

# **Multi-Dimensional Wave Digital Filters and Wavelets**

## **Inauguraldissertation**

zur Erlangung des akademischen Grades eines

Doktors der Naturwissenschaften

der Universität Mannheim

von

**MSc. Achim GOTTSCHER**

aus Grombach

*Mannheim, 1998*

Dekan der Fakultät:

Referent:

Korreferent:

Tag der mündlichen Prüfung:

Professor Dr. Reinhard Männer, Universität Mannheim

Professor Dr. -Ing. Dr.-Ing. E.h. N. J. Fliege, Universität Mannheim

Professor Dr. Gabriele Steidl, Universität Mannheim

23. September 1998

# Preface

The presented dissertation is the result of my work which I carried out in several places. Hence I am very grateful to several people that have helped and organisations that have sponsored me during that time.

Prof. Dr. N. Fliege, Universität Mannheim, Lehrstuhl für Elektrotechnik, Germany  
Prof. Dr. G. Steidl, Universität Mannheim, Fakultät für Mathematik und Informatik, Germany  
Prof. Dr. A. Fettweis, Ruhr Universität Bochum, Lehrstuhl für Nachrichtentechnik, Germany  
Prof. Dr. M. Vetterli, Ecole Polytechnique Federale de Lausanne, Dept. d'Electricite, LCAV, Switzerland  
Prof. Dr. P. Tchamitchian, Jerome Universite Aix, Laboratoire de Mathematique, France  
Prof. Dr. A. Nishihara, Tokyo Institute of Technology, Dept. of Physical Electronics, Japan  
Deutscher Akademischer Austauschdienst (DAAD), Germany  
Japanisches Kultusministerium (Monbusho), Japan  
Universität Mannheim, Germany

A special thank goes to Prof. N. J. Fliege who gave me the chance for this dissertation. Also I thank him for the constructive critical discussions on it.

Furthermore, I am thankful to Prof. G. Steidl for useful discussions on the thesis and who accepted the Korreferat.

In addition, I like to thank for their invitation as a visiting researcher to Professors A. Fettweis, M. Vetterli, P. Tchamitchian, and A. Nishihara.

Last but not least, I am delighted about the support I have received from my parents, wife and friends.

Grombach, September 1998

Achim GOTTSCHER.



## List of Abbreviations

WDF	wave digital filter
ASIC	application specific integrated circuit
FCCS	face centered cubic sampling
BCCS	body centered cubic sampling
FIR	finite impulse response
IIR	infinite impulse response
$\mathbf{V}, \mathbf{M}$	sampling matrix
FCCS	face centered cubic sampling
BCCS	body centered cubic sampling
2-D	two dimensional
$M_{rec} = \begin{bmatrix} 2 & 0 \\ 0 & 2 \end{bmatrix}$	rectangular sampling matrix
$M_q = \begin{bmatrix} 1 & 1 \\ 1 & -1 \end{bmatrix}$	quincunx sampling matrix (well behaved, i.e., $M_q^2 = M_{rec}$ )
$y(t)$	continuous output signal
$x(t)$	continuous input signal
$t$	time variable
$h(t)$	filter function
$R$	resistance
$C$	capacitance
$L$	inductance
$r$	gyrator factor
$\lambda$	transformator factor
$i(t)$	electrical current
$u(t)$	electrical voltage
$\text{sinc}(t) = \frac{\sin(\pi t)}{\pi t}$	sinus cardinal function
$ H(s) ^2$	magnitude squared of an analog filter transfer function $H(s)$
$H(e^{j\omega})$	digital filter transfer function
$K(s)$	characteristic function
$s$	Laplace variable
$\Omega = 2\pi f$	circular frequency (analog signals)
$\omega = 2\pi f$	circular frequency (digital signals, one dimensional)
$\boldsymbol{\omega}$	circular frequency (multi-dimensional)
$R_N$	Chebyshev rational function
$\epsilon_s, \epsilon_p$	stopband-, passband-ripple factor
$N \in \mathbf{N}$	filter order
$a_s$	specified minimum attenuation in the stopband in dB
$a_p$	maximal allowable attenuation spread in the passband in dB
$\Omega_s$	stopband edge
$\Omega_p$	passband edge
$m, n \in \mathbf{Z}$	time instaces, related to $t$
$L, M$	up-, down-sampling factors
$T, T_s$	sampling time interval
$z$	z-transform variable
$E_k$	$k^{th}$ type 1 polyphase component
$G(z), H(z), Q(z)$	digital filter

$\varphi, H_0, H_L, H_{LP}$	low-pass filter
$H_1, H_H, H_{HP}$	high-pass filter
$\psi, H_{BP1}, H_{BP2}$	band-pass filter
$V_i, W_i$	subspaces of $L_2(\mathbf{R})$
$\varphi(t)$	scaling function (father wavelet)
$\psi(t)$	basic wavelet (mother wavelet)
MA	multiresolution analysis
PR	perfect reconstruction
FB	filter bank
QMF	quadrature mirror filter
$L_2(\mathbf{R})$	space of square integrable signals
$L_k(t)$	Lagrange basis polynomials
$A_1, A_2, a_1, a_2, B_1, B_2, b_1, b_2$	wave quantities
$Z_1, Z_2$	impedance
<b>S</b>	scattering matrix
<b>E</b>	unit matrix

# Contents

<b>1</b>	<b>Introduction</b>	<b>1</b>
<b>2</b>	<b>Circuits and Filters</b>	<b>4</b>
2.1	Circuits and filters . . . . .	4
2.1.1	Analog filters . . . . .	4
2.1.2	Digital filters . . . . .	9
2.2	Tools for circuit design . . . . .	11
2.2.1	Multirate techniques . . . . .	11
2.2.2	Filter bank . . . . .	12
2.2.3	Mallats multiresolution analysis . . . . .	14
2.2.4	Scaling function and wavelet relations . . . . .	16
2.3	Sampling . . . . .	17
2.3.1	Polynomial sampling theorem . . . . .	17
2.3.2	Shannon sampling theorem . . . . .	18
2.3.3	Wavelet sampling theorem . . . . .	19
2.3.4	Sampling in multiresolution subspaces . . . . .	20
<b>3</b>	<b>Wave Digital Filter</b>	<b>23</b>
3.1	Wave Digital Filter . . . . .	23
3.1.1	Analog relationships . . . . .	23
3.1.2	Digital relationships . . . . .	26
3.1.3	Lattice Wave Digital Filter . . . . .	26
3.1.4	IIR Wave Digital Filter and Perfect Reconstruction . . . . .	28
3.1.5	Ladder Wave Digital Filter . . . . .	29
3.2	Implementation of non-causal filters (for infinite length signals) . . . . .	30

<b>4</b>	<b>Wavelets</b>	<b>32</b>
4.1	Some Properties . . . . .	32
4.1.1	Convolution . . . . .	32
4.1.2	Fractional Shift . . . . .	32
4.1.3	Shift operation on the expansion coefficients . . . . .	34
4.1.4	Performance Simulations . . . . .	39
4.2	Wavelet bases . . . . .	41
4.2.1	Sinc Wavelet . . . . .	41
4.2.2	Meyer Wavelets . . . . .	42
4.2.3	Raised Cosine Wavelets . . . . .	43
4.2.4	Haar Wavelet . . . . .	46
4.2.5	Daubechies Wavelets . . . . .	47
4.2.6	Butterworth Wavelets . . . . .	49
4.2.7	Chebyshev Wavelets . . . . .	50
4.3	Conclusion . . . . .	50
<b>5</b>	<b>Two-Channel Multidimensional Systems</b>	<b>52</b>
5.1	Two-Dimensional Nonseparable Orthonormal Wavelets . . . . .	52
5.1.1	Paraunitary Filter Bank . . . . .	53
5.1.2	Constructing 2-D Wavelet Bases from LWDFs . . . . .	57
5.2	Discussions . . . . .	58
5.2.1	Minimum sampling density for $\mathbf{V}$ related to $\mathbf{M}_q$ . . . . .	58
5.3	Conclusion . . . . .	59
<b>6</b>	<b>Four-Channel Multidimensional Systems</b>	<b>64</b>
6.1	Preliminaries . . . . .	64
6.2	Three-Dimensional Nonseparable Orthogonal Perfect Reconstruction Filter Bank using Wave Digital Filters . . . . .	65
6.3	Four-channel two-dimensional nonseparable orthogonal perfect recon- struction filter bank . . . . .	71
6.4	Infinite recursive tree structure (4-channel) . . . . .	72
6.5	Conclusion . . . . .	72
<b>7</b>	<b>Ladder Wave Digital Filter</b>	<b>81</b>



7.1	Explicit formulas for IIR filters . . . . .	81
7.2	Four channel polyphase arrangements . . . . .	83
7.3	Conclusion . . . . .	87
<b>8</b>	<b>Conclusion</b>	<b>89</b>
<b>A</b>	<b>Sampling lattice</b>	<b>90</b>
<b>B</b>	<b>Zusammenfassung</b>	<b>96</b>
<b>C</b>	<b>Bibliography</b>	<b>99</b>

# Chapter 1

## Introduction

Even though this thesis is mainly concerned with digital (discrete) signal processing, analog (continuous) signal processing is the overall goal. What links them together is a sampling theorem. The principal impact of a sampling theorem is that it allows the replacement of a continuous (filtered) signal by a discrete sequence of its samples without loss of any information. Also it specifies a minimum sampling rate that is necessary in order to be able to reconstruct the original continuous signal. The main reason why one is using a digital circuit to process analog (continuous) signals is: In some frequency range, digital circuits are less subject to distortion and interference than are analog circuits.

If a discrete sequence is convolved with a digital filter then the filter structure (possible choices are, e.g., direct-, parallel-, cascade-, lattice-, ladder-structures) for the desired application was chosen beforehand. A very good choice for an application that requires good coefficient accuracy, dynamic range and stability under finite arithmetic conditions are the lattice or ladder wave digital filter (WDF) structures. Recursive WDFs, e.g. Butterworth and Cauer (elliptic) filters, can be designed by using explicit formulas. Nonrecursive WDFs are designed with optimization methods and numerical problems can occur for high filter degrees. In order to meet the same filter specification, nonrecursive digital filters need a higher filter degree than recursive digital filters. Linear phase filters and multiplierless structures are possible to be realized for both types.

Digital filters that are arranged in a filter bank and fulfil additional requirements can be used to generate wavelets. Biorthogonal filters are such filters. Orthogonal filters are a special case of biorthogonal filters that have the lowest complexity. Design methods of orthogonal filters have been found for the one dimensional case [Gas85, Fli94, Vai93, Vet95]. The design of orthogonal filters in higher dimensions for nonseparable sampling, except for one trivial filter (Haar filter), have not been found. Unlike separable sampling (diagonal matrix), which is build with tensor products of their one-dimensional counterparts and results in one scaling function and three different basic (mother) wavelets for a two-channel, two-dimensional filter bank,

nonseparable sampling results in one scaling function and one basic wavelet. A similar statement on the number of basic wavelets is true for more than two channels and higher dimensional filter banks.

Possible candidates for a sampling theorem are the wavelet sampling theorem and the Nyquist sampling theorem. The filter with which an analog signal gets convolved before sampling takes place is called scaling function (father wavelet). Possible candidates for a nonseparable sampling matrix in two dimensions are a quincunx matrix for a two channel and a hexagonal matrix for a four channel filter bank. A face centered cubic sampling (FCCS) matrix can be used for two channels and a body centered cubic sampling (BCCS) matrix can be used for four channels in three dimensions.

The strength of wavelet methods lies in their ability to describe local phenomena more accurately than a traditional expansion in sines and cosines can. Hence, wavelets are ideal in applications where an approach to transient behaviour is needed; such as in seismic signals or in image processing. Operators associated with wavelets, i.e., Calderon-Zygmund operators seem to enable to solve outstanding classical problems in complex analysis and partial differential equations. Thus, wavelets are very much needed in multidimensional problems and efficient orthogonal filters designed as wave digital filters for nonseparable sampling matrices are desirable. In fact, they are needed by engineers that deal with subband coding, physicists in quantum physics that deal with coherent states and mathematicians that deal with Calderon-Zygmund operators but they are not restricted to them. Various industrial standards have already incooperated the wavelet transform, as an example see [Rao96].

The main target of this thesis is the design of orthogonal multidimensional wave digital filters for nonseparable sampling matrices. In order to be able to find an easy access to filter design, some basic background knowledge of electrical circuits and filters of analog as well as digital type are reviewed in chapter 2. To indicate an application, an electrical circuit that represents a three-dimensional Navier-Stokes equation is presented. And it can be used when calculating numerical values of this equation. Important ingredients that link a digital filter to a wavelet transform are summarised and it is referred to other literature for a more detailed discussion. Furthermore important sampling theorems are discussed and a comparison on the minimum sampling rate is given that shows interesting aspects.

Chapter 3 recapitulates relationships of WDFs to their analog reference filters and how a perfect reconstruction system can be build without the need of a spectral factorization method. Feldkeller's equation plays an important role during the design of ladder or lattice WDFs. It is exemplarily shown how to build a perfect reconstruction system with recursive orthogonal lattice WDFs. How infinite length signals are processed and how non-causal filters are implemented is also discussed.

Known wavelet bases such as Meyer wavelets, Sinc-wavelets (Littlewood-Paley wavelets), Haar wavelets, Daubechies wavelets and Butterworth wavelets are listed in chapter

4 and known filters are presented that, under some restrictions, can be used to generate new orthonormal wavelet bases such as raised-cosine wavelets and Chebyshev wavelets. Also presented are two properties of the wavelet transform, i.e., convolution and shift. Using known filter design tools the known shift property is extended to a shift  $\tau \in \mathbf{R}$ .

The novelties of chapter 5, 6 and 7 are: Two channel nonseparable orthogonal wave digital filters for quincunx sampling are designed in chapter 5. The design method is based on one-dimensional filters as well as well-behaved sampling matrices. A polyphase decomposition is applied and results in a very efficient realization of the filters. Four-channel nonseparable orthogonal wave digital filters for hexagonal sampling as well as for BCCS matrices are designed in Chapter 6. As in chapter 5, well behaved sampling matrices are found and used during the design process which again can be brought back to one-dimensional filters. As an example, Butterworth filters are used. However, the design process is not restricted to that type of filters.

The chapters 5 and 6 use lattice WDFs since they can be implemented very efficiently. However, it can be seen in chapter 7 that for hexagonal sampling a ladder WDF implementation is more efficient than a lattice WDF implementation. A new proposed design method that uses explicit formulas for four-channel systems is given.

Finally the thesis is concluded in chapter 8.

# Chapter 2

## Circuits and Filters

This chapter is divided into three sections. It provides some background knowledge for later chapters on analog and digital filters. Furthermore, tools for circuit design, that can increase the efficiency with which signals can be processed, are given, i.e., multirate system, filter bank, Malats multiresolution analysis and wavelet transform. In addition, sampling theorems that link digital circuits to analog circuits are presented.

### 2.1 Circuits and filters

The theory of analog and digital filters is huge. Here, only some parts of it are presented that are necessary to follow the main idea of the new presented material in this thesis. It is referred to [Fet86, Fli94, Vet95, Vai93] and reference therein for more details.

#### 2.1.1 Analog filters

Convolution was used by Oliver Heaviside in the late nineteenth century to calculate electrical circuit output current when the input voltage waveform was more complicated than a simple battery source. The use of the methods of Heaviside predates the use of the analytical methods developed by Fourier and Laplace [Skl88]. Analog filters are electrical circuits. The theory of analog filters also owes its origin to Wagner and Campbell, who in 1915 advanced the concept of passive electrical wave filters [The73]. Fig. A.2 shows a block diagram of an electrical filter. In what follows<sup>1</sup>,  $t \in \mathbf{R}$ . In Fig. A.2, the output variable<sup>2</sup>  $y(t)$  is related to the input variable  $x(t)$  through a

---

<sup>1</sup>Very often  $t$  represents time. For such cases  $t$  has the unit seconds.

<sup>2</sup>A function as well as a function value is denoted in the same way, e.g.  $y(t)$ . However, for notational convenience, the dependency on the independent variable is sometimes neglected.

convolution integral as

$$y(t) = \int_{\tau=-\infty}^{\infty} h(t, \tau)x(\tau)d\tau, \quad (2.1)$$

or, when the analog filter is a time-invariant network, as

$$y(t) = \int_{\tau=-\infty}^{\infty} h(t - \tau)x(\tau)d\tau. \quad (2.2)$$

A passive electrical filter may be composed for example of some electrical resistances



**Figure 2.1:** Electrical Filter. (Two port.)

$R$ , capacitances  $C$ , inductances  $L$ , gyrators  $r$  and ideal transformers  $\lambda$ . The voltage  $u(t)$  and the current  $i(t)$  are related as

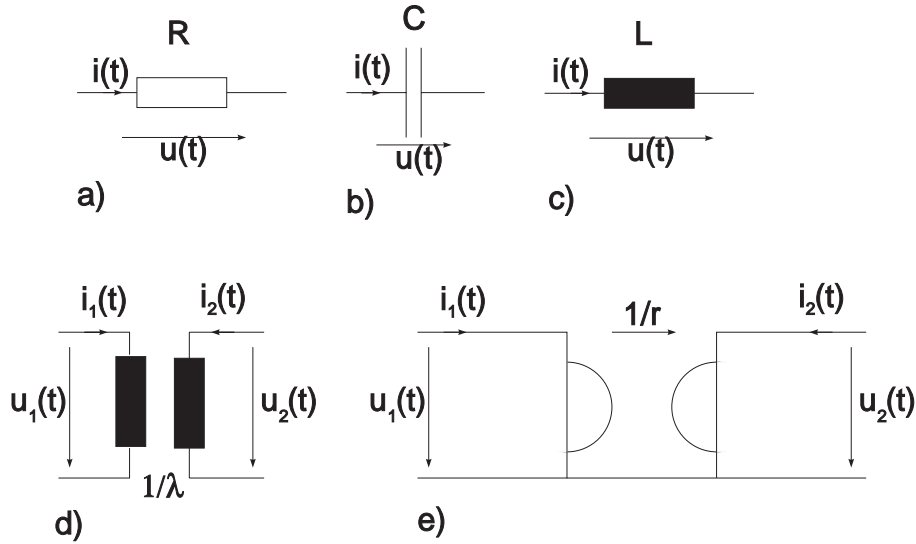


**Figure 2.2:** Symbol for a) Resistance, b) capacitance, c) inductance, d) ideal transformer, e) gyrator.

$$u(t) = R \cdot i(t),$$

$$i(t) = C \frac{du(t)}{dt},$$

$$u(t) = L \frac{di(t)}{dt},$$

$$\begin{pmatrix} u_1(t) \\ u_2(t) \end{pmatrix} = \begin{pmatrix} 0 & -r \\ r & 0 \end{pmatrix} \begin{pmatrix} i_1(t) \\ i_2(t) \end{pmatrix}$$

$$\begin{pmatrix} u_2(t) \\ i_1(t) \end{pmatrix} = \begin{pmatrix} \lambda & 0 \\ 0 & -\lambda \end{pmatrix} \begin{pmatrix} u_1(t) \\ i_2(t) \end{pmatrix}$$

The associated circuit elements<sup>3</sup> are illustrated in Fig. 2.2.

A one dimensional circuit as well as multidimensional circuits may be determined by finding differential equations that result from the application of Kirchhoff's voltage rule and Kirchhoff's current rule. These rules are shown e.g. in [Hem95] for multidimensional circuits. It is interesting to note at this point that entirely different physical systems may correspond to the same mathematical description. For example, an analogy between mechanical and electrical systems exists. Hence, it is possible to describe mechanical problems with electrical circuits. Also note that discretised versions of these electrical circuits can be used for methods that solve numerically multidimensional partial differential equations of any type. Such methods require additional filter circuits. They are designed with the help of approximations for which the Laplace transform is suitable. Using the Laplace transform,

$$A(s) = \int_{s=-\infty}^{\infty} a(t)e^{-st}ds,$$

(2.2) can be written as

$$Y(s) = H(s)X(s).$$

An ideal noncausal filter e.g.

$$h_{sinc}(t) = \frac{\sin(\pi t)}{\pi t} = sinc(t),$$

$$h_{raised-cosine}(t) = sinc(t) \frac{\cos(\alpha \pi t)}{1 - 2\alpha t^2},$$

$0 \leq \alpha \leq 1$ , or

$$h_{cosine}(t) = sinc(t) \frac{\sin(\pi t - 1)}{\pi(t - 1)},$$

may be approximated with the causal filter transfer function  $H(s)$  as:

$$|H(s)|_{s=j\Omega}^2 = [H(s)H(-s)]_{s=j\Omega} = \frac{1}{1 + K^2(s)} = \frac{a_0 + a_1\Omega^2 + \dots + a_M\Omega^{2M}}{b_0 + b_1\Omega^2 + \dots + b_N\Omega^{2N}}, \quad (2.3)$$

where  $N, M \in \mathbf{Z}$  and<sup>4</sup>  $\Omega \in \mathbf{R}$ .  $K(s)$  denotes the so-called characteristic function.

Common approximations are Bessel, Butterworth, Chebyshev type I, Chebyshev type II and Cauer (elliptic) approximation. For a Butterworth approximation (maximally flat)

$$K^2(s) = (-s)^{2N}, \quad (2.4)$$

and for a Cauer approximation (Chebyshev pass- and stop-band)

$$K^2(s) = \epsilon^2 R_N^2(s); \quad (2.5)$$

<sup>3</sup>It is referred to [Hem95] for the definition of multidimensional versions of these circuit elements.

<sup>4</sup>Very often  $\Omega = 2\pi f$  represents circular frequency. For such cases  $\Omega$  has the unit radians per second.

here  $\epsilon \in \mathbf{R}$  is a small number. The Chebyshev rational function  $R_N(\Omega)$  is defined by [Dav95, p.2182][Tan95, p.2616]

$$R_N(\Omega) = \begin{cases} \frac{(\delta^{-2}-1)^{1/4}}{\epsilon^{1/2}} \Omega \prod_{i=1}^{(N-1)/2} \frac{\Omega^2 - \Omega_r \operatorname{sn}^2[\frac{2iK(\Omega_r)}{N}, \Omega_r]}{\Omega^2 \Omega_r \operatorname{sn}^2[\frac{2iK(\Omega_r)}{N}, \Omega_r] - 1} & N=\text{odd}, \\ \frac{(\delta^{-2}-1)^{1/4}}{\epsilon^{1/2}} \Omega \prod_{i=1}^{N/2} \frac{\Omega^2 - \Omega_r \operatorname{sn}^2[\frac{(2i-1)K(\Omega_r)}{N}, \Omega_r]}{\Omega^2 \Omega_r \operatorname{sn}^2[\frac{(2i-1)K(\Omega_r)}{N}, \Omega_r] - 1} & N=\text{even} \end{cases}$$

Here,  $(\Omega_p$  is the so-called passband edge,  $\Omega_s$  is the so-called stopband edge)  $\Omega_r = \Omega_p/\Omega_s$ ,  $K(t)$  is the complete elliptic integral of the first kind given by

$$K(t) = \int_{\phi=0}^{\pi/2} \frac{d\phi}{[1 - t^2 \sin^2 \phi]^{1/2}} = \int_{x=0}^1 \frac{dx}{[(1-x^2)(1-t^2x^2)]^{1/2}}$$

The Jacobian elliptic sine function  $\operatorname{sn}[u, t]$  is defined as

$$\operatorname{sn}[u, t] = \sin \varphi \text{ if } u = \int_{\phi=0}^{\varphi} \frac{d\phi}{[1 - t^2 \sin^2 \phi]^{1/2}}$$

The integral

$$F(\varphi, t) = \int_{\phi=0}^{\varphi} \frac{d\phi}{[1 - t^2 \sin^2 \phi]^{1/2}} = \int_{x=0}^{\sin \varphi} \frac{dx}{[(1-x^2)(1-t^2x^2)]^{1/2}}$$

is called the elliptic integral of the first kind. Note that  $K(t) = F(\pi/2, t)$ . Bessel-, Chebyshev type I- and Chebyshev type II filters are not used in this thesis. Thus, see e.g. [Dav95, Tan95] for the definition of their characteristic function. The choice of the filter degree  $N$  depends on how good the ideal filter should be approximated and can be specified by the parameters

$a_s$  specified minimum attenuation in the stopband in decibels

$a_p$  maximum allowable attenuation spread in the passband in decibels

$\Omega_s$  stopband edge

$\Omega_p$  passband edge.

One can also use instead of  $a_s$  and  $a_p$  the ripple factors

$$\epsilon_s = \sqrt{10^{a_s/10} - 1}$$

$$\epsilon_p = \sqrt{10^{a_p/10} - 1},$$

respectively. Figure 2.3 shows the specifications for an analog lowpass filter. The filter order for a normalized filter with specification

$$(1 + \epsilon_p^2)^{-1} \leq |H(s)|^2 \leq 1 \quad \text{for the passband} \quad (2.6)$$

$$0 \leq |H(s)|^2 \leq \epsilon_s^2 \quad \text{for the stopband} \quad (2.7)$$



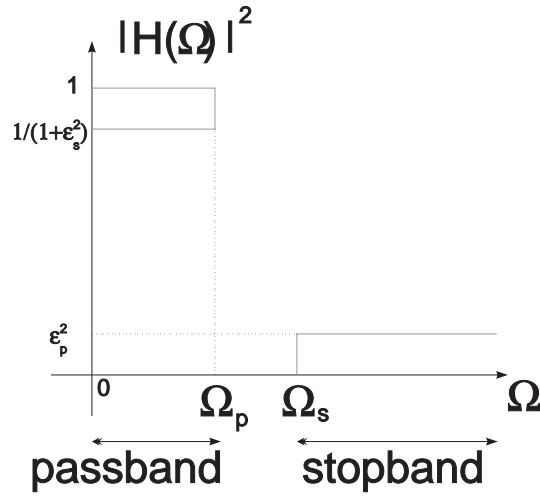


**Figure 2.3:** Specification for an analog low-pass filter.

can be estimated from

$$N \geq \frac{\log[\epsilon_p/(\epsilon_s^{-2} - 1)^{1/2}]}{\log[\Omega_p/\Omega_s]} \quad (\text{Butterworth case}) \quad (2.8)$$

$$N \geq \frac{1}{\log[\beta]} \log\left[\frac{\epsilon_p^2}{16(\epsilon_s^{-2} - 1)}\right] \quad (\text{Cauer case}) \quad (2.9)$$

with

$$\beta = e^{-\pi K[(1-\Omega_r^2)^{1/2}]/K[\Omega_r]}.$$

Having obtained an explicit approximation formula for (2.3) by using say (2.4), it is

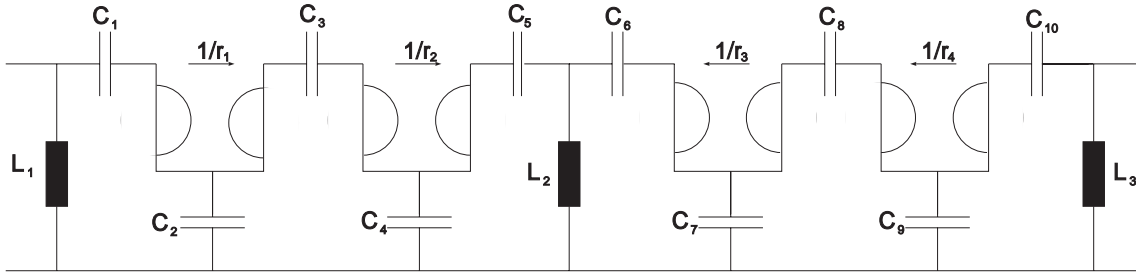


**Figure 2.4:** Example for an analog low-pass filter. Note, there are many possible filter circuits that correspond to (2.10)

necessary, because of passivity yielding stability, to calculate the values of the elements ( $R, L, C, \dots$ ) of a passive<sup>5</sup> analog filter. This can be done with a method shown for example in [The73, Sch90, Unb93].

As an example Fig. 2.4 shows a one dimensional low-pass filter with the transfer

<sup>5</sup>Active filters can be split up into a passive and active part [Hem95].

function (see also (7.7) of chapter 7)

$$H(s) = 2 \frac{(s-2)(s^3 + 6s^2 - 8)}{(s+1)(s+2)(s^2 + s + 1)(s^3 - 6s^2 + 8)(s^6 + s^3 + 1)} \quad (2.10)$$

and Fig. 2.5 indicates a three dimensional circuit that models a lossless fluid dynamic system. A detailed description of the electrical circuit (Network) in Fig. 2.5 is given in [Fet92]. Also [Hem95, Nit93, Fri96] describe similar circuits.

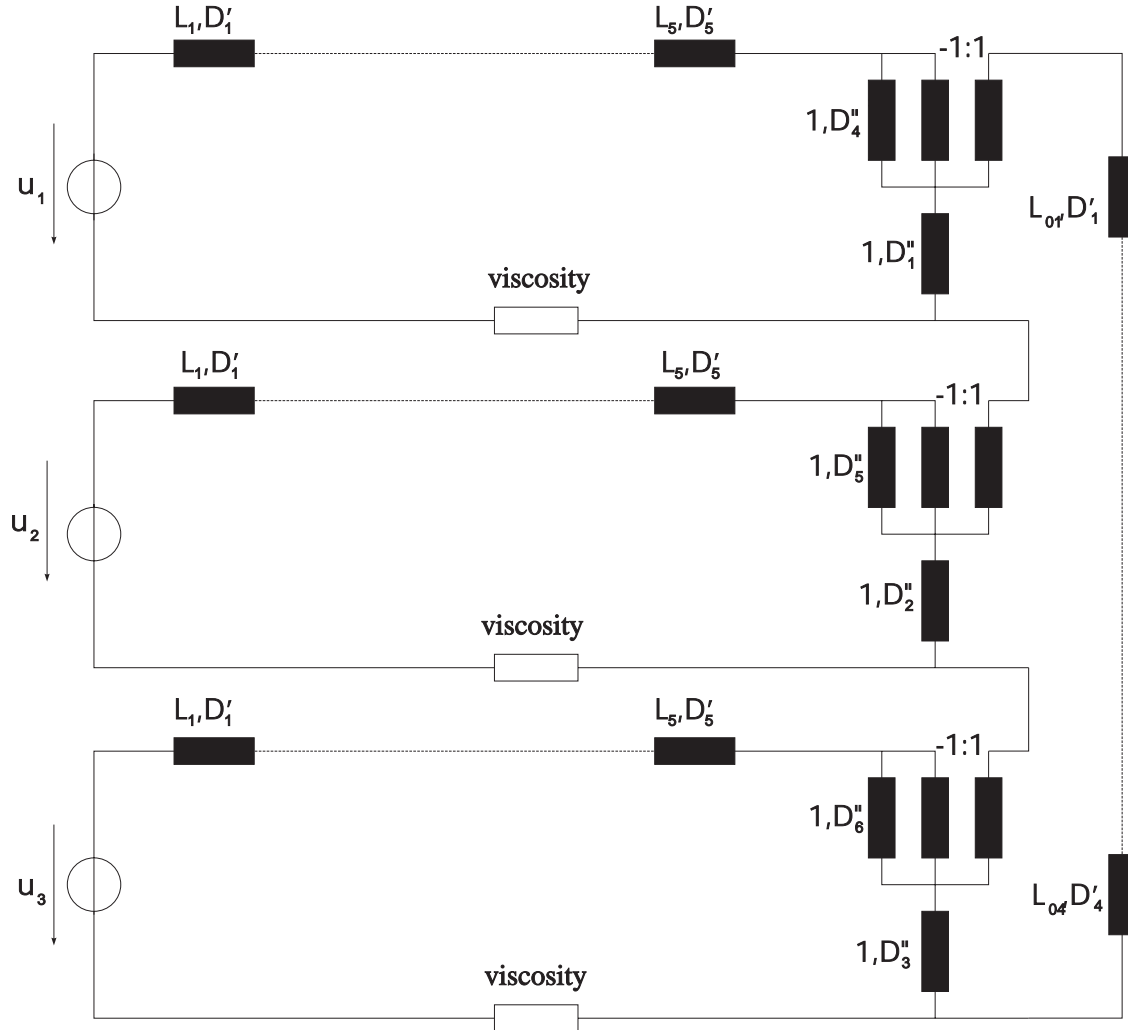


**Figure 2.5:** Electrical circuit representing the general three-dimensional fluid dynamic equations.  $u_1, u_2$  and  $u_3$  represent ideal voltage sources. It is referred to [Hem95, Fet92] for the definition of the multidimensional elements, where  $\mathbf{L}$  must not be a constant and  $\mathbf{D}$  represents a differential operator. The complex resistant (viscosity) is nonlinear.

### 2.1.2 Digital filters

There exist many methods to design digital filters. One method that relates a digital filter to an analog (reference) filter is called wave digital filter (WDF) and it owes its

origin to Alfred Fettweis, who in 1970 [Fet70] made it possible to design systematically passive digital filters (WDF) (yielding low-sensitivity filters) by making full use of analog filter design techniques. Although this method is more complicated than other existing digital filter design methods, it always guaranties (when properly used) a stable passive digital filter [Fet86]. Discussions of standard WDF design (IIR or FIR), including the bireciprocal case which leads to filters that when used in an iterated perfect reconstruction filter bank yield orthonormal wavelets, can be found in [Fet86, Gas85]. Two main WDF structures are the lattice WDF<sup>6</sup> and the ladder WDF. In a two channel filter bank lattice WDF yield more computationally efficient realizations than ladder WDF. This is not true for four channel filter banks, see chapter 7. Since the next Chapter is devoted to WDF, this section presents only general digital filter relationships.

In what follows<sup>7</sup>  $n, m \in \mathbf{Z}$ . Discrete versions of (2.1) and (2.2) are

$$y(m'T_2) = \sum_n h(m'T_2, nT_1)x(nT_1),$$

and

$$y(m'T_2) = \sum_n h(m'T_2 - nT_1)x(nT_1),$$

$T_1 = LT$  and  $T_2 = MT$  denote sampling instants,  $M$  represents a positive integer downsampling factor,  $L$  represents a positive integer upsampling factor,  $m' = m - 1 + \Delta$ ,  $0 \leq \Delta \leq 1$ ,  $1/T$  critical sampling rate to be defined later,  $M/L \leq 1$  and assuming the filter  $h$  to be a low-pass filter, the cutoff frequency is the lesser of  $\pi/L$  and  $\pi/M$ . (Throughout this thesis, it is always assumed that the filters are time-invariant.) Assuming  $T_1 = T_2 = T$ ,  $\Delta = 1$  and using the z-transform

$$A(z) = \sum_{n=-\infty}^{\infty} a(nT)z^{-n}, \quad (2.11)$$

a IIR-filter may be represented as

$$H(z) = \frac{\sum_{m=0}^M b_m z^{-m}}{1 + \sum_{n=1}^N a_n z^{-n}}$$

and a FIR-filter may be represented as

$$H(z) = \sum_{n=0}^{N-1} b_n z^{-n}.$$

Note, instead of (2.11), also for  $\Delta \neq 1$ , a modified z-transform [Kov95]

$$A(z, \Delta) = \sum_{n=-\infty}^{\infty} a([n - 1 + \Delta]T)z^{-n},$$

can be used. Without going into details it should be noticed that adaptive FIR and IIR filters exist, see e.g. [Nar94, Hay95].

---

<sup>6</sup>Note, lattice digital filters [Lim95] and lattice WDFs [Fet86] are different. Whereas analytical formulas exist for lattice WDF, they do not exist for lattice digital filters. Their filter structure is also different. The filter structure for lattice WDF is always robust.

<sup>7</sup>Note, the time instances  $n, m$  are related to  $t$ .

Digital filters are composed of adders, multipliers and delay elements. Unlike passive analog filters, passive digital filters can be designed to have exactly linear phase. Whereas the design of linear phase FIR filters is well known, the design of linear phase IIR filters is under current research. Recent publications on this topic are [Vet95, Sel97]. Noncausal digital filters can also be realized. This is true for FIR and IIR filters. Linear phase IIR filters have a causal and noncausal part. A realizable passive filter cannot have negative element values in the analog case but in the digital case it is possible. Note, analog reference filters from which a digital filter is derived may have negative element values.

As an example, a linear phase IIR low-pass filter  $H_0(z)$ , that can be used for a two-channel orthogonal perfect reconstruction filter bank from which wavelet bases can be generated, is shown next.

$$H_0(z) = A(z^2) + z^{-1}A(z^{-2})$$

$$A(z) = \frac{1 + 6z^{-1} + (15/7)z^{-2}}{(15/7) + 6z^{-1} + z^{-2}}.$$

The filter coefficients in the FIR case are usually obtained from the application of optimization techniques that use a weighted Chebyshev method. Closed-form formulas exist (e.g. Lagrange polynomial), but they often lead to filters that are not optimal in some respect. Nevertheless, useful exceptions exist, see chapter 4. A well known computer program using the weighted Chebyshev method is due to [Cle79]. The filter coefficients in the IIR case can be obtained in two ways: a) from explicit formulas, b) from algorithms executed by computer programs [lee79]. Both ways give good results in some respect. However, unlike FIR filters, IIR filters can be unstable. Since WDF have very good properties concerning coefficient accuracy requirements, dynamic range and especially all aspects of stability under finite-arithmetic conditions, this thesis makes use of them also because they are very much suited for multirate systems.

## 2.2 Tools for circuit design

Since there is no general tool which can be used to design a filter for any purpose in a most efficient way, many tools are necessary and some of them which are used in connection with the wavelet transform are presented below.

### 2.2.1 Multirate techniques

Multirate techniques can often be used to improve the computational efficiency of digital filters suffering from a certain redundancy. A system contains redundancy if the bandwidth or transition bandwidth is less than half the sampling rate [Fli94]. A powerful tool of multirate systems is the polyphase decomposition (polyphase transform).

It can be defined as:

$$H(z) = \sum_{k=0}^{M-1} z^{-k} E_k(z^M) \quad (2.12)$$

where

$$E_k(z) = \sum_{n=-\infty}^{\infty} h(Mn + k) z^{-n}.$$

Equation (2.12) is called type 1 polyphase decomposition. Note, that  $E_k$  for  $k = 0$  is called  $0^{th}$ -type 1 polyphase component and, as will be seen later, is of some importance. Periodically time-varying systems with period  $N$  and a time-scale change are e.g. down/up-samplers [Vet95]. Such systems can be analyzed with polyphase transforms. For a downsampler, depicted in Fig. 2.6 a),  $Y(z)$  is related to  $X(z)$  as

$$Y(z) = \frac{1}{M} \sum_{k=0}^{M-1} X(z^{\frac{1}{M}} e^{-j2\pi k/M}).$$

And for a upsampler, depicted in Fig. 2.6 b),  $Z(z)$  is related to  $Y(z)$  as

$$Z(z) = Y(z^M).$$

Cascading arbitrarily units of filters and down/up-samplers, can result in arbitrar-

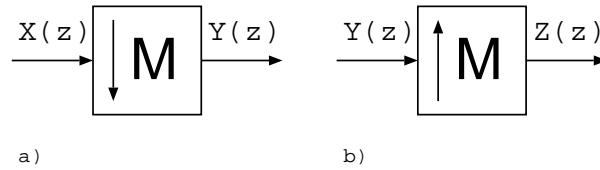


**Figure 2.6:** Block diagram representation of a (a) downsampler (b) upsampler.

ily tree-structured filter banks. Wavelet packets are obtained from arbitrarily tree-structured filter banks [Wic92]. To give an example for an application, they are very suitable for the goal of computing the evolution of turbulent flows [Far92]. And a four-channel unit offers more possible combinations than a two-channel unit. Thus one has more choice in the detection of the characteristic scaling of the different regions of the flow. In other words, efficient compression of datas is possible when using multi-rate systems. Other applications which take advantage of multirate techniques are in speech and image compression as well as statistical and adaptive signal processing.

## 2.2.2 Filter bank

The counter part of an analog filter bank is a digital filter bank. There is a similarity between a modulator/demodulator in continuous systems and a decimator/interpolator in a discrete system, see [Cro83] and references therein. However, modulation is also used in discrete systems, e.g., modulated digital filter banks, see [Fli94, Kar97]. Among digital filter banks (in the following called FB), there are some which have a perfect

reconstruction (PR) property. A PR FB can be viewed as a transformation. Dependent on how the filters are designed, different transformations are applied to an input signal. Examples of transformations are: Fourier transform, Cosine transform and Wavelet transform [Fli94, Vet95, Vai93]. Figure 2.7, for example, shows a four channel FB. The related equations in case of a PRFB are:

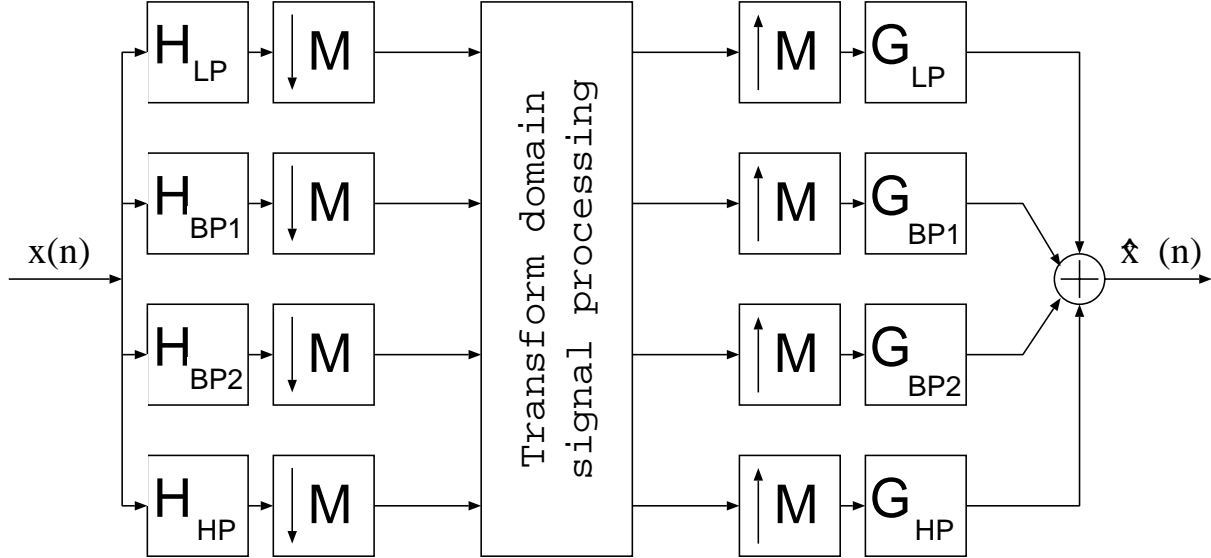


**Figure 2.7:** FB having  $M=4$  channels, where  $x(n) = \hat{x}(n)$  for a PRFB without any processing of signals in the transform domain.  $M$  represents the down/up-sampling matrix.  $H_i$  and  $G_i$ ,  $i = LP, BP1, BP2, HP$  are filters.

$$\begin{bmatrix} X_0(z) \\ X_1(z) \\ X_2(z) \\ X_3(z) \end{bmatrix} = \frac{1}{4} \begin{bmatrix} H_{LP}(z^{\frac{1}{4}}) & H_{LP}(-jz^{\frac{1}{4}}) & H_{LP}(-z^{\frac{1}{4}}) & H_{LP}(jz^{\frac{1}{4}}) \\ H_{BP1}(z^{\frac{1}{4}}) & H_{BP1}(-jz^{\frac{1}{4}}) & H_{BP1}(-z^{\frac{1}{4}}) & H_{BP1}(jz^{\frac{1}{4}}) \\ H_{BP2}(z^{\frac{1}{4}}) & H_{BP2}(-jz^{\frac{1}{4}}) & H_{BP2}(-z^{\frac{1}{4}}) & H_{BP2}(jz^{\frac{1}{4}}) \\ H_{HP}(z^{\frac{1}{4}}) & H_{HP}(-jz^{\frac{1}{4}}) & H_{HP}(-z^{\frac{1}{4}}) & H_{HP}(jz^{\frac{1}{4}}) \end{bmatrix} \begin{bmatrix} X(z^{\frac{1}{4}}) \\ X(-jz^{\frac{1}{4}}) \\ X(-z^{\frac{1}{4}}) \\ X(jz^{\frac{1}{4}}) \end{bmatrix}$$

$$\hat{X}(z) = \begin{bmatrix} G_{LP}(z) & G_{BP1}(z) & G_{BP2}(z) & G_{HP}(z) \end{bmatrix} \begin{bmatrix} X_0(z^4) \\ X_1(z^4) \\ X_2(z^4) \\ X_3(z^4) \end{bmatrix}$$

$$\begin{aligned} \hat{X}(z) &= \begin{bmatrix} G_{LP}(z) & G_{BP1}(z) & G_{BP2}(z) & G_{HP}(z) \end{bmatrix} \\ &\quad \cdot \frac{1}{4} \begin{bmatrix} H_{LP}(z) & H_{LP}(-jz) & H_{LP}(-z) & H_{LP}(jz) \\ H_{BP1}(z) & H_{BP1}(-jz) & H_{BP1}(-z) & H_{BP1}(jz) \\ H_{BP2}(z) & H_{BP2}(-jz) & H_{BP2}(-z) & H_{BP2}(jz) \\ H_{HP}(z) & H_{HP}(-jz) & H_{HP}(-z) & H_{HP}(jz) \end{bmatrix} \begin{bmatrix} X(z) \\ X(-jz) \\ X(-z) \\ X(jz) \end{bmatrix} \end{aligned}$$

This expands to

$$\begin{aligned}
\hat{X}(z) = & \frac{1}{4}[[G_{LP}(z)H_{LP}(z) + G_{BP1}(z)H_{BP1}(z) + G_{BP2}(z)H_{BP2}(z) + G_{HP}(z)H_{HP}(z)]X(z) \\
& + [G_{LP}(z)H_{LP}(-jz) + G_{BP1}(z)H_{BP1}(-jz) + G_{BP2}(z)H_{BP2}(-jz) + G_{HP}(z)H_{HP}(-jz)]X(-jz) \\
& + [G_{LP}(z)H_{LP}(-z) + G_{BP1}(z)H_{BP1}(-z) + G_{BP2}(z)H_{BP2}(-z) + G_{HP}(z)H_{HP}(-z)]X(-z) \\
& + [G_{LP}(z)H_{LP}(jz) + G_{BP1}(z)H_{BP1}(jz) + G_{BP2}(z)H_{BP2}(jz) + G_{HP}(z)H_{HP}(jz)]X(jz)] \quad (2.13)
\end{aligned}$$

The last three terms of (2.13) have to be zero for a PR system. And the inner part of the first term must be equal to 4.

### 2.2.3 Mallats multiresolution analysis

One can find the content of this subsection for example in [Fli94, Vet95, Tch96, Mey92, Mal89, Jaw94, Dau92]. The concept of multiresolution analysis consists of a

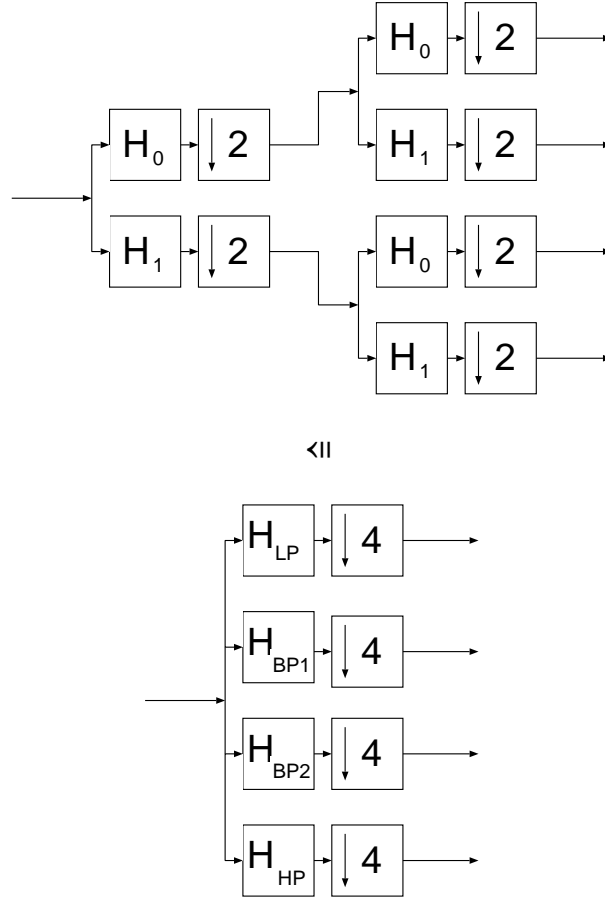


**Figure 2.8:** Two equivalent 4-channel PRFBs (analysis part).  $H_{LP}(z) = H_0(z)H_0(z^2)$ ,  $H_{BP1}(z) = H_0(z)H_1(z^2)$ ,  $H_{BP2}(z) = H_1(z)H_1(z^2)$ ,  $H_{HP}(z) = H_1(z)H_0(z^2)$ .

sequence of nested signal subspaces  $V_i$  of  $L_2 \in (\mathbf{R})$  (Note, that the notation of the nesting order varies in the literature)

$$V_2 \subset V_1 \subset V_0 \subset V_{-1} \subset V_{-2} \dots \quad (2.14)$$

such that

$$\begin{aligned} \overline{\bigcup_{i \in \mathbf{Z}} V_i} &= L_2(\mathbf{R}), \quad \bigcap_{i \in \mathbf{Z}} V_i = \{0\} \\ x(t) \in V_i &\iff x(2^i t) \in V_0 \end{aligned} \quad (2.15)$$

$$x(t) \in V_0 \implies x(t - n) \in V_0, \quad \text{for all } n \in \mathbf{Z} \quad (2.16)$$

There exists a scaling function  $\varphi(t) \in V_0$  which together with its translations

$$\varphi_n = \varphi(t - n), \quad (n \in \mathbf{Z}) \quad (2.17)$$

constitutes an orthonormal basis<sup>8</sup> of the space  $V_0$ , written in the Fourier domain

$$\sum_{k=-\infty}^{\infty} |\Phi(\omega + 2k\pi)|^2 = 1. \quad (2.18)$$

It is shown in [Fli94, Mey92] how to obtain from the continuous signal  $x(t)$  the discrete signal  $x(n)$  or  $\alpha_0(n)$  as well as the other expansion coefficients (wavelet coefficients). And it will be repeated below. Furthermore, in [Dau92] it is shown that:

### Theorem 2.1

Let  $\varphi_{i,n}(t) = 2^{-\frac{i}{2}} \varphi(2^{-i}t - n)$  ( $i, n \in \mathbf{Z}$ ). If  $\varphi(t) \in L_2(\mathbf{R})$  satisfies

$$0 < \alpha \leq \sum_{k \in \mathbf{Z}} |\Phi(\omega + 2\pi k)|^2 \leq \beta < \infty \quad (2.19)$$

and if the subspace  $V_i \in L_2$  is spanned by functions  $\{\varphi_{i,n} : n \in \mathbf{Z}\}$ , i.e.,

$$V_i = \overline{\text{span}\{\varphi_{i,n} : n \in \mathbf{Z}\}}$$

then

$$\bigcap_{i \in \mathbf{Z}} V_i = \{0\}.$$

See [Dau92] for a proof.

### Theorem 2.2

For  $\varphi(t) \in L_2(\mathbf{R})$  satisfying (2.19) and  $V_i$  defined as above, if  $\Phi(\Omega)$  is bounded for all  $\Omega$  and continuous near  $\Omega = 0$ , with  $\Phi(0) \neq 0$ , then

$$\overline{\bigcup_{i \in \mathbf{Z}} V_i} = L_2(\mathbf{R}).$$

See [Dau92] for a proof.

---

<sup>8</sup>Since the vectors  $\varphi(t - n)$  form an orthonormal basis for  $V_0$ ,  $\delta(n) = \int \varphi(t) \varphi^*(t + n) dt$  holds, where  $\delta(n) = \begin{cases} 1 & \text{for } n=0, \\ 0 & \text{elsewhere} \end{cases}$ . Furthermore, the above autocorrelation function with its spectral factor  $\varphi(t)$  can be written (applying Parseval's formula and the shift property of the Fourier transform) as  $\delta(n) = \frac{1}{2\pi} \int |\Phi(\omega)|^2 e^{jn\omega} d\omega$ . Here, as  $n \in \mathbf{Z}$  results in sampling of  $\Phi(\Omega)$ , i.e.,  $\tilde{\Phi}(e^{j\omega}) = \frac{1}{T} \sum_{n=-\infty}^{\infty} \Phi(\frac{\Omega + 2\pi n}{T})$  and assuming  $T = 1$ , it follows that  $\delta(n) = \frac{1}{2\pi} \int_{\omega=0}^{2\pi} e^{jn\omega} \sum_{k=-\infty}^{\infty} |\Phi(\omega + 2\pi k)|^2 d\omega$ . Hence, because  $\frac{1}{2\pi} \int_{\omega=0}^{2\pi} e^{jn\omega} d\omega = \delta(n)$ , the infinite summation must be equal to 1.



### 2.2.4 Scaling function and wavelet relations

As described above a multiresolution is composed of a scaling function  $\varphi(t) \in V_0$  satisfying (2.14-2.18). It follows that the subspace  $V_0$  can be constructed from the functions in (2.17) and from there all the other subspaces  $V_i$  can be generated.

The above presented multiresolution analysis (MA) corresponds to a two-channel PR FB but is not restricted to it. See e.g. Fig. 2.8 for  $M=4$ . The extension to  $M > 4$  is straightforward.

Let  $\psi_{i,n}(t) = 2^{-\frac{i}{2}}\psi(2^{-i}t-n)$  ( $i, n \in \mathbf{Z}$ ) and let in  $V_{i-1}$  the spaces  $V_i = \overline{\text{span}(\{\varphi_{i,n} : n \in \mathbf{Z}\})}$  and  $W_i = \overline{\text{span}(\{\psi_{i,n} : n \in \mathbf{Z}\})}$  form an orthogonal complement, such that  $V_{i-1} = V_i \oplus W_i$ . One can show [Fli94, Vet95, Vai93] that if a normalized regular<sup>9</sup> low-pass filter  $H_0(e^{j\omega})$  satisfies  $|H_0(e^{j0})| = \sqrt{2}$ ,  $\sum_n |h_0(n)|^2 = 1$  and  $|H_0(e^{j\pi})| = 0$ , then the scaling function can be expressed in the frequency domain as

$$\Phi(\omega) = \frac{1}{\sqrt{2}}H_0(e^{\frac{j\omega}{2}})\Phi\left(\frac{\omega}{2}\right), \quad (2.20)$$

in the time domain as

$$\varphi(t) = \sqrt{2} \sum_{n \in \mathbf{Z}} h_0(n) \varphi(2t - n). \quad (2.21)$$

The mother wavelet in the frequency domain can be expressed as

$$\Psi(\omega) = \frac{1}{\sqrt{2}}H_1(e^{\frac{j\omega}{2}})\Phi\left(\frac{\omega}{2}\right),$$

and in the time domain as

$$\psi(t) = \sqrt{2} \sum_{n \in \mathbf{Z}} h_1(n) \psi(2t - n).$$

It is shown, e.g. in [Vet95, Dau92], that one can relate the two filters  $H_0(e^{j\omega})$  and  $H_1(e^{j\omega})$  (in the orthonormal case) as  $H_1(e^{j\omega}) = -e^{-j\omega}H_0(-e^{-j\omega})$ . Hence, in the orthonormal case, a wavelet can also be constructed by<sup>10</sup>

$$\Psi(\omega) = -\frac{1}{\sqrt{2}}e^{-\frac{j\omega}{2}}H_0(-e^{-j\frac{\omega}{2}})\Phi\left(\frac{\omega}{2}\right).$$

The number of wavelets  $C$  is determined by the number of cosets [Vet95], i.e.,

$$C = M - 1,$$

where  $M$  represents the downsampling factor of the associated FB. The integral wavelet transform is defined as [Dau92] (general definition)

$$WT\{x(t), a, b\} = \frac{1}{\sqrt{|a|}} \int_{t=-\infty}^{\infty} x(t) \psi^*\left(\frac{t-b}{a}\right) dt$$

where  $b$  (time shift) and  $a > 0$  (scaling factor) are real valued continuous variables. (See [Dau92] for the conditions on  $\psi$  that the transformation exists). The discrete

<sup>9</sup>For a scaling function  $\Phi(\Omega) = \prod_{i=1}^{\infty} H_0(e^{j2^{-i}\Omega})$  needs to be satisfied. Regularity is used for smoothness of a scaling function and also to count zeros of  $H_0(e^{j\omega})$  at  $\omega = \pi$ . In other words, a regular filter  $H_0(e^{j\omega})$  leads to a scaling function with some degree of smoothness. It is referred to [Vet95, p.256] for more details.

<sup>10</sup>Note, this is only one possible choice out of many.

choice, e.g. see [Fli94, Vet95, Vai93],  $a = 2^{-i}$ ,  $b = 2^{-i}k$ ,  $i, k \in \mathbf{Z}$  and ("\*" denotes complex conjugation)  $\psi(t) = h^*(-t)$  leads to

$$WT\{x(t), i, k\} = 2^{\frac{i}{2}} \int_{t=-\infty}^{\infty} x(t)h(k - 2^i t)dt$$

Considering the two-channel discrete-time case ( $M = 2$ ,  $V_0 = V_1 \oplus W_1$ ), the expansion coefficients (also called wavelet coefficients),  $x_q(n)$ , can be expressed as

$$x_q(n) = \sum_{m=-\infty}^{\infty} x(m)h_q(2n - m),$$

$q = 0, 1$ . For the two-channel discrete-time case, the inverse wavelet transform follows as

$$x(m) = \sum_{q=0}^1 \sum_{n=-\infty}^{\infty} x_q(n)g_q(m - 2n).$$

A wavelet can be interpreted as an analog bandpass filter. The number of vanishing moments, defined in [Dau92], of a wavelet corresponds to the number of zeros at the aliasing frequencies of the associated digital filter. They determine the so-called flatness of the digital filter. High frequency selectivity means that the transition bandwidth is small. For equiripple filters, a low stop-band attenuation means low pass-band ripple. Frequency selectivity as well as flatness of a filter improves as the filter degree increases. For some filter types, frequency selectivity and flatness can be controlled independently. This is true for IIR and FIR filters.

## 2.3 Sampling

In this section three sampling theorems are presented, i.e., sampling of polynomials, Shannon sampling and wavelet sampling. They can be used to link digital signal processing to analog signal processing.

### 2.3.1 Polynomial sampling theorem

For  $n + 1$  arbitrary distinct points  $0 \leq t_0 < t_1 < \dots < t_n \leq 1$  and  $n + 1$  real values  $v_0, v_1, \dots, v_n$ , there exists a unique polynomial  $p_n(t)$  of degree  $n$ , which satisfies [Che95]

$$p_n(t_k) = v_k \quad k = 0, 1, \dots, n.$$

This polynomial is given by

$$p_n(t) = \sum_{k=0}^n v_k L_k(t)$$

with the Lagrange basis polynomials

$$L_k(t) = \frac{(t - t_0) \dots (t - t_{k-1})(t - t_{k+1}) \dots (t - t_n)}{(t_k - t_0) \dots (t_k - t_{k-1})(t_k - t_{k+1}) \dots (t_k - t_n)} \quad k = 0, \dots, n.$$

If not only functional values, but also derivative values, are available and required to be interpolated by the polynomial

$$p_n^{i_k}(t_k) = v_{k,i_k}, \quad i_k = 0, \dots, m_k \quad k = 0, 1, \dots, n$$

then, we have a Hermite interpolation problem [Che95]. An algebraic polynomial of degree  $d = n + \sum_{k=0}^n m_k$  always exists as a Hermite interpolant. An explicit closed-form formula for the Hermite interpolant also can be constructed. For example, if only the functional values  $\{v_k\}_{k=0}^n$  and the first derivative values  $\{w_k\}_{k=0}^n$  are given and required to be interpolated, then the Hermite interpolant is given by

$$p_{2n}(t) = \sum_{k=0}^n \{v_k A_k(t) + w_k B_k(t)\}$$

where, with the notation  $L_k'(t_k) = (d/dt)L_k(t)|_{t=t_k}$ ,

$$A_k(t) = [1 - 2(t - t_k)L_k'(t_k)]L_k^2(t) \text{ and } B_k(t) = (t - t_k)L_k^2(t).$$

However, if the derivative values are not consecutively given, we have a Hermite-Birkhoff interpolation problem, which is not always uniquely solvable [Lor83].

### 2.3.2 Shannon sampling theorem

A bandlimited signal  $x(t)$  having no spectral components at and above  $2\pi f_m = \Omega_m$ , can be uniquely determined by values sampled at uniform intervals of  $T_s = 1/f_s$  seconds, where [Skl88, Jer77, Fli91]

$$T_s \leq \frac{1}{2f_m}.$$

The sampling rate  $f_s = 2f_m$  is also called the Nyquist (or critical sampling) rate. The Nyquist rate is a sufficient condition to allow an analog signal to be reconstructed uniquely from a set of uniformly spaced discrete-time samples.

In other words, if the Fourier transform of a signal  $x(t)$  is defined as

$$X(\Omega) = \int_{t=-\infty}^{\infty} x(t)e^{-j\Omega t}dt,$$

and

$$X(\Omega) = \begin{cases} X(\Omega) & \text{for } |\Omega| < \Omega_m, \\ 0 & \text{elsewhere} \end{cases}$$

then [Skl88, Jer77, Fli91], with  $\varphi(t) = \text{sinc}(t)$ ,

$$x(t) = \sum_{n=-\infty}^{\infty} x(nT_s)\varphi\left(\frac{t - nT_s}{T_s}\right). \quad (2.22)$$

For notational convenience, the normalized expression  $x(n)$  is often used instead of  $x(nT_s)$ .

Let the inverse Fourier transform be defined as

$$x(t) = \frac{1}{2\pi} \int_{t=-\infty}^{\infty} X(\Omega)e^{j\Omega t}d\Omega,$$

then, due to the symmetry of the Fourier transform pairs, the Shannon sampling theorem is also valid for time-limited functions, i.e. for the Fourier transform  $X(\omega)$  of a function  $x(t)$ , which is zero for  $|t| \geq T_m/2$  [Jer77, Fli91], it holds that (using  $\Phi(\Omega) = \text{sinc}(\Omega/\pi)$ )

$$X(\Omega) = \sum_{n=-\infty}^{\infty} X(n\Omega_s) \Phi\left(\frac{T_s}{2\pi}[\Omega - n\Omega_s]\right).$$

Sampling with the value of the function and its derivatives increases the sampling spacing required, or in other words, it allows the reconstruction of the bandlimited signal with a sampling rate less than the Nyquist rate [Jer77].

### 2.3.3 Wavelet sampling theorem

Using orthonormal wavelet bases, introduced above, a signal  $x(t) \in V_i$  can be represented as [Fli94, Mey92]

$$x(t) = \sum_{n=-\infty}^{\infty} \alpha_0(n) \varphi_0(t - n) \in V_0, \quad (2.23)$$

with the expansion coefficients (uniformly spaced discrete-time samples)

$$\alpha_0(n) = \int_{t=-\infty}^{\infty} x(t) \varphi_0^*(t - n) dt. \quad (2.24)$$

Equation (2.23) looks similar to equation (2.22). Unlike the Shannon case, for wavelet sampling,  $\varphi(t)$  or  $\Phi(\Omega)$  do neither have to be time limited nor band limited, respectively. If  $\varphi(t)$  ( $\Phi(\Omega)$ ) is time limited (band limited), then  $\varphi(t)$  ( $\Phi(\Omega)$ ) is of compact support.

A closed form analytic formula for

$$\Phi(\Omega) = \prod_{i=1}^{\infty} H_0(e^{j2^{-i}\omega})$$

exists for example for the Haar scaling function, splines, Shannon scaling function, raised cosine scaling functions and for Meyer scaling functions. However, a ‘graphical’ scaling function exists, for example, for Daubechies scaling functions, Butterworth scaling functions and for Chebyshev scaling functions. Figure 2.9 illustrates the wavelet signal processing arrangement (sampling and reconstruction).

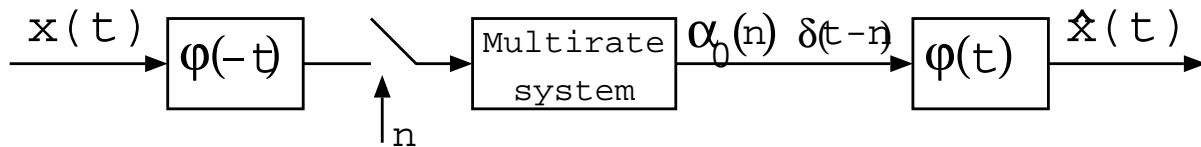


**Figure 2.9:** Wavelet signal processing arrangement [Fli94].

### 2.3.4 Sampling in multiresolution subspaces

The wavelet transformation (WT) is defined for square integrable signals ( $L_2(\mathbf{R})$ ). Furthermore, wavelets can be used to process some signals in  $L_1([0,1])$  [Mey92, Dau92]. If these signals are processed with realizable electrical filters (analog and digital filters), then one can only realize scaling functions that have infinite support in time as well as in frequency domain (causality). Hence, in the realizable ideal case digital IIR filters, with a finite number of filter coefficients, are of interest and causal, exactly linear phase filters are then impossible. Noncausal digital IIR linear phase filters are possible to be implemented, see [Vet95]. Linear phase wavelets are possible with IIR filters, see e.g. [Ans96]. Examples of wavelets based on IIR-filters are the Butterworth wavelets [Her93] or Chebyshev wavelets [Got98]. However, one can approximate linear phase with causal digital IIR filters. The wave digital filter (WDF) method is especially suited for designing digital filters since the well known benefits (such as low-sensitivity, low roundoff noise and all aspects of stability under finite word length conditions) can be obtained in one as in multiple dimensions [Fet86, Gas85]. And there is no need for a spectral factorization method<sup>11</sup> when designing the digital filters, neither in one nor in multiple dimensions [Fet86, Got97].

The validity of the wavelet transform requires, that a discrete signal is obtained from the related continuous signal  $x(t)$  as in (2.24). Nevertheless, in reality, this ideal sampling process is approximated; independent of whether  $\varphi(t)$  has compact support or not. The question of how good the discrete-to-continuous signal representation is approximated depends on the realization of the scaling function  $\varphi(t)$  in (2.24).

In conventional signal processing, there are many different continuous signals  $x(t)$  having the same discrete sample values, unless the signal  $x(t)$  is bandlimited before it undergoes the sampling process (Shannons sampling theorem).

For the wavelet transform, there exists the wavelet sampling theorem (see also [Wal92, Xia93, Djo94, Mey92]) where  $\varphi(t)$  does not need to have compact support and the  $\alpha_0(n)$ 's are obtained from  $x(t)$  with a normalized maximal sampling spacing of  $T_s = 1$  [Fli94, Mey92]. Alternatively, Shannons sampling theorem can be applied to cases, where  $\varphi(t)$  has compact support either in frequency domain or in time domain, see [Jer77]. In particular, the minimum sampling rate  $f_s = 1/T_s$  for the sinc case follows as  $\omega_m = \pi/2 \Rightarrow f_m = 1/4 \Rightarrow T_s \leq \frac{1}{2f_m} = 2$  and for the Meyer case  $\omega_m = 2\pi/3 \Rightarrow f_m = 1/3 \Rightarrow T_s = 3/2$ , where the bandlimited signal has no spectral components at and above  $\omega_m$ . Comparing both sampling theorems on the sinc-wavelet, Shannon's sampling theorem allows much less samples to uniquely represent the associated continuous time signal, compared to the wavelet sampling theorem. This can be particularly seen in the case of partial differential equations (PDE), where a bandlimited signal  $x(t)$  can be uniquely recovered from samples of

---

<sup>11</sup>Very often a digital half band filter (every second filter coefficient is 0) is used as a prototype filter (which can be interpreted as an autocorrelation of two filters) from which the filters (spectral factors) that are used in a PRFB are obtained. This is done with the help of a spectral factorization method. Such a method is only known in one dimension.

$x(t)$  and its derivative at half the sampling rate [Jer77, Djo94].

Increasing the order of e.g. Daubechies filters, splines, Butterworth filters or Chebyshev filters, results in higher regularity which is desired in many applications when using the WT. By doing so, a wanted side effect occurs, i.e., the associated scaling function then has approximately compact support in frequency domain. And hence, Shannon's sampling theorem can be applied. As an example, in the Butterworth case a filter order of 9 is used in [Gas85, Got97], where in the one dimensional case 4 coefficients only are necessary. Note, B-splines can be viewed as Butterworth wavelets [Her93]. Thus, according to conventional digital signal processing, and because of economical reasons, one may classify scaling functions into two groups; some examples are listed in Table 2.1. This classification is meant to stress the fact that the Shannon sampling theorem provides a more economic discrete representation of an associated continuous signal than the wavelet sampling theorem. Of course all the scaling functions in Table 2.1 are valid ones when using the wavelet sampling theorem.

In practice, one designs an “approximating” scaling function such that the aliasing error (well known from conventional signal processing, compare [Skl88, Jer77]), when compared to a “valid” scaling function, is minimized (discretization problem). Alternatively, one can use

$$h_0(n) = \sqrt{2} \int_{t=-\infty}^{\infty} \varphi^*(2t - n) \varphi(t) dt \quad (2.25)$$

$$= \frac{1}{2\sqrt{2}\pi} \int_{\omega=-\infty}^{\infty} e^{-j\omega n} \Phi^*\left(\frac{\omega}{2}\right) \Phi(\omega) d\omega \quad (2.26)$$

in order to approximate a “valid” scaling function directly. (Equation (2.26) is obtained from (2.25) by using the shift property, scaling property, modulation theorem and Parsevals formula.) And since a valid scaling function has compact support in the frequency domain, the integral in (2.26) becomes zero outside  $\omega = \pm \frac{4\pi}{3}$ . However,  $h_{a0}(n)$  will in general not form a perfect reconstruction filter bank, since in practice, one uses only a finite set out of  $\{h_{a0}(n)\}$ , which contains an infinite number of non-zero filter coefficients.

"Valid" scaling functions (for Shannon sampling)		"Approximating" scaling functions (for Shannon sampling)
-----related to a digital filter having-----		
infinite number of filter coefficients		finite number of filter coefficients
sinc scaling function (IIR-filter)  Meyer scaling functions (IIR-filter)  raised-cosine scaling functions (IIR-filter)		Daubechies scaling functions (FIR-filter)  Haar scaling function (FIR-filter)  Butterworth scaling functions (IIR-filter)  Chebyshev scaling functions (IIR-filter)

**Table 2.1** Scaling functions.

# Chapter 3

## Wave Digital Filter

Among different digital filters, wave digital filters are best suited for multirate systems that are used to compute a wavelet transform. Their low circuit complexity and robustness outperform other known digital filters. However, the theory of wave digital filters is very complex. In what follows, only main parts of the wave digital filter theory is presented. It is referred to [Fet86] for more details. Another part of this chapter shows how one can implement noncausal recursive filters that process infinite length signals.

### 3.1 Wave Digital Filter

Wave digital filters are derived from analog (reference) filters. This derivation is shown in the first subsection. How perfect reconstruction can be achieved is also shown for the analog case. A bilinear transform connects a reference filter to a wave digital filter. Finally, two main wave digital filter structures are presented, ladder structure and lattice structure. Exemplarily, perfect reconstruction relations are shown for the latter one.

#### 3.1.1 Analog relationships

Figure 3.1 shows a doubly terminated analog filter (reference filter). Assuming  $R_1 = R_2 = R$ , the wave quantities  $A_1$ ,  $A_2$ ,  $B_1$  and  $B_2$  can be defined as ( $i = 1, 2$ ):

$$\begin{aligned} A_i &= U_i + RI_i \\ B_i &= U_i - RI_i \quad (\text{voltage wave}) \end{aligned} \tag{3.1}$$

or

$$\begin{aligned} \overline{A}_i &= \frac{U_i + RI_i}{2\sqrt{R}} \\ \overline{B}_i &= \frac{U_i - RI_i}{\sqrt{R}} \quad (\text{power wave}). \end{aligned}$$



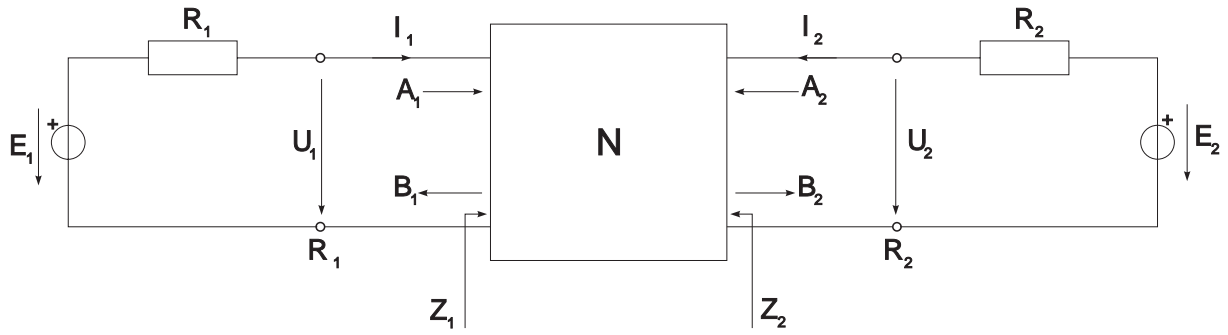


**Figure 3.1:** Doubly terminated analog filter. (Two port.)

In what follows, the first case is used. The scattering matrix  $\mathbf{S}$  is defined as

$$\begin{pmatrix} B_1 \\ B_2 \end{pmatrix} = \mathbf{S} \begin{pmatrix} A_1 \\ A_2 \end{pmatrix}$$

$$\mathbf{S} = \begin{pmatrix} S_{11} & S_{12} \\ S_{21} & S_{22} \end{pmatrix}$$

with

$$S_{11} = \frac{Z_1 - R}{Z_1 + R}$$

$$S_{22} = \frac{Z_2 - R}{Z_2 + R}$$

$$S_{21} = \frac{2U_2}{E_1} \Big|_{E_2=0}$$

$$S_{12} = \frac{2U_1}{E_2} \Big|_{E_1=0}.$$

The elements of  $\mathbf{S}$  can be interpreted as filters. See e.g. [Unb93, p.126] for the definition of  $Z_1$  and  $Z_2$ .

A PRFB can be build when the analysis and the synthesis filters form a paraunitary system, i.e. [Fet85, Lei94], written in matrix form<sup>1</sup>  $\mathbf{S}_* \mathbf{S} = \mathbf{E}$ , where  $\mathbf{E}$  denotes the identity matrix. If in addition each filter of  $\mathbf{S}$  is stable, the scattering matrix  $\mathbf{S}$  is said to be lossless. In the case of IIR WDFs, the filters of  $\mathbf{S}_*$  are unstable if the filters of  $\mathbf{S}$  are stable [Fet85, Lei94]. Nevertheless, it will be shown below how to implement the unstable filters of  $\mathbf{S}_*$  in a stable way.

It follows from  $\mathbf{S}_* \mathbf{S} = \mathbf{E}$ , that (possible forms of the Feldtkeller equation [Bel68])

$$|S_{11}|^2 + |S_{21}|^2 = 1$$

$$|S_{12}|^2 + |S_{22}|^2 = 1$$

---

<sup>1</sup> $h(n) \rightarrow h(-n) \Rightarrow H(\omega) \rightarrow H_*(\omega)$ , where for a real rational function  $F = F(\omega)$  the paraconjugate  $F_* = F_*(\omega)$  is defined by  $F_*(\omega) = F(-\omega)$ . For a matrix, paraconjugation implies not only paraconjugation of each entry, but also transposition. Note,  $H_* = H^{*T}$  where  $T$  means transpose and  $H_*(z) = H^*(z^{-1})$ . Note, as defined before  $H^*$  is the complex conjugate of  $H$ .

$$S_{11}S_{12}^* + S_{21}S_{22}^* = 0.$$

The characteristic function,  $K(s)$ , is defined as

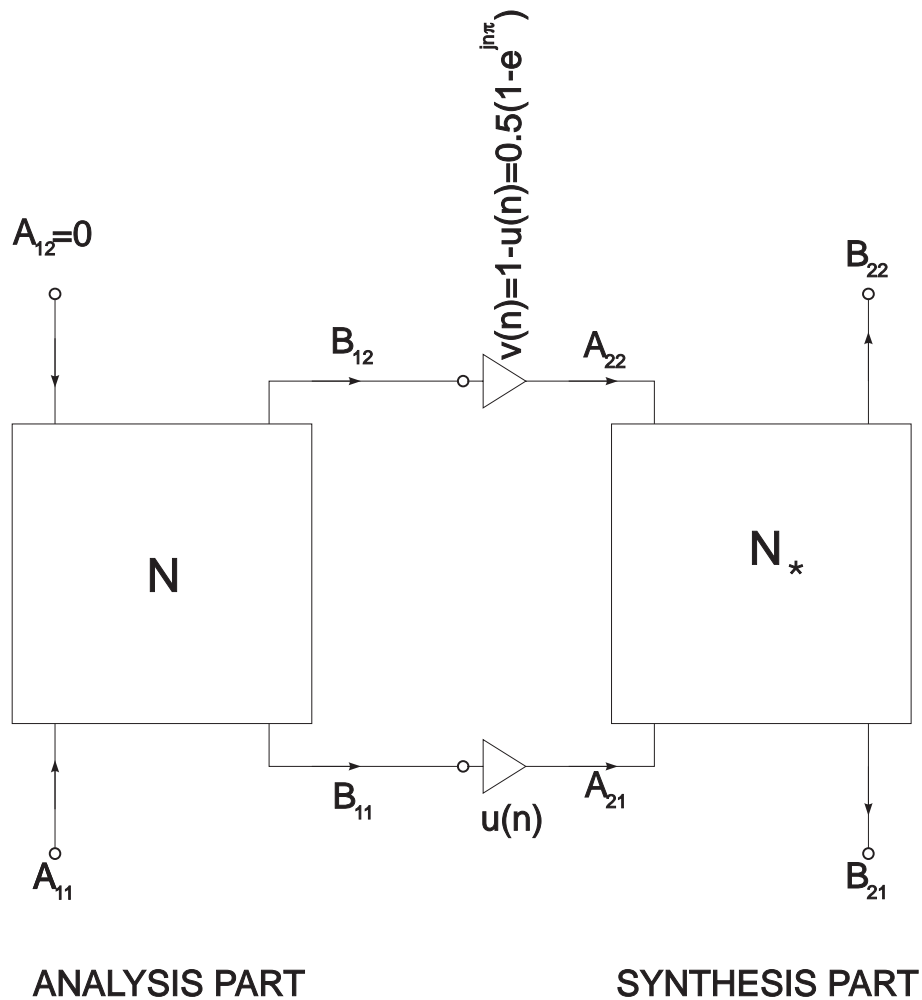


**Figure 3.2:** WDF arrangement for a 2-channel PRFB. The wave quantities  $A_1$ ,  $A_2$ ,  $B_1$ , and  $B_2$  are defined in (3.1)

$$K(s) = \frac{S_{11}(s)}{S_{21}(s)}.$$

For symmetric filters [Bel68]

$$K_*(s) = -K(s).$$

For antimetric filters [Bel68]

$$K_*(s) = K(s).$$

The characteristic function for symmetric/antimetric filters is bireciprocal (selfreciprocal) [Fet86], i.e.,

$$K\left(\frac{1}{s}\right) = 1/K(s).$$

WDFs in a 2-channel system form a PRFB if they fulfill [Lei94]

$$|H_0(s)|^2 + |H_1(s)|^2 = 1$$

and

$$|H_0(s)| = |H_1(\frac{1}{s})|.$$

### 3.1.2 Digital relationships

Let

$$s = j\Omega = \tanh\left(\frac{pT}{2}\right) = \frac{z-1}{z+1} \quad z = e^{pT} \quad (3.2)$$

be a bilinear transform of the  $z$ -variable, where  $p = j\omega$  is the complex frequency of a digital filter,  $F = \frac{1}{T}$  the sampling frequency and

$$\Omega = \tan\left(\frac{\omega T}{2}\right).$$

Assume then an arrangement depicted in Fig. 3.2. PR can be shown for ladder WDFs (see Fig. 3.6) as well as for lattice WDFs (see Fig. 3.3). However, it will be shown using a lattice WDF arrangement.

### 3.1.3 Lattice Wave Digital Filter

Lattice WDF are related to an analog filter, illustrated in Fig. 3.3. Using

$$2\mathbf{S} = \begin{pmatrix} S_a + S_b & S_b - S_a \\ S_b - S_a & S_a + S_b \end{pmatrix}$$

with

$$S_i = \frac{Z_i - R}{Z_i + R}, \quad i = a, b$$

then Fig. 3.2 can be redrawn as illustrated in Fig. 3.4. Real WDF coefficients are obtained if  $S_a$  and  $S_b$  are composed of second order all-pass sections. In addition, either  $S_a$  or  $S_b$  needs to be cascaded with a first order all-pass section. Thus the resulting filter degree is odd. In what follows, it is assumed that  $S_a$  contains one first order all-pass section. With the knowledge that the general transfer function of stable all-pass filters can be expressed as (for  $i \in \mathbf{Z}$ ,  $\text{Re}\{s_{\infty i}\} < 0$  and  $s_{0i} = -s_{\infty i}^*$ )

$$H_{all-pass}(s) = c_n \frac{\prod_{i=1}^n (s + s_{\infty i})}{\prod_{i=1}^n (s - s_{\infty i})} = (-1)^n c_n \frac{N(-s)}{N(s)},$$

and with<sup>2</sup>

$$S_a(s) = \frac{g_1(-s)}{g_1(s)}$$

$$S_b(s) = \frac{g_2(-s)}{g_2(s)}$$

---

<sup>2</sup>The minus sign of  $S_a(s)$  is already incorporated in the structure.

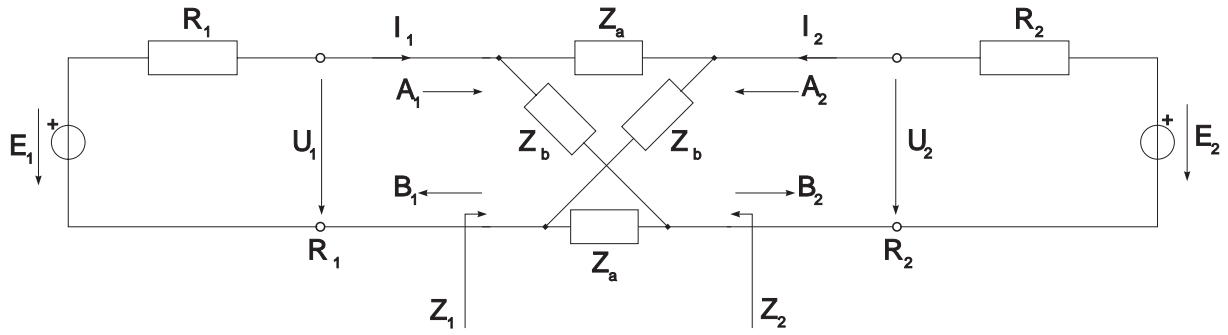


**Figure 3.3:** Lattice reference filter.  $Z_a$  and  $Z_b$  are LC-Networks.

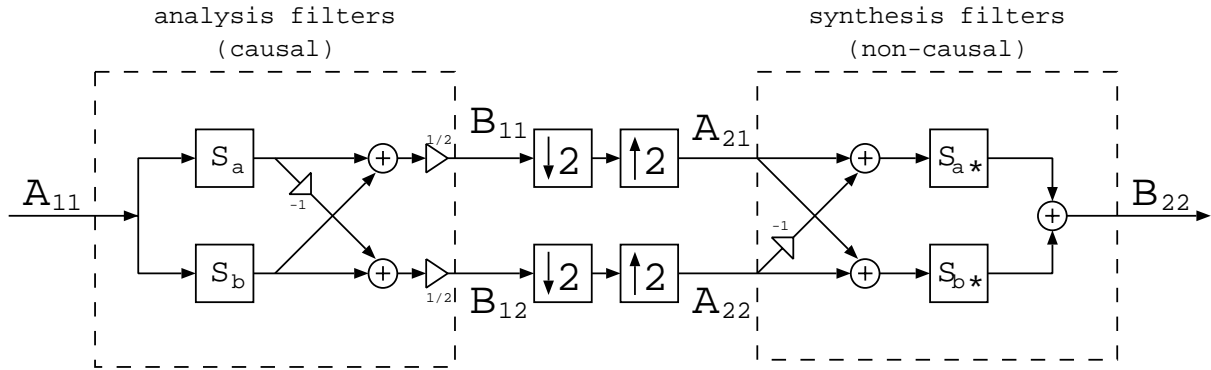


**Figure 3.4:** Lattice WDF arrangement for a 2-channel PRFB. (s-domain).

where  $g_1(s)$  and  $g_2(s)$  are Hurwitz polynomials (all the zeros of the polynomials are on the left half s-plane) [Bel68] it can be shown that:

$$S_{11}(s) = \frac{h(s)}{g(s)} = \frac{g_1(s)g_2(-s) + g_1(-s)g_2(s)}{2g_1(s)g_2(s)} \quad \text{Reflectance}$$

$$S_{21}(s) = \frac{f(s)}{g(s)} = \frac{g_1(s)g_2(-s) - g_1(-s)g_2(s)}{2g_1(s)g_2(s)} \quad \text{Transmittance.}$$

Thus, because of losslessness,

$$\mathbf{S} = \frac{1}{g(s)} \begin{pmatrix} h(s) & \sigma f_*(s) \\ f(s) & -\sigma h_*(s) \end{pmatrix}$$

with

$$g(s)g_*(s) = h(s)h_*(s) + f(s)f_*(s) \quad (\text{Feldtkeller equation})$$

where  $\sigma$  is a unimodular constant,  $g(s)$  is again a Hurwitz polynomial and here  $\sigma f_*(s) = f(s)$ ,  $\sigma h_*(s) = h(s)$ . Using (3.2) and assuming a bi-recursive characteristic function,

$$S_a(s)|_{s=\frac{z-1}{z+1}} = z^{-1}E_1(z^2)$$

and

$$S_b(s)|_{s=\frac{z-1}{z+1}} = E_0(z^2),$$

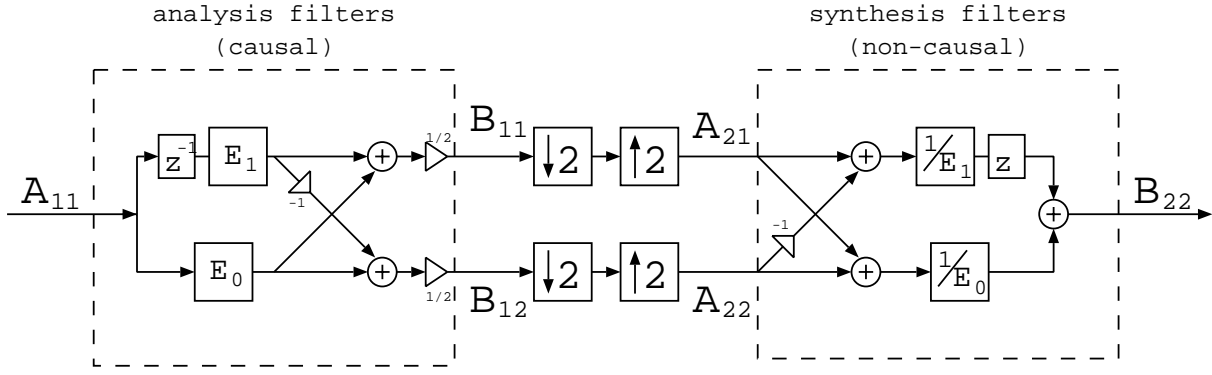


**Figure 3.5:** Bireciprocal lattice WDF arrangement for a 2-channel PRFB. (z-domain).

where  $E_0(z^2)$  and  $E_1(z^2)$  are the polyphase components of a 2-channel FB [Lei94, Nos83].

### 3.1.4 IIR Wave Digital Filter and Perfect Reconstruction

For the bireciprocal case, Fig. 3.4 can be redrawn as shown in Fig. 3.5. It follows that

$$H_0(z) = \frac{1}{2}(E_0(z^2) + z^{-1}E_1(z^2)) \quad (3.3)$$

$$H_1(z) = H_0(-z) = \frac{1}{2}(E_0(z^2) - z^{-1}E_1(z^2)) \quad (3.4)$$

$$G_0(z) = 2H_0(z^{-1}) = E_0(z^{-2}) + z^1E_1(z^{-2}) = \frac{1}{E_0(z^2)} + \frac{1}{z^{-1}E_1(z^2)} \quad (3.5)$$

$$G_1(z) = 2H_1(z^{-1}) = E_0(z^{-2}) - z^1E_1(z^{-2}) = \frac{1}{E_0(z^2)} - \frac{1}{z^{-1}E_1(z^2)} \quad (3.6)$$

Note, the factor  $\frac{1}{2}$  in (3.3) and (3.4) causes

$$H_0(e^{j\omega})|_{\omega=0} = H_1(e^{j\omega})|_{\omega=\pi} = 1.$$

PR with sampling rate changes in a 2-channel FB may be expressed as

$$\begin{aligned} \hat{X}(z) &= \frac{1}{2}[G_0(z)H_0(z) + G_1(z)H_1(z)]X(z) \\ &\quad + \frac{1}{2}[G_0(z)H_0(-z) + G_1(z)H_1(-z)]X(-z) \end{aligned} \quad (3.7)$$

Substituting (3.3 -3.6) into the first term of (3.7), results in

$$\begin{aligned} &\frac{1}{2}\left[\left(\frac{1}{E_0(z^2)} + \frac{1}{z^{-1}E_1(z^2)}\right)\frac{1}{2}(E_0(z^2) + z^{-1}E_1(z^2))\right. \\ &\quad \left.+ \left(\frac{1}{E_0(z^2)} - \frac{1}{z^{-1}E_1(z^2)}\right)\frac{1}{2}(E_0(z^2) - z^{-1}E_1(z^2))\right]X(z) = \\ &\quad \frac{1}{2} \frac{2(E_0(z^2)z^{-1}E_1(z^2))}{E_0(z^2)z^{-1}E_1(z^2)}X(z) = X(z) \end{aligned} \quad (3.8)$$

and for the second term of (3.7) follows after using (3.3 - 3.6)

$$\begin{aligned}
 & \frac{1}{2} \left[ \left( \frac{1}{E_0(z^2)} + \frac{1}{z^{-1}E_1(z^2)} \right) \frac{1}{2} (E_0(z^2) - z^{-1}E_1(z^2)) \right. \\
 & \left. + \left( \frac{1}{E_0(z^2)} - \frac{1}{z^{-1}E_1(z^2)} \right) \frac{1}{2} (E_0(z^2) + z^{-1}E_1(z^2)) \right] X(-z) = \\
 & \frac{1}{2} \left[ \frac{(E_0(z^2)z^{-1}E_1(z^2)) \frac{1}{2} (E_0(z^2) - z^{-1}E_1(z^2))}{E_0(z^2)z^{-1}E_1(z^2)} \right. \\
 & \left. - \frac{(E_0(z^2)z^{-1}E_1(z^2)) \frac{1}{2} (E_0(z^2) + z^{-1}E_1(z^2))}{E_0(z^2)z^{-1}E_1(z^2)} \right] X(-z) = 0
 \end{aligned} \tag{3.9}$$

### 3.1.5 Ladder Wave Digital Filter

Ill-conditioning is equivalent to high sensitivity. Lattice WDFs have low passband sensitivity. Ladder WDFs have low pass- and stop-band sensitivity. One possible structure of a Ladder-reference filter is depicted in Fig.3.6.

Compared to lattice WDFs, ladder WDFs need a smaller word-length to meet the

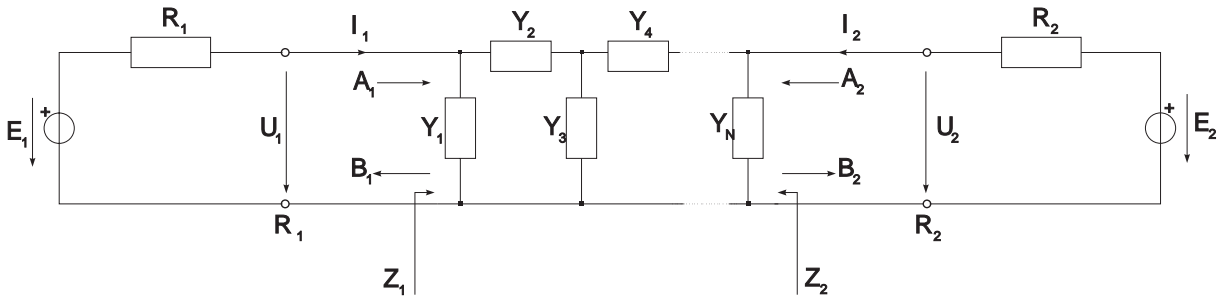


**Figure 3.6:** Example of a LC-ladder reference filter.  $Y_i$ ,  $i = 1, \dots, N$ , are LC-Networks.

same accuracy specifications. However, in 1-dimensional 2-channel systems, bi-recursive lattice WDFs need much less filter coefficients than ladder WDFs. In some cases, Bartlett's Bisection Theorem can be used to derive an equivalent LC-lattice WDF from a LC ladder WDF [Law90]. In 2-dimensional 4-channel hexagonally sampled systems, ladder WDFs need much less filter coefficients than lattice WDFs. Using so-called unit elements in a ladder WDF structure, the number of filter coefficients can be reduced compared to a LC realization [Owe92, Thi77].

The next step, once a reference filter has been found, is to find a WDF. In general there are many possibilities to choose a WDF-structure. This is due to the fact that not only the analog elements need to be transformed into digital elements, but also the so-called adaptors must be used in the digital circuit. The book [Law90] shows a different approach. The components can be performed directly without the use of adaptors. The main point of the two methods is to fulfill a digital representation

of Kirchhoff's rule at a junction. Furthermore, the latter method is less flexible and hence the choice of a desired WDF-structure may not be possible.

### 3.2 Implementation of non-causal filters (for infinite length signals)

It is shown in [Lei94, Mit92] how to implement non-causal filters with which one can process infinite length signals. This will be summarized next for bireciprocal lattice WDF. A detailed description for all WDF can be found in [Lei94]. A stable realiza-

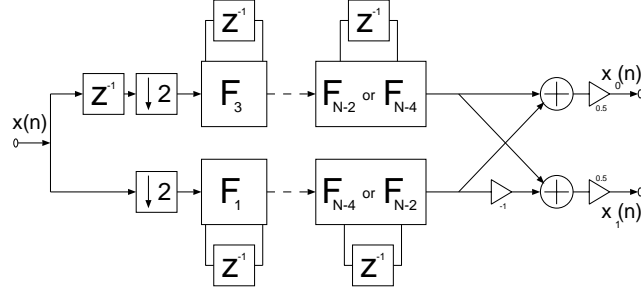


**Figure 3.7:** Block diagram of the analysis filters of a two-channel LWDF FB (bireciprocal case) for  $N = 5, 9, 13, \dots$  or  $N = 7, 11, 15, \dots$  in polyphase representation.

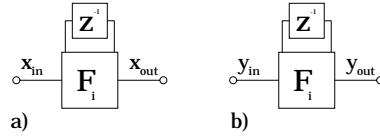


**Figure 3.8:** All-pass section  $F_i$ : a) analysis, b) synthesis side.

tion of the filters of  $\mathbf{S}_*$  is achieved in three steps. Step 1 requires to properly initialize the synthesis filters before filtering takes place.

Considering the analysis filters of a two-channel LWDF bank, polyphase representation in Fig. 3.7, the all-pass sections  $F_i(z)$  have the special form (bireciprocal case)

$$F_i(z) = \frac{z^{-1} - \alpha_i}{1 - \alpha_i z^{-1}}.$$

Since the same all-pass filters are used in the analysis and synthesis FB, a state-variable representation of each single all-pass section, compare Fig. 3.8, is useful. For the analysis side:  $\mathbf{T}_a(n+1) = \mathbf{a}\mathbf{T}_a(n) + \mathbf{b}x_{in}(n)$ ,  $x_{out}(n) = \mathbf{c}\mathbf{T}_a(n) + \mathbf{d}x_{in}(n)$ , and in case for the synthesis side,  $\mathbf{T}_a, x_{in}$  and  $x_{out}$  are replaced with  $\mathbf{T}_s, y_{in}$  and  $y_{out}$ , respectively.  $\mathbf{T}_a, \mathbf{T}_s$  denote the state-variable vectors of the analysis and synthesis side, which are related as  $\mathbf{T}_s(0) = \mathbf{G}\mathbf{T}_a(P)$  by the matrix

$$\mathbf{G} = \begin{bmatrix} 0 & 1 \\ 1 & 0 \end{bmatrix}, \quad (3.10)$$

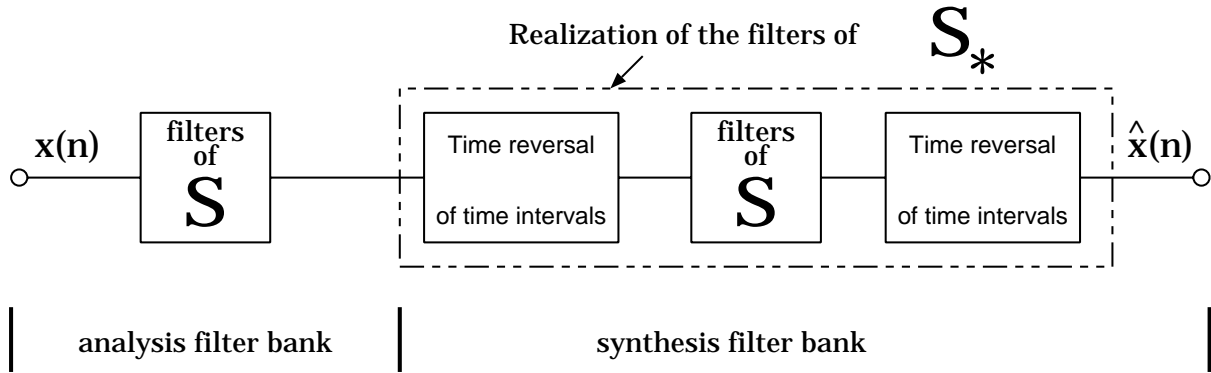


**Figure 3.9:** System for perfect reconstruction, FIR or IIR, for infinite length signals.

where  $y_{out}(n) = x_{in}(P - n - 1)$  for  $n = 0, 1, \dots, P - 1$ ,  $P$  the number of samples in the time interval. Step 2 is indicated in Fig. 3.9, where an infinite length signal is divided in time intervals which are then fed into the filters of the synthesis filter bank in a time reversed manner. Step 3, also shown in Fig. 3.9, requires the time intervals to be time reversed after the filtering process and to be joined together to form the output signal  $\hat{x}(n)$ . Note, the time reversal of the time intervals is done in blocks. The block length is a multiple of the sampling interval  $T$ , and time reversal is simply implemented by a reversal of the relevant pointers to the samples in the blocks.



# Chapter 4

## Wavelets

Two properties, i.e., convolution and shift are presented in this chapter. And for the shift property a new, computational efficient circuit realization is given. Furthermore, two new wavelet bases are presented in this chapter, i.e., the raised cosine wavelets and the Chebyshev wavelets. Known wavelet bases are also presented in order to be able to see advantages of the new introduced bases.

### 4.1 Some Properties

Two main properties, convolution and shift, will be discussed next for the wavelet transform. The considered shift operation on the expansion coefficients must not be an integer, i.e., it can be shifted by an amount of  $\tau \in \mathbf{R}$ .

#### 4.1.1 Convolution

It is shown in [Vai93] how to convolve two sequences  $x(n)$  and  $g(n)$  by means of FBs, compare Fig. 4.1. This can be done by directly convolving the expansion coefficients of a paraunitary FB and adding the results. The advantage using a FB for convolution of two sequences is that one can quantize and obtain a coding gain over direct convolution (increased accuracy for a given bit rate). Thus

$$x(n) * g^*(-n) \iff X(z)G_*(z) = \sum_{k=0}^{M-1} X_k(z^M) \sum_{m=0}^{M-1} z^{-m} G_{*m}^{(k)}(z^M)$$

where  $G_m^{(k)}(z)$  is the subband signal obtained by replacing  $g(n)$  with  $g(n - m)$ .

#### 4.1.2 Fractional Shift

In [Bey92] the nonstandard form of the shift operator for the wavelet decomposition of all circulant shifts of a vector is reported, and [Can94] shows an algorithm to approximate the shift operator for real shifts in the finest scale, where in both cases the

shift operator is related to the analysis filters and is a recursive algorithm, respec-

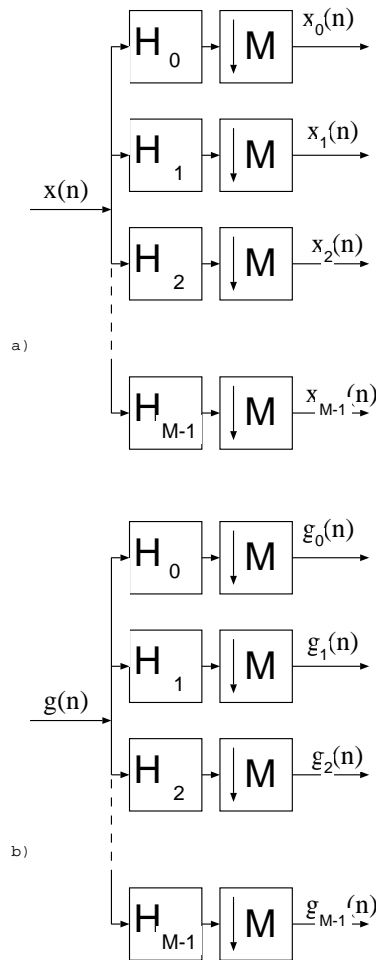


**Figure 4.1:** A maximally decimated FB (analysis part): a) with input  $x(n)$  and b) with input  $g(n)$ .

tively. However, the shift operation presented below is neither related to the analysis filters nor to the synthesis filters of the filter bank. In particular the shift operation in this realization is done directly on the expansion coefficients.

A practical tool to perform a translation  $\tau$ ,  $\tau \in \mathbf{R}$ , more suitable for filter bank implementations of the wavelet transform is provided below. The shift problem, here shown for the two-channel case, may be described as follows: For filter banks with perfect reconstruction one can write by using the z-transform representation with the output signal  $\hat{X}(z)$  and the input signal  $X(z)$  [Fli94]

$$\begin{aligned} \hat{X}(z) &= \frac{1}{2}[G_0(z)H_0(z) + G_1(z)H_1(z)]X(z) + \frac{1}{2}[G_0(z)H_0(-z) + G_1(z)H_1(-z)]X(-z) \\ &= F_0(z)X(z) + F_1(z)X(-z) \end{aligned} \quad (4.1)$$

where for FIR filters<sup>1</sup>  $F_0(z) = z^{-k}$  (for IIR filters  $F_0(z) = 1$ ) and  $F_1(z) = 0$ .

This can be written in matrix form as

$$\hat{X}(z) = \frac{1}{2} \begin{bmatrix} G_0(z) & G_1(z) \end{bmatrix} \begin{bmatrix} H_0(z) & H_0(-z) \\ H_1(z) & H_1(-z) \end{bmatrix} \begin{bmatrix} X(z) \\ X(-z) \end{bmatrix}.$$

The intermediate process where the input signal  $X(z)$  is split up in two channels,

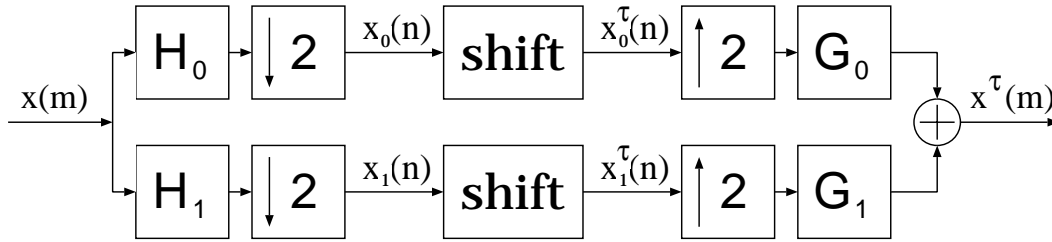


**Figure 4.2:** Shift Operation in orthonormal compactly supported wavelet bases, M=2.

filtered by the analysis filters  $H_0(z)$  and  $H_1(z)$  and down sampled by the factor M = 2, follows for the subsignals  $X_0(z)$  and  $X_1(z)$  in matrix form as

$$\begin{bmatrix} X_0(z) \\ X_1(z) \end{bmatrix} = \frac{1}{2} \begin{bmatrix} H_0(z^{\frac{1}{2}}) & H_0(-z^{\frac{1}{2}}) \\ H_1(z^{\frac{1}{2}}) & H_1(-z^{\frac{1}{2}}) \end{bmatrix} \begin{bmatrix} X(z^{\frac{1}{2}}) \\ X(-z^{\frac{1}{2}}) \end{bmatrix}.$$

The output signal  $\hat{X}(z)$  of the synthesis filters results from this intermediate process after upsampling by the factor L = 2 and filtering with  $G_0(z)$  and  $G_1(z)$  in

$$\hat{X}(z) = \begin{bmatrix} G_0(z) & G_1(z) \end{bmatrix} \begin{bmatrix} X_0(z^2) \\ X_1(z^2) \end{bmatrix}$$

Having the expansion coefficients (subsignals)  $x_0(n)$  and  $x_1(n)$ , the task is in finding the new coefficients (shifted subsignals)  $x_0^\tau(n)$  and  $x_1^\tau(n)$  such, that  $x^\tau(m)$  is a shifted version of  $x(m)$ , where  $x^\tau(m)$  is the  $\tau$  shifted output signal and  $x(m)$  the input signal. Fig. 4.2 illustrates this in a pictorial way.

### 4.1.3 Shift operation on the expansion coefficients

The overall filter bank with perfect reconstruction has a constant group delay. And it is possible to realize filter banks where the output signal is exactly the same as the input signal (theoretically). However, our aim is to have an output signal which is a shifted version of the input signal. And we aim to perform it on the expansion coefficients.

Since a rotation in the expansion coefficients leads to an integer shift, the shift  $0 \leq \tau \leq 1$  only needs to be considered. See also [Vet95, p.261].

---

<sup>1</sup>In the case of FIR filters either the analysis filters or the synthesis filters are made causal by multiplying them with  $z^{-k}$ . In the case of IIR filters it is referred to section 3.2.

A signal  $x(n)$  passed through an L-fold expander followed by the joined interpolator and decimator filter  $H(z)$  and a M-fold decimator where  $L = M$ , shown in Fig. 4.3, results in  $y(n) = x(n + k)$ ,  $k \in \mathbf{N}$ .

Observing the fact that two sampling rate conversions (first upsampling by a factor

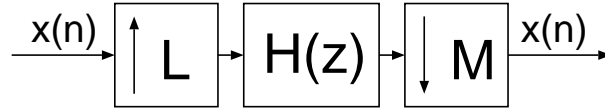


**Figure 4.3:** L-fold expander followed by the interpolator filter  $H(z)$  and a M-fold decimator (fractional sampling rate alteration),  $L = M$  and  $H(z)$  has a cutoff frequency of  $\pi/M$ .

L and second downsampling by the same factor  $M = L$ ) on the expansion coefficients  $x_0(n)$  and  $x_1(n)$ , but discarding by the downsampling process also the original values and therefore keeping other values (coset), results in a set of shifted expansion coefficients  $x_0^T(n)$  and  $x_1^T(n)$ , we can immediately draw the conclusion that this yields finally to a shift of the sequence  $x(m)$ . Theoretically one can perform any desired shift by using this technique. In practice for some fractional shifts a dramatic increase of the sampling rate conversion circuit complexity follows. The solution to this problem is a continuously variable delay element (FIR-filter,  $\tau \in \mathbf{R}$ ) described below, which has a reasonable complexity.

Let  $\{x(nT_s)\}$  designate the sequence of the signal samples uniformly sampled with a sampling rate  $1/T_s$  and  $n$  the sampling index of the signal samples. Also let  $\{y(kT_i)\}$  designate the sequence of interpolated samples with a intermediate sampling rate  $1/T_i$  where  $k$  denotes the interpolator output index. The interpolator equation, for the  $k^{th}$  interpolator output sample, may then be expressed as

$$y(kT_i) = \sum_{n=M_1}^{M_2} x(nT_s) h_I(kT_i - nT_s). \quad (4.2)$$

$M_1$  and  $M_2$  are limits determined by the finite response duration of a time-continuous, time-invariant, linear phase FIR filter  $h_I(t)$ . Since it is assumed also to have shifts  $\tau \in \mathbf{R}$ , the ratio  $T_i/T_s$  becomes irrational. Unlike conventional digital interpolation/decimation methods this method enables one to obtain an interpolated value  $y(kT_i)$  which must not be related to a rational factor  $L/M$  of the sampling rate, where  $L$  and  $M$  are integer values. In order to synthesize a controllable delay  $\tau$ , in equation (4.2) a change of the indexing is required. The first control parameter  $n_k$ , the index for the  $k^{th}$  interpolant, is defined as

$$n_k = \text{largest integer less or equal to the real number } \frac{kT_i}{T_s}$$

The second control parameter  $\tau$  (delay), length of a fractional interval for the  $k^{th}$  interpolant ( $0 \leq \tau < 1$ ), is defined as

$$\tau = \frac{kT_i}{T_s} - n_k.$$

The filter index  $i$ , index on filter coefficients, is defined as

$$i = n_k - n.$$

Equation (4.2) may be rewritten as

$$y(kT_i) = \sum_{i=I_1}^{I_2} x[(n_k - i)T_s] h_I[(i + \tau)T_s].$$

The new limits  $I_1$  and  $I_2$  are large enough to include all nonzero coefficients of the finite impulse response of the filter; these modified limits are fixed numbers and do not depend upon  $n$ . The basepoint set length  $I = I_2 - I_1 + 1$  and ranging from  $t_1$  to  $t_2$ , indicates the required number of coefficients  $h_I[(i + \tau)T_s]$  (taps) in the FIR filter. Interpolants  $y(kT_i)$  are computed for times corresponding to

$$t = kT_i = (\tau + n_k)T_s.$$

For  $t < t_2$  or  $t \geq t_1$  ( $t_2 > t_1$ ) follows  $h_I(t) = 0$ . Thus the duration of the impulse response,  $T_0$ , is defined as

$$T_0 = t_2 - t_1.$$

It is straightforward that the inequality  $IT_s \geq T_0$  must be imposed for any method of implementing the interpolator in order that all non-zero portions of the continuous-time function are sampled correctly. A conventional interpolating polynomial, such as the Lagrange polynomial  $I_N(t)$ , leads to piecewise polynomials  $L_i(t)$  (=Lagrange functions).

$$h_I(t) = \begin{cases} L_1(t) \\ L_2(t) \\ L_3(t) \\ . \\ . \\ . \end{cases}$$

The  $N^{th}$  degree polynomial  $I_N(t)$ , with the Lagrange functions  $L_i(t)$ , both given below, is fitted to the interpolant  $y(kT_i)$  in such a way that the Lagrange functions  $L_i(t)$  become identified with the coefficients of the interpolating filter  $h_I(t)$  [Sch73].

$$I_N(t) = \sum_{i=0}^N L_i(t) x_i$$

and

$$L_i(t) = \prod_{j=0, j \neq i}^N \frac{t - t_j}{t_i - t_j}. \quad (4.3)$$

Equation (4.4) is obtained from equation (4.3) by substituting  $t = (\tau + n_k)T_s$

$$L_i(kT_i) = \prod_{j=I_1, j \neq i}^{I_2} \frac{\tau + j}{j - i}. \quad (4.4)$$

Replacing  $x_i$  with  $x[(n_k - i)T_s]$  and  $I_N(t)$  with  $y(kT_i)$  yields to the interpolation

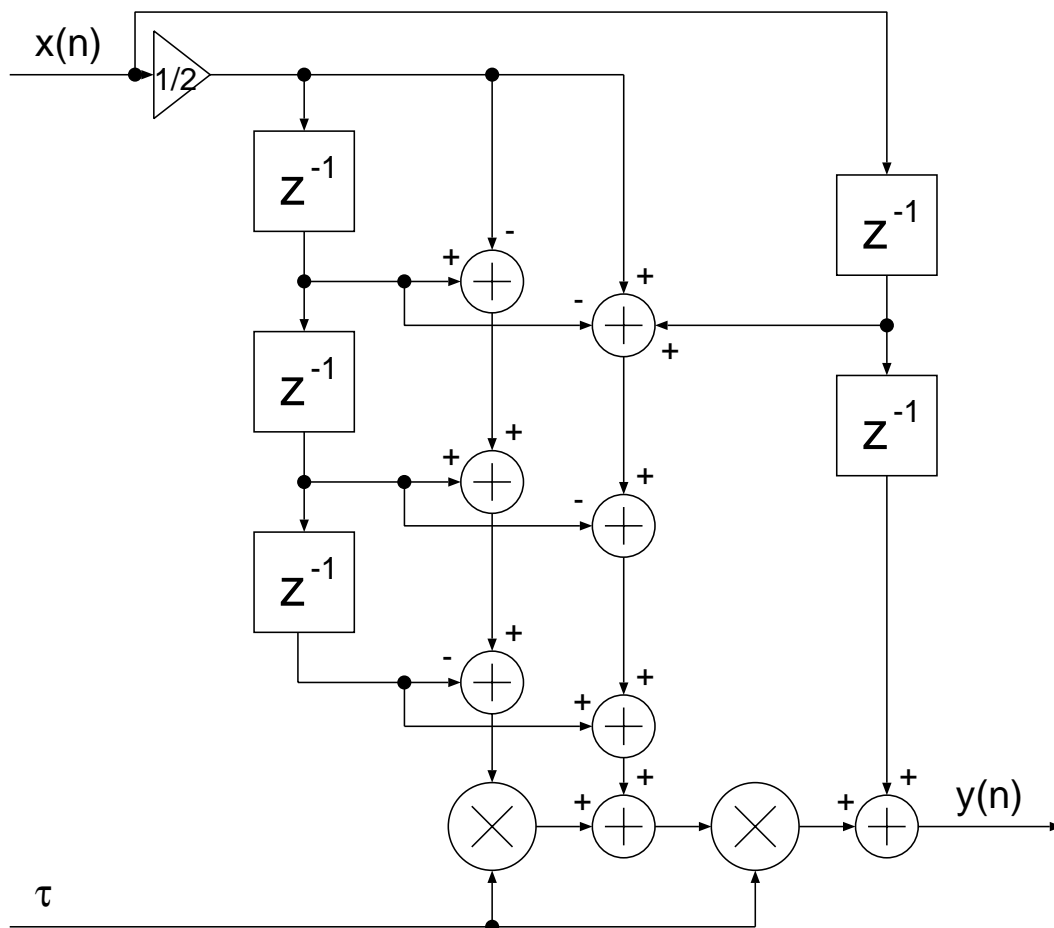


**Figure 4.4:** FIR filter for shift operation on the expansion coefficients.

function

$$y(kT_i) = \sum_{i=I_1}^{I_2} x[(n_k - i)T_s] L_i(kT_i)$$

$i \downarrow j \rightarrow$	0	1	2
-2	0	$-\alpha$	$\alpha$
-1	0	$\alpha+1$	$-\alpha$
0	1	$\alpha-1$	$-\alpha$
1	0	$-\alpha$	$\alpha$

**Table 4.1** Filter coefficients  $b_j(i)$  for the continuously controllable delay element,  $N = 2$ ,  $I_1 = -2$ , and  $I_2 = 1$ .

where each Lagrange function  $L_i(kT_i) = L_i((n_k + \tau)T_s)$  of degree  $N$  is also defined as

$$L_i(\tau) = \sum_{j=0}^N b_j(i) \tau^j$$

and describes  $h_I(t)$  in the  $i^{\text{th}}$   $T_s$  interval. Only odd degree Lagrange functions [Sch73] ( $N$  odd) should be employed in order to have a linear phase FIR interpolation filter with impulse response  $h_I(t)$ . Using this technique to realize a continuously variable delay element, [Far88, Eur93] show examples with an odd degree Lagrange function, which one of them we adopt here for demonstrating a shift in orthonormal wavelet bases.

The coefficients  $b_j(i)$  for the filter structure realizing a controllable delay, shown in Fig. 4.4, are given in Table 4.1 with  $\alpha = 0.5$ ,  $N = 2$ ,  $I_1 = -2$  and  $I_2 = 1$ . Note, that having  $\alpha \neq 0.5$  results in a dramatic increase of the delay element complexity. Using higher odd-degree order Lagrange functions [Ram84] yield to higher accuracy. Performance simulations are given in the next section.

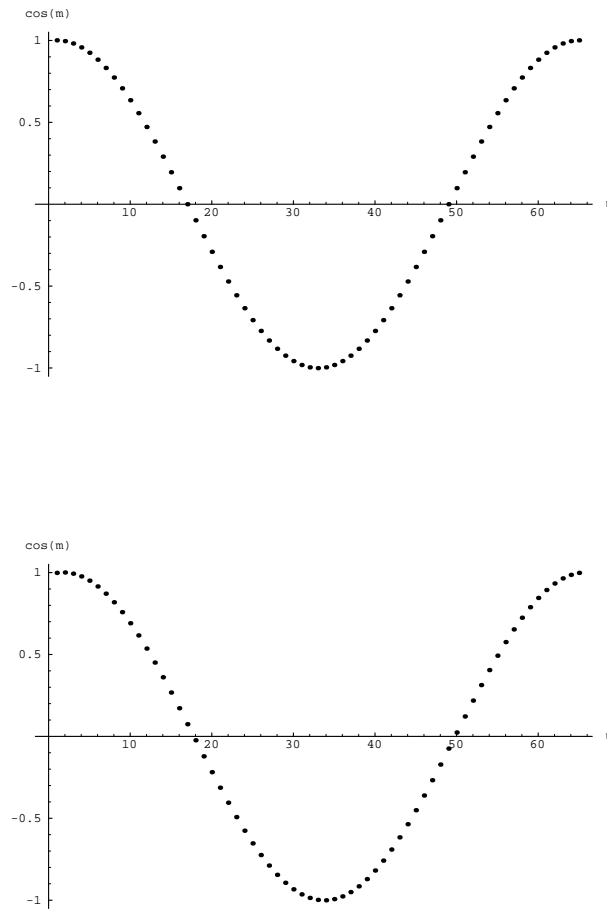


**Figure 4.5:** Translations on the function  $x(m) = \cos(m)$  for the shifts  $\tau = 0$  and  $\tau = 0.379$ .

### 4.1.4 Performance Simulations

Using the above given method this section presents some simulation results of the shift operation in orthonormal wavelet bases. Simulations were done by using the Daubechies wavelets with 12 coefficients and on complex valued wavelets reported

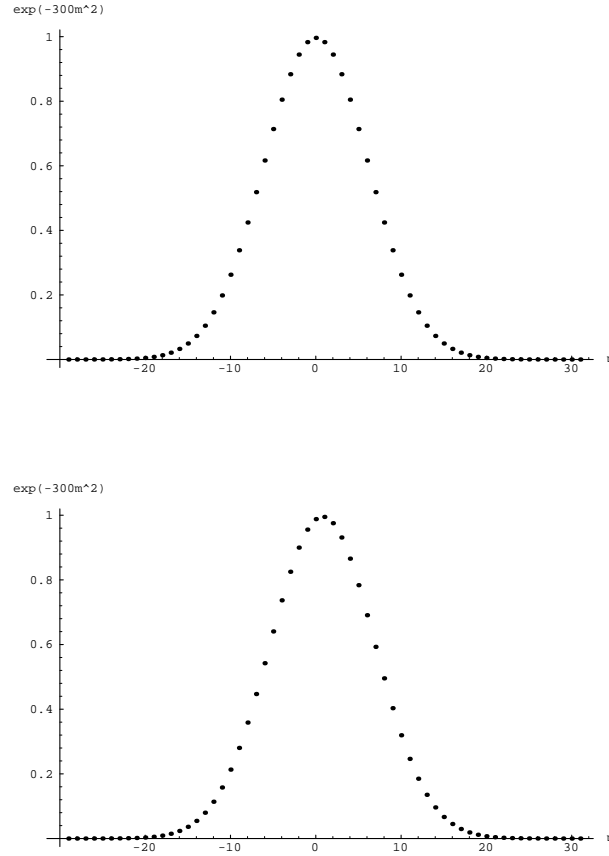


**Figure 4.6:** Translations on the function  $x(m) = \exp(-300m^2)$  for the shifts  $\tau = 0$  and  $\tau = 0.379$ .

in [Law93], in order to test translations on the periodic function  $x(m) = \cos(m)$  and the nonperiodic function  $x(m) = \exp(-300m^2)$ .

As both functions are real valued a method similar to the Fourier transform approach for the complex valued wavelets where  $2N$  real samples are transformed with an  $N$ -sample complex transform is used. In other words, the imaginary part of the discrete transform is used to compute also real values which can be done by breaking the  $2N$ -point function  $x(m)$ ,  $m = 0, 1, 2, \dots, 2N-1$ , into two  $N$ -sample functions. Function  $x(m)$  can be divided in half as follows:

$$a(m) = x(2m)$$

$$b(m) = x(2m + 1)$$

with  $m = 0, 1, 2, \dots, N-1$ .

Function  $a(m)$  is equal to the even-numbered samples of  $x(m)$ , and  $b(m)$  is equal



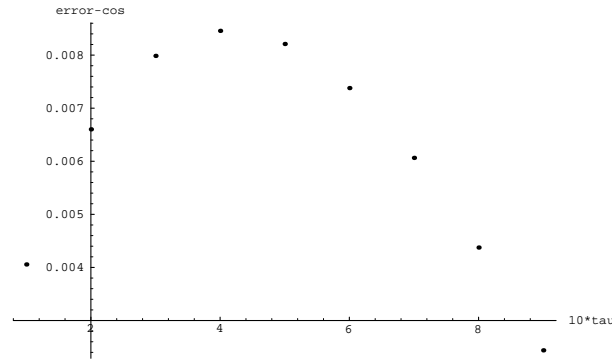


**Figure 4.7:** Maximal absolute error,  $x(m) = \cos(m)$ .

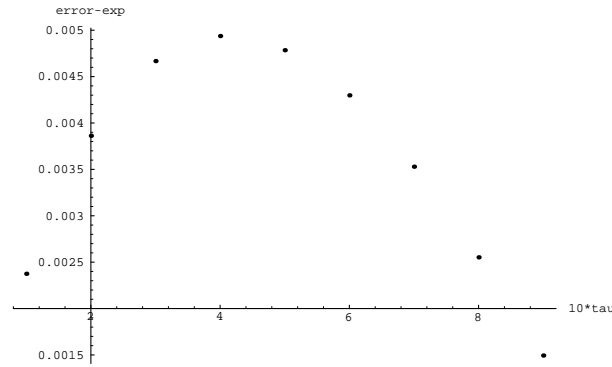


**Figure 4.8:** Maximal absolute error,  $x(m) = \exp(-300m^2)$ .

to the odd-numbered samples of  $x(m)$ . Now, in order to use efficiently the wavelet transform,  $a(m)$  and  $b(m)$  are used to form the complex function  $e(m)$ .

$$e(m) = a(m) + jb(m)$$

with  $m = 0, 1, 2, \dots, N-1$ .

The Figs. 4.5 and 4.6 show shifts for  $\tau = 0$  and  $\tau = 0.379$  for both test functions  $x(m) = \cos(m)$  and  $x(m) = \exp(-300m^2)$  on the expansion coefficients (using Daubechies filters), respectively. We do not show here the plots for the expansion coefficients (using complex filters) as there can not be seen any difference within this graphical resolution to that for the Daubechies case.

Having used one particular delay element out of many possible ones, the accuracy of the delay element itself was tested by using the periodic function  $x(m) = \cos(m)$  and the non-periodic function  $x(m) = \exp(-300m^2)$ . The maximal absolute error  $e(\tau)$ , where  $e(\tau) = x(m) - x(m + \tau)$ , is shown in Fig. 4.7 for the periodic input function (error-cos) with respect to  $10\tau$  and for the non-periodic input function (error-exp) with respect to  $10\tau$  in Fig. 4.8. For example, the maximal absolute error  $e(\tau)$  in Fig. 4.7 for  $\tau = 0.2$  is 0.0066.

## 4.2 Wavelet bases

Next, seven wavelet bases are presented, two of them are new. The wavelets are separated into two groups. "Valid" wavelets (assuming Shannon sampling) and "approximating" wavelets, see also Table 2.1 in chapter 2. First, three "valid" wavelets are presented, sinc-wavelet, Meyer wavelet and the newly introduced raised-cosine wavelet. Then, four "approximating" wavelets are presented, Haar wavelet, Daubechies wavelet, Butterworth wavelet and the newly introduced Chebyshev wavelet (based on IIR elliptic filters). The new wavelets are obtained from already known filters that, under some restrictions, yield wavelet bases. Hence, the selection criteria for the choice of a filter, known from filter theory, can be used. Since the choice of a filter depends on the application, it is up to the user what is best in some respect.

### 4.2.1 Sinc Wavelet

The sinc wavelet (also referred to as Littlewood-Paley wavelet or Shannon wavelet) is described in detail in [Vet95]. Main time and frequency domain relations are summarized below.

The scaling function (interpretable as an analog low pass filter) in time domain can be written as

$$\varphi(t) = \text{sinc}(t)$$

and in frequency domain as

$$\Phi(\Omega) = \begin{cases} 1 & \text{for } -\pi \leq \Omega \leq \pi \\ 0 & \text{elsewhere} \end{cases}$$

The  $2\pi$ -periodic digital low-pass filter for  $-\pi \leq \omega \leq \pi$  follows in frequency domain as

$$H_0(e^{j\omega}) = \sqrt{2} \sum_{k \in \mathbf{Z}} \Phi[2(\omega + 2k\pi)] = \begin{cases} \sqrt{2} & \text{for } \frac{-\pi}{2} \leq \omega \leq \frac{\pi}{2} \\ 0 & \text{elsewhere} \end{cases}$$

and in time domain as

$$h_0(n) = \frac{1}{\sqrt{2}} \text{sinc}(n/2)$$

The wavelet (interpretable as an analog band-pass filter) may be written in time domain as [Vai93]

$$\psi(t) = \sqrt{2} \sum_{n=-\infty}^{\infty} (-1)^{-n+1} h_0(n) \varphi(2t + n - 1) = \text{sinc}(t/2) \cos(3\pi t/2)$$

and in frequency domain as

$$\Psi(\Omega) = \begin{cases} 1 & \text{for } -2\pi \leq \Omega \leq -\pi \text{ and } \pi \leq \Omega \leq 2\pi \\ 0 & \text{elsewhere} \end{cases}$$

The  $2\pi$ -periodic digital high-pass filter for  $-\pi \leq \omega \leq \pi$  follows in frequency domain as

$$H_1(e^{j\omega}) = \begin{cases} -\sqrt{2}e^{-j\omega} & \text{for } -\pi \leq \omega \leq -\frac{\pi}{2} \text{ and } \frac{\pi}{2} \leq \omega \leq \pi \\ 0 & \text{elsewhere} \end{cases}$$

and in time domain as

$$h_1(n) = (-1)^n h_0(-n + 1).$$

### 4.2.2 Meyer Wavelets

The Meyer wavelet can be found in [Vet95, Dau92]. Some important relations are listed below.

The scaling function in frequency domain is defined as

$$\Phi(\Omega) = \begin{cases} \sqrt{\theta(2 + \frac{3\Omega}{2\pi})} & \text{for } \Omega \leq 0 \\ \sqrt{\theta(2 - \frac{3\Omega}{2\pi})} & \text{for } 0 \leq \Omega \end{cases}$$

where

$$\theta(x) = \begin{cases} 0 & \text{for } x \leq 0 \\ 1 & \text{for } 1 \leq x \end{cases}$$

and  $\theta(x) + \theta(1 - x) = 1$  for  $0 \leq x \leq 1$ ,  $\theta(x)$  differentiable.

For example, one choice for  $\theta(x)$  is

$$\theta(x) = \begin{cases} 0 & \text{for } x \leq 0 \\ 3x^2 - 2x^3 & \text{for } 0 \leq x \leq 1 \\ 1 & \text{for } 1 \leq x \end{cases}$$

The  $2\pi$ -periodic digital low-pass filter for  $-\pi \leq \omega \leq \pi$  can be obtained from

$$H_0(e^{j\omega}) = \sqrt{2} \sum_{k \in \mathbf{Z}} \Phi[2\omega + 4k\pi]$$

The wavelet written in frequency domain may be expressed as

$$\Psi(\Omega) = \begin{cases} 0 & \text{for } 0 \leq \Omega \leq 2\pi/3 \\ -\frac{1}{\sqrt{2}}e^{-j\Omega/2}\Phi(\Omega - 2\pi) & \text{for } 2\pi/3 \leq \Omega \leq 4\pi/3 \\ -\frac{1}{\sqrt{2}}e^{-j\Omega/2}\Phi(\Omega/2) & \text{for } 4\pi/3 \leq \Omega \leq 8\pi/3 \\ 0 & \text{for } 8\pi/3 \leq \Omega \end{cases}$$

### 4.2.3 Raised Cosine Wavelets

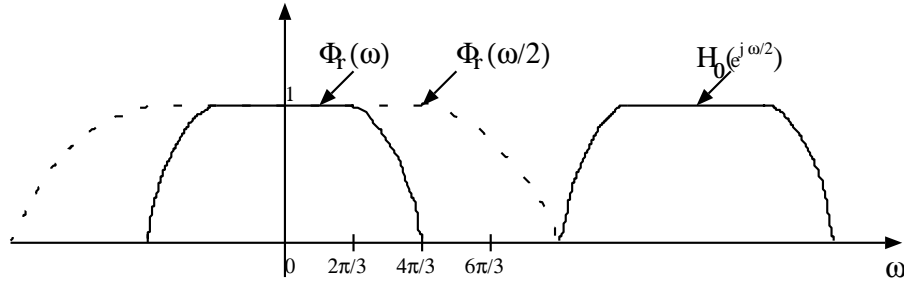


**Figure 4.9:**  $H_0(e^{j\omega/2})$ ,  $\Phi_r(\omega)$  and  $\Phi_r(\omega/2)$  for  $\alpha = 1/3$ .

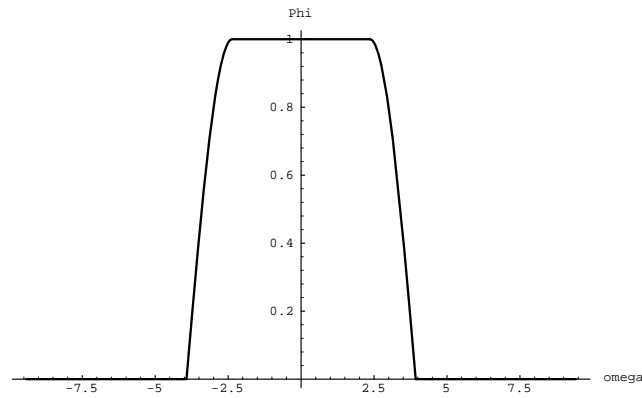


**Figure 4.10:** Raised-cosine scaling function  $|\Phi_r(\Omega)|$  for  $\alpha = 0.25$ .

In the following, orthonormal wavelet bases are derived from the raised cosine filter (compact support in frequency domain) where the roll-off factor  $\alpha$  ranges between

$$0 \leq \alpha \leq \frac{1}{3}.$$

As a special case, the sinc-scaling function follows for  $\alpha = 0$  and for  $\alpha = 1/3$  a Meyer scaling function is almost fullfilled. (only one point is not continuous.)

Let  $W$  be the absolute bandwidth,  $W_0 = \frac{1}{2T}$ ,  $\alpha = \frac{(W - W_0)}{W_0}$  the roll-off factor,  $T$  the sampling period, then the raised-cosine filter can be defined as

$$h_{\text{raised-cosine}}(t) = 2W_0 \text{sinc}(2W_0 t) \frac{\cos[2\pi(W - W_0)t]}{1 - 4(W - W_0)t^2}.$$

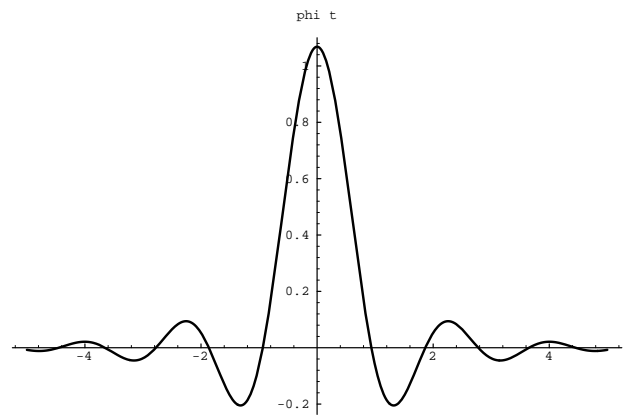


**Figure 4.11:** Raised-cosine scaling function  $\varphi_r(t)$  for  $\alpha = 0.25$ .

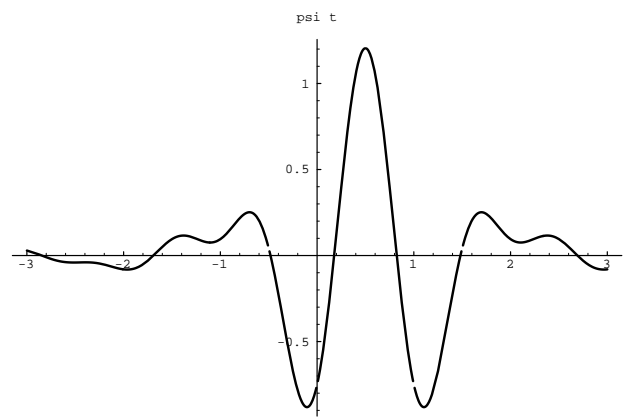


**Figure 4.12:** Raised-cosine wavelet  $\psi_r(t)$  for  $\alpha = 0.25$ .

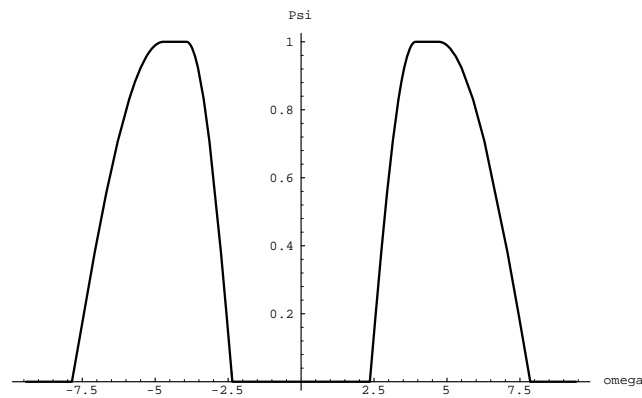


**Figure 4.13:** Raised-cosine wavelet  $|\Psi_r(\omega)|$  for  $\alpha = 0.25$ .

**Theorem 4.1**

A "valid" scaling function is obtained from the raised-cosine filter if  $T=1$  ( $W_0 = \frac{1}{2}$ ) and  $\alpha$  ranges between

$$0 \leq \alpha \leq \frac{1}{3}.$$

Thus,

$$\varphi_r(t) * \varphi_r(t) = \text{sinc}(t) \frac{\cos[\pi \alpha t]}{1 - 2\alpha t^2}.$$

(\* stands for convolution) or in frequency domain

$$\Phi_r(\Omega) = \begin{cases} 1 & \text{for } |\Omega| < \pi(1 - \alpha) \\ \cos\left(\frac{|\Omega| + (\alpha - 1)\pi}{4\alpha}\right) & \text{for } \pi(1 - \alpha) < |\Omega| < \pi(1 + \alpha) \\ 0 & \text{for } |\Omega| > \pi(1 + \alpha) \end{cases}.$$

$\Phi_r(\Omega)$  is the Fourier transform of the raised cosine scaling function and different  $\alpha$  result in different wavelets.

**Proof :**

To prove that  $\Phi_r(\Omega)$  satisfies a multiresolution analysis (2.14-2.18), it is enough to check (2.18) in the interval  $\Omega \in [0, 2\pi]$ , since  $\Phi_r(\Omega)$  is symmetric and has compact support. It follows that

$$|\Phi_r(\Omega)|^2 + |\Phi_r(\Omega - 2\pi)|^2 = 1$$

for  $\Omega \in [0, (1 - \alpha)/2]$  and for  $\Omega \in [(1 - \alpha)/2, (1 + \alpha)/2]$ . And thus, orthonormality is given. Next, define  $V_0$  to be the closed subspace spanned by this orthonormal set.  $V_i$  is similarly defined which satisfies (2.14) if  $H_0(e^{j\omega})$  is  $2\pi$ -periodic and if  $H_0(e^{j\omega})$  is square integrable on  $[0, 2\pi]$  such that (2.20) is valid. Then a  $2\pi$ -periodic filter exists if  $0 \leq \alpha \leq \frac{1}{3}$  (Compare Fig. 4.9, (2.20) and (4.5)). By definition,  $\Phi_r(\Omega)$  is zero outside  $W$  and the integral over  $\Phi_r^2(\Omega)$  is bounded by a finite number. It follows that a  $2\pi$ -periodic, square integrable low-pass filter  $H_0(e^{j\omega})$  on  $[0, 2\pi]$  exists. As (2.14) is satisfied, then the rest of the multiresolution analysis follows from theorem 2.1 and theorem 2.2 as well as from the definitions (2.15) and (2.16) themselves.  $\diamond$

The wavelet can be obtained as follows:

Sampling a bandlimited analog signal  $X_a(\Omega)$  in frequency domain results in [Vai93]

$$X(e^{j\omega}) = \frac{1}{T} \sum_{k=-\infty}^{\infty} X_a\left(\Omega + \frac{2\pi k}{T}\right) \Big|_{\Omega=\frac{\omega}{T}}$$

where the Fourier transform of  $x(n)$  and  $x_a(t)$  are  $X(e^{j\omega})$  and  $X_a(\Omega)$ , respectively. In this case one can therefore write

$$H_0(e^{j\omega}) = \sqrt{2} \sum_{k \in \mathbf{Z}} \Phi_r(2\Omega + 4k\pi) \quad (4.5)$$

for the digital low-pass filter.

The wavelet follows as

$$\Psi_r(\Omega) = -\frac{1}{\sqrt{2}} e^{-j\frac{\omega}{2}} \sum_{k \in \mathbf{Z}} \Phi_r(\Omega + 2\pi(2k + 1)) \Phi_r\left(\frac{\Omega}{2}\right)$$

and because as only for  $k = 0$  and  $k = -1$  the support of  $\Phi_r(\frac{\Omega}{2})$  and  $\Phi_r(\Omega + 2\pi(2k+1))$  overlaps (resulting from compact support of the scaling function in frequency domain)

$$\Psi_r(\Omega) = -\frac{1}{\sqrt{2}}e^{-j\frac{\Omega}{2}}[\Phi_r(\Omega + 2\pi) + \Phi_r(\Omega - 2\pi)]\Phi_r(\frac{\Omega}{2}).$$

As an example, Figs. 4.11-4.13 show plots of a Raised cosine scaling function and a raised cosine wavelet for  $\alpha = 0.25$ .

#### 4.2.4 Haar Wavelet

The Haar wavelet is described in detail in [Vet95, Dau92]. And the main relations are summarized below.

The scaling function in time domain is defined as

$$\varphi(t) = \begin{cases} 1 & \text{for } 0 \leq t < 1 \\ 0 & \text{elsewhere} \end{cases}$$

and in frequency domain as

$$\Phi(\Omega) = e^{-j\Omega/2} \text{sinc}(\Omega/(2\pi)).$$

The  $2\pi$ -periodic digital low-pass filter follows in frequency domain as

$$H_0(e^{j\omega}) = \sqrt{2}e^{-j\omega/2} \cos(\omega/2)$$

or in z-domain as

$$H_0(z) = \frac{1}{\sqrt{2}} + \frac{1}{\sqrt{2}}z^{-1}$$

The  $2\pi$ -periodic digital high-pass filter follows in frequency domain as

$$H_1(e^{j\omega}) = j\sqrt{2}e^{-j\omega/2} \sin(\omega/2)$$

and in z-domain as

$$H_1(z) = \frac{1}{\sqrt{2}} - \frac{1}{\sqrt{2}}z^{-1}$$

The wavelet in time domain can be written as

$$\psi(t) = \varphi(2t) - \varphi(2t - 1) = \begin{cases} 1 & \text{for } 0 \leq t < 1/2 \\ -1 & \text{for } 1/2 \leq t < 1 \\ 0 & \text{elsewhere} \end{cases}$$

and in frequency domain as

$$\Psi(\Omega) = je^{-j\Omega/2} \frac{\sin^2(\Omega/4)}{(\Omega/4)}.$$

### 4.2.5 Daubechies Wavelets

The digital filters used for the Daubechies wavelets can be designed in different ways. There are two design procedures for deriving the digital low-pass filter  $H_0(z)$ . The first is based on spectral factorization and the second is based on FIR lattice structures (or FIR WDF). Factorization becomes numerically ill-conditioned as the filter size grows. There exists no such a problem for FIR lattice (or FIR WDF) structures.

#### Spectral factorization

Let, for orthogonal FBs,  $P(z)$  be a half-band filter, such that

$$P(z) + P(-z) = H_0(z)G_0(z) + H_1(z)G_1(z) = 2.$$

The spectral factor  $H_0(z)$  can be obtained from [Str96]

$$P(z) = 2 \left( \frac{1+z}{2} \right)^p \left( \frac{1+z^{-1}}{2} \right)^p \sum_{k=0}^{p-1} \binom{p+k-1}{k} \left( \frac{1-z}{2} \right)^k \left( \frac{1-z^{-1}}{2} \right)^k.$$

Complete factorisations used during the design process are not unique (freedom of choice) [Vet95]. The other filters of a 2-channel system follow as

$$H_1(z) = z^{-(N-1)} H_0(-z^{-1}) \quad (4.6)$$

$$G_0(z) = z^{-(N-1)} H_0(z^{-1}) \quad (4.7)$$

$$G_1(z) = z^{-(N-1)} H_1(z^{-1}). \quad (4.8)$$

A low sensitivity procedure starts from a paraunitary matrix.

#### FIR lattice structures (FIR WDF)

Starting with

$$H_p = \begin{pmatrix} H_{00}(z) & H_{10}(z) \\ H_{01}(z) & H_{11}(z) \end{pmatrix} = U_0 \left[ \prod_{i=1}^{\frac{N}{2}-1} \begin{pmatrix} 1 & 0 \\ 0 & z^{-1} \end{pmatrix} U_i \right]$$

where

$$U_i = \begin{pmatrix} \cos(\alpha_i) & -\sin(\alpha_i) \\ \sin(\alpha_i) & \cos(\alpha_i) \end{pmatrix},$$

the FIR low-pass filter of a 2-channel system is given as

$$H_0(z) = H_{00}(z^2) + z^{-1} H_{01}(z^2),$$

and the other filters are obtained as in (4.6 - 4.8).

The same filters in the FIR lattice structure are obtained when one starts with an analog reference filter. Then the obtained digital filter is also called FIR WDF [Fet86, Oko71].



WDF are related to an analog reference filter by a bilinear transform. This is true in the FIR and IIR case. Since  $H_{LP}(e^{j\omega})$  can be factored as [Vet95, Dau92]

$$H_{LP}(e^{j\omega}) = \left( \frac{1 + e^{j\omega}}{2} \right)^N \cdot R(\omega),$$

$N \in \mathbb{N} \setminus \{0\}$ , the following theorem holds [Vet95, Dau92]:

**Theorem 4.2**

If

$$\sup_{\omega \in [0, 2\pi]} |R(\omega)| < 2^{N-1}$$

then (2.21) exists.

See [Vet95] for a proof.

In [Fet86, Oko71] this is shown in a more general sense for FIR WDFs, and will be reviewed next.

Making use of (3.2) ,i.e.,  $z = \frac{s+1}{1-s}$ , the transfer function of any nonrecursive filter follows as

$$H_{LP}(s) = \frac{f(s)}{g(s)}$$

$$g(s) = (s + 1)^N = \left( \frac{2e^{pT}}{e^{pT} + 1} \right)^N$$

$N$  is equal to the degree of  $H_{LP}(s)$  in  $z$  and  $f(s)$  is also a polynomial in  $s$ .

Since  $|H_{LP}(s)| \leq 1$  for all  $\Omega$ , it follows for the special case when the equal sign is reached, that the associated WDFs, when iterated in a paraunitary filter bank [Vet95, Lei94], are related to a wavelet transform, compare [Fet86]. The structure for FIR WDFs [Fet86, Oko71] is depicted in Fig. 4.14, and the necessary equations related to the filter coefficients  $\beta_1, \dots, \beta_{N-1}, \alpha$  as well as the wave quantities  $a_1, a_2, b_1, b_2$  can be found in [Fet86, Oko71] and references therein, see also Chapter 3.

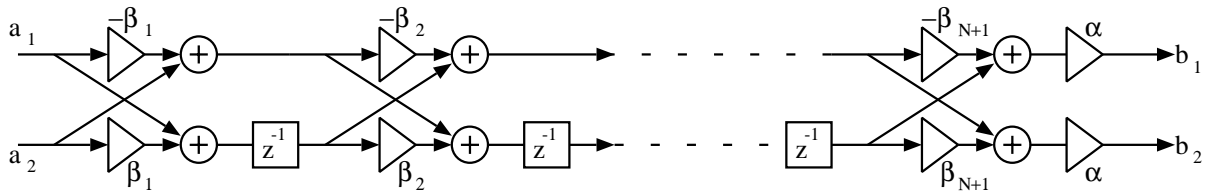


**Figure 4.14:** FIR WDF structure [Fet86, Oko71].

## Graphical Limit Functions

The graphical limit functions can be obtained using [Fli94]

$$\begin{aligned}
\Phi_i(\Omega) &= \prod_{m=1}^i \frac{1}{\sqrt{2}} H_0(e^{j2^{-m}\omega}) \\
\Psi_i(\Omega) &= \frac{1}{\sqrt{2}} H_1(e^{j\frac{\omega}{2}}) \prod_{m=2}^i \frac{1}{\sqrt{2}} H_0(e^{j2^{-m}\omega}) \\
h_{0k}(n) &= \begin{cases} h_0(n) = \sqrt{2}h_0(m) & \text{if } n = 2^k m \\ 0 & \text{elsewhere} \end{cases} \\
h_0^i(n) &= \prod_{k=1}^i *h_{0k}(n) \\
\varphi^i(t) &= 2^{\frac{i}{2}} h_0^i(n), \quad n2^{-i} \leq t \leq (n+1)2^{-i} \\
h_{1i}(n) &= \begin{cases} h_1(n) = \sqrt{2}h_1(m) & \text{if } n = 2^i m \\ 0 & \text{elsewhere} \end{cases} \\
h_1^i(n) &= h_{1i}(n) * \prod_{k=1}^{i-1} *h_{0k}(n) \\
\psi^i(t) &= h_1^i(n), \quad n2^{-i} \leq t \leq (n+1)2^{-i}
\end{aligned}$$

which approximate the scaling function and wavelet as  $i \rightarrow \infty$ .

### 4.2.6 Butterworth Wavelets

There exist, similar to the Daubechies wavelets, also two ways of filter designs. One using a spectral factorization and the other not, see [Smi91, Ans96]. However, the filters are related differently to each other. In the case that a spectral factorization method is used, the filters are related to  $H_0(z)$  as:

$$\begin{aligned}
H_1(z) &= z^{-(N-1)} H_0(-z^{-1}) \\
G_0(z) &= z^{-(N-1)} H_0(z^{-1}) \\
G_1(z) &= z^{-(N-1)} H_1(z^{-1}).
\end{aligned}$$

In the WDF case the filters are related as:

$$\begin{aligned}
H_1(z) &= H_0(-z) \\
G_0(z) &= 2H_0(z^{-1}) \\
G_1(z) &= 2H_1(z^{-1}).
\end{aligned}$$

Noting that for  $K(s)$  of (2.4)

$$K\left(\frac{1}{s}\right) = \frac{1}{K(s)}$$

and using the results of subsection 3.1.4, one can obtain graphical limit functions similar to the Daubechies case. Note, B-splines can be viewed as Butterworth wavelets [Her93].

### 4.2.7 Chebyshev Wavelets

For the Chebyshev rational function  $R_N(s)$  in (2.5), it is assumed that

$$K\left(\frac{1}{s}\right) = \frac{1}{K(s)} \quad (4.9)$$

holds, compare [Tan95, p.2182].

Butterworth filters have the property that, for a low pass filter, all the zeros are at the aliasing frequency. Elliptic filters (having a Chebyshev pass- and stop-band) can also be of the bireciprocal WDF type, see (4.9). Odd order elliptic bireciprocal WDFs have a zero at the aliasing frequency. Even order ones do not<sup>2</sup>. Thus wavelet bases can be generated from odd order bireciprocal WDFs. The Chebyshev response for a 7<sup>th</sup> order bireciprocal WDF (elliptic function) is shown in Fig. 4.15. And the filter coefficients as well as the transfer function are [Fet85]:

$$\begin{aligned} \gamma_1 &= (1/2) \\ \gamma_2 &= (1/8) + (1/32) \\ \gamma_3 &= (1/8) + (1/32) + (1/128) \\ H_{LP}(e^{j\omega}) &= 0.5(e^{j\omega} \frac{e^{j2\omega} + \gamma_1}{1 + \gamma_1 e^{j2\omega}} + \frac{e^{j2\omega} + \gamma_2}{1 + \gamma_2 e^{j2\omega}} \frac{e^{j2\omega} - \gamma_3 + 1}{1 + (1 - \gamma_3)e^{j2\omega}}) \end{aligned}$$

A design method for bireciprocal WDF is shown in [Gas85]. The filter coefficients can be calculated in a straight forward manner. The main advantage of Chebyshev wavelets compared to Butterworth wavelets is that, for a given filter degree, they have a better frequency selectivity. See Fig. 4.16 for a Butterworth response (9<sup>th</sup> order bireciprocal WDF.) The above elliptic filter is a low-sensitivity filter.

## 4.3 Conclusion

New presented material in this chapter is:

- a) a very efficient way to obtain fractional shifts of the expansion coefficients (wavelet coefficients) by an amount of  $\tau \in \mathbf{R}$ .
- b) the raised cosine wavelet that has compact support in frequency domain and is attractive for Shannon sampling.

---

<sup>2</sup>Even order IIR filters yield complex coefficients.

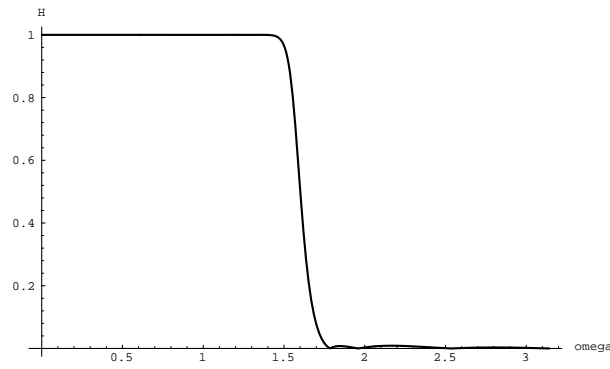


**Figure 4.15:** Chebyshev response for a 7<sup>th</sup> order bireciprocal WDF (elliptic function) having only 3 filter coefficients. Chebyshev wavelets can be generated from this filter in the usual way [Vet95, Str96].

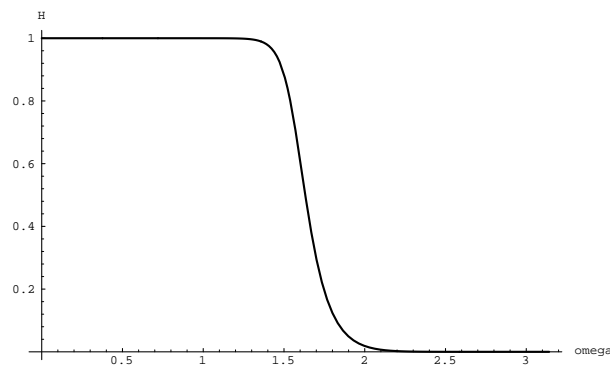


**Figure 4.16:** Butterworth response for a 9<sup>th</sup> order bireciprocal WDF having 4 filter coefficients.

and c) the Chebyshev wavelet that needs, for a given frequency selectivity, less filter coefficients than a Butterworth wavelet.

## Chapter 5

# Two-Channel Multidimensional Systems

Sofar no design method for orthonormal filters was reported that can be used for nonseparable sampling in dimension two or higher. Only one single trivial filter, the Haar filter, was known. In this chapter a novel design method for two-channel multidimensional nonseparable orthonormal filters is presented. In the next chapter it is extended to four-channel multidimensional systems. The presented filters can be used to generate multidimensional orthonormal nonseparable wavelets.

### 5.1 Two-Dimensional Nonseparable Orthonormal Wavelets

Motivated by the fact that for a given filter specification IIR-filters have much less complexity compared to FIR-filters, the following is concerned with the design of nonseparable 2-dimensional IIR-filters by means of wave digital filters (WDFs). They are suitable for multirate systems to generate nonseparable orthonormal wavelet bases. An implementation of perfect reconstruction filter banks using IIR filters for infinite length signals was first shown in [Mit92]. This method was modified in [Lei94] for 1-dimensional WDFs. It is summarized in section 3.2 and will be used for non-separable 2-dimensional lattice WDFs using quincunx sampling.

In the 1-dimensional case wavelet bases can be constructed from Butterworth filters [Her93], or elliptic filters leading, when used in an iterated perfect reconstruction filter bank, to Butterworth or Chebyshev wavelets, respectively. The implementation as lattice wave digital filters of those filters is very efficient [Gas85] and will be used when constructing a nonseparable perfect reconstruction filter bank for quincunx sampling.

### 5.1.1 Paraunitary Filter Bank

In the 1-dimensional case, a bandlimited (by means of an analog filter  $\varphi(t)$ ) signal  $x_a(t)$  having no spectral components at and above  $2\pi f_m$ , can be determined uniquely by values sampled at uniform intervals of  $T$  seconds where  $T \leq \frac{1}{2f_m}$ . In the D-dimensional case, the minimum sampling density  $\rho_{min}$  (number of lattice points per unit hypervolume) is defined as [Vai93]

$$\rho_{min} = \frac{1}{|\det \mathbf{V}|} \quad (5.1)$$

where  $\mathbf{V}$  is the sampling matrix used when sampling bandlimited signals. The minimum sampling density  $\rho_{min}$  depends on  $\mathbf{V}$  and on the support of the bandlimited signal. The support of the bandlimited signal is determined by the shape of  $\varphi(\mathbf{t})$ .

In a 1-dimensional multirate system, a signal  $x(n)$ , bandlimited to the region  $|\omega| < \frac{\pi}{C}$  (by means of a digital filter  $h_0(n)$ ,  $C$  = number of channels), can be alias-free downsampled. In the D-dimensional case, alias-free downsampling is directly related to the matrix  $\mathbf{M}$ . The decimation ratio  $r$  is defined as  $r = |\det \mathbf{M}|$ . In case that an orthonormal wavelet transform is performed by means of a multirate system, the analog filter  $\varphi(t)$  and the digital filter  $h_0(n)$  are related in frequency domain as [Fli94, Vet95]  $\Phi(\omega) = \prod_{k=1}^{\infty} M_0(2^{-k}\omega)$ , where  $M_0(\omega) = H_0(e^{j\omega})/H_0(1)$ . The ideal filter  $H_0(e^{j\omega})$  in a D-dimensional multirate filter design has the form

$$H_0(e^{j\omega}) = \begin{cases} 1 & \text{if } \omega = \pi \mathbf{M}^{-T} \mathbf{x} + 2\pi \mathbf{m}, \\ & \text{for some } \mathbf{x} \in [-1, 1)^D, \mathbf{m} \in N \\ 0 & \text{elsewhere} \end{cases}$$

where  $\omega = [\omega_0 \ \omega_1 \ \dots \ \omega_{D-1}]^T$ ,  $\mathbf{M}$  is a  $D \times D$  nonsingular matrix,  $M^{-T}$  stands for  $(M^{-1})^T$  and  $2\pi \mathbf{m}$  represents the periodicity.

The analog and digital low-pass filters are then related as [Vet95, Kov92, Coh93]

$$\Phi(\omega) = \prod_{k=1}^{\infty} M_0(\mathbf{M}^{-k} \omega) \quad (5.2)$$

where  $M_0(\omega) = H_0(e^{j\omega})/H_0(\mathbf{1})$ . As  $\mathbf{M}$  in (5.2) determines the shape of  $\varphi(\mathbf{t})$ , it follows that  $\mathbf{V}$  in (5.1) is related to  $\mathbf{M}$ .

Note, that for Shannon sampling  $\varphi(\mathbf{t})$  must be an analog filter having compact support in frequency domain in order to be able to uniquely reconstruct, by means of an interpolation formula, an analog signal from its discretely represented signal. This means that the associated digital low-pass filter  $h_0(\mathbf{n})$  has in general an infinite number of nonzero filter coefficients and can therefore not exactly be realized. However, assuming wavelet sampling, in the following an exact realizable  $h_0(\mathbf{n})$  (2-dimensional case) will be designed for a perfect reconstruction system having a finite number of non-zero filter coefficients, that yield an  $\varphi(\mathbf{t})$  which has infinite support in frequency domain.

Considering the 2-dimensional non-separable case, one choice of  $\mathbf{M}$  for quincunx sam-

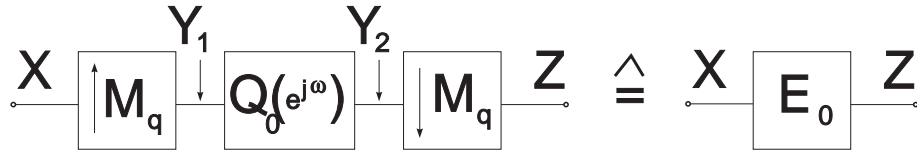


**Figure 5.1:** 0th type 1 polyphase component of  $Q_0(e^{j\omega})$ .

pling is (symmetry dilation matrix)

$$\mathbf{M}_q = \begin{bmatrix} 1 & 1 \\ 1 & -1 \end{bmatrix}.$$

$\mathbf{M}_q$  is said to be well behaved [Kov92]. Based on  $\mathbf{M}_q$ , 2-dimensional nonseparable wavelets will be derived.

Figure 5.1 shows the 0th type 1 polyphase component [Mer83, Lin84, Che91, Fet90] of  $Q_0(e^{j\omega})$ . Assuming

$$Q_0(e^{j\omega}) = H_L(e^{j\omega_0})H_L(e^{j\omega_1}) + H_H(e^{j\omega_0})H_H(e^{j\omega_1})$$

and using the transforms

$$Y_1(\omega) = X(\mathbf{M}^T \omega) \quad (5.3)$$

and

$$Z(\omega) = \frac{1}{|\det \mathbf{M}|} \sum_{\mathbf{k} \in N(\mathbf{M}^T)} Y_2(\mathbf{M}^{-T}(\omega - 2\pi \mathbf{k})), \quad (5.4)$$

representing upsampling and downsampling respectively,  $\mathbf{k}$  the set of integer vectors inside the fundamental parallelepiped, it turns out that  $E_0(\omega)$  equals the ideal low-pass filter  $H_0(e^{j\omega})$  associated to the quincunx sampling matrix  $\mathbf{M}_q$ . Compare Fig. 5.2 for a proper choice of  $Q_0(e^{j\omega})$ . This way of realizing  $H_0(e^{j\omega})$  is very attractive as will be seen later. A pictorial proof that  $E_0(\omega)$  indeed represents  $H_0(e^{j\omega})$  is illustrated in

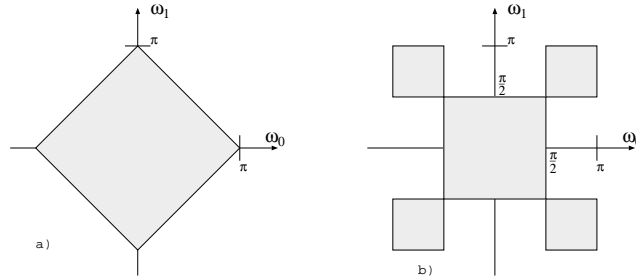


**Figure 5.2:** a) Ideal digital low-pass filter shape  $E_0(\omega) = H_0(e^{j\omega})$  for quincunx sampling with  $\mathbf{M}_q$ , b)  $Q_0(e^{j\omega})$ . The dotted areas indicate the pass-band of the filters in  $-\pi \leq \omega_0 \leq \pi$ ,  $-\pi \leq \omega_1 \leq \pi$ .

Fig. 5.3. See also appendix A. In general, when upsampling/downsampling with  $\mathbf{M}$ , the lattice is squeezed/stretched by  $|\det \mathbf{M}|$  and after downsampling  $\mathbf{M}$  also rennumbers the lattice points. Concrete, the input lattice  $\mathbf{V}$ , written in frequency domain as

$$\mathbf{U} = 2\pi \mathbf{V}^{-T} = 2\pi \begin{bmatrix} 1 & 0 \\ 0 & 1 \end{bmatrix}$$

and shown in Fig. 5.3 a), undergoes an interpolation with  $\mathbf{M}_q$  by (5.3 ). This results in the lattice which is illustrated in Fig. 5.3 b). Figure 5.3 b) also shows one period of  $Q_0(e^{j\boldsymbol{\omega}})$ . Downsampling according to (5.4) finally gives back the desired input lattice filtered by the ideal low-pass filter  $H_0(e^{j\boldsymbol{\omega}})$ , where only one period of  $H_0(e^{j\boldsymbol{\omega}})$  is depicted. If  $H_L(e^{j\omega_0}) = 0$  and  $H_L(e^{j\omega_1}) = 0$  at  $\omega_0 = \pi$  and  $\omega_1 = \pi$ , respectively, then  $H_0(e^{j\boldsymbol{\omega}}) = 0$  at  $\boldsymbol{\omega} = (\pi, \pi)$ . Similarly one can design a high-pass filter

$$Q_1(e^{j\boldsymbol{\omega}}) = H_H(e^{j\omega_0})H_L(e^{j\omega_1}) + H_L(e^{j\omega_0})H_H(e^{j\omega_1}),$$

see Fig. 5.4. Since  $\mathbf{M}_q\mathbf{M}_q = \mathbf{M}_{rec}$ ,

$$\mathbf{M}_{rec} = \begin{bmatrix} 2 & 0 \\ 0 & 2 \end{bmatrix}$$

the 2-dimensional nonseparable PR filter bank, using  $\mathbf{M}_q$ , can be implemented with

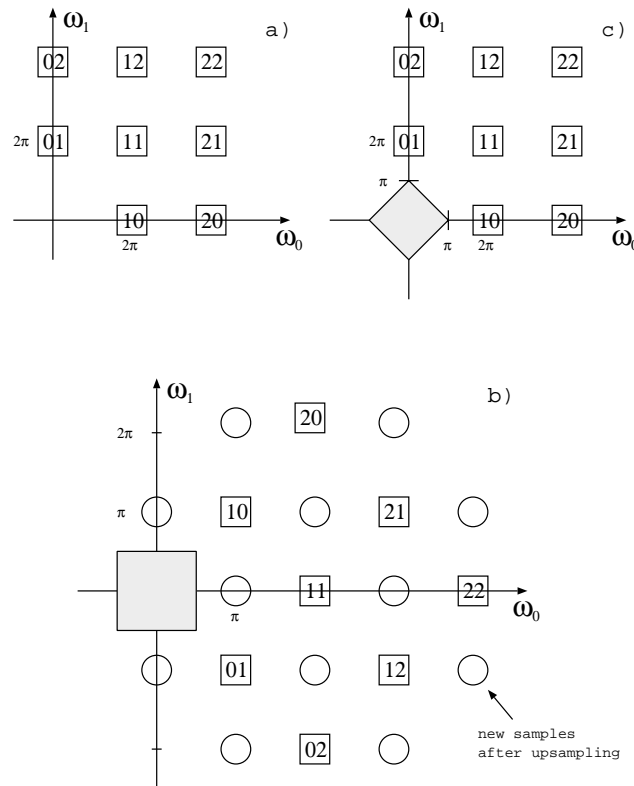


**Figure 5.3:** Lattice representations in frequency domain, a) input lattice, b) after upsampling with  $\mathbf{M}_q^T$ ,  $Q_0(e^{j\boldsymbol{\omega}})$  is indicated, and c) after downsampling with  $\mathbf{M}_q^{-T}$ .

separable filters. And when realized with LWDF this structure becomes very simple. The designed perfect reconstruction filter bank can be used to perform a nonseparable 2-dimensional wavelet transform. Clearly, the final structure representing a 2-dimensional nonseparable perfect reconstruction filter bank with quincunx sampling is shown in Fig. 5.5. This structure can be applied for FIR and IIR filters. It can be very efficiently implemented, especially in the bireciprocal LWDF case. Figure 5.6 shows an example for a Butterworth implementation of a LWDF,  $N=9$ , maximum



number of zeros at  $\boldsymbol{\omega} = (\pi, \pi)$ . This structure uses 12 filter coefficients (only 4 of them being different) and they can be calculated with a pocket calculator by using the method shown in [Gas85]. Filter coefficients used in Fig. 5.6:

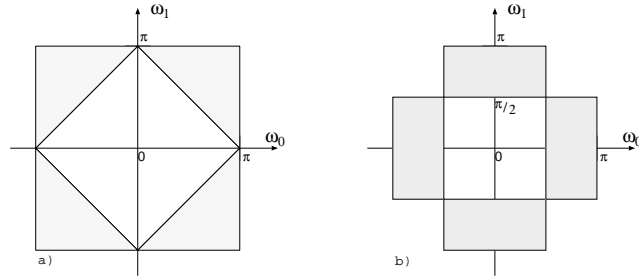


**Figure 5.4:** a) Ideal digital high-pass filter shape  $H_1(e^{j\boldsymbol{\omega}})$  for quincunx sampling with  $\mathbf{M}_q$ , b)  $Q_1(e^{j\boldsymbol{\omega}})$ .

$$\begin{aligned}\alpha_1 &= -0.132\ 47 \\ \alpha_2^* &= \ 0.295\ 91 \\ \alpha_3 &= -0.031\ 09 \\ \alpha_4 &= -0.333\ 33\end{aligned}$$

With  $\alpha_2 = -(1 - \alpha_2^*)$ , the 1-dimensional frequency response of  $H_L(e^{j\omega_0})$  follows as

$$H_L(e^{j\omega_0}) = 0.5(e^{j\omega_0} \frac{e^{j2\omega_0} - \alpha_1}{1 - \alpha_1 e^{j2\omega_0}} \frac{e^{j2\omega_0} - \alpha_2}{1 - \alpha_2 e^{j2\omega_0}} + \frac{e^{j2\omega_0} - \alpha_3}{1 - \alpha_3 e^{j2\omega_0}} \frac{e^{j2\omega_0} - \alpha_4}{1 - \alpha_4 e^{j2\omega_0}}) \quad (5.5)$$

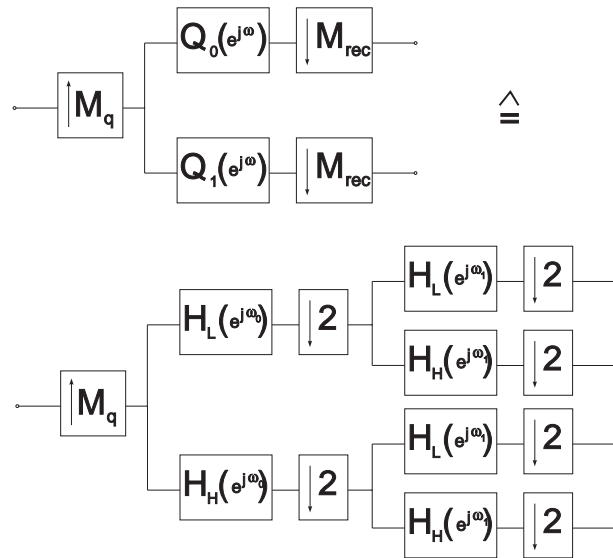


**Figure 5.5:** Efficient structure for a 2-dimensional nonseparable perfect reconstruction filter bank with quincunx sampling (analysis part).

### 5.1.2 Constructing 2-D Wavelet Bases from LWDFs

In general the number of wavelets is determined by

$$|\det(\mathbf{M})| - 1 = r - 1.$$

Unlike the 2-D separable case,  $\mathbf{M}_{rec}$ , in which three mother wavelets  $\psi_1, \psi_2, \psi_3$  and one scaling function  $\varphi$  exist, in the quincunx case,  $\mathbf{M}_q$ , there exist only one mother wavelet  $\psi$  and one scaling function  $\varphi$  [Vet95, Coh93]. The corresponding iterated filter bank for quincunx  $\mathbf{M}_q$ , representing the scaling function and wavelet, is indicated in Fig. 5.7.

Figure 5.8 shows various dilated versions of the ideal basic filters for  $\mathbf{M}_q$ , which take part in the infinite products of (5.2) and

$$\Psi(\boldsymbol{\omega}) = M_1(\mathbf{M}^{-1}\boldsymbol{\omega}) \prod_{k=2}^{\infty} M_0(\mathbf{M}^{-k}\boldsymbol{\omega})$$

where  $M_1(\boldsymbol{\omega}) = H_1(e^{j\boldsymbol{\omega}})/H_1(\mathbf{0})$ . For  $\mathbf{M}_q$  and the ideal basic filters, the scaling function  $\varphi$  is separable in the sense that it can be expressed directly in terms of one dimensional functions, i.e.,

$$\Phi_q(\boldsymbol{\omega}) = \Phi(\omega_0)\Phi(\omega_1)$$

or in time domain as

$$\varphi_q(\mathbf{t}) = \varphi(t_0)\varphi(t_1).$$

For Shannon sampling, the ideal filter  $\Phi_q(\boldsymbol{\omega})$  needs to be approximated with e.g. Butterworth filters. The wavelet follows as (only one wavelet!):

$$\Psi_q(\boldsymbol{\omega}) = \Phi_q(\mathbf{M}^{-1}\boldsymbol{\omega})M_1(j\mathbf{M}^{-1}\boldsymbol{\omega}).$$

For the separable case

$$\Phi_{rec}(\omega_1, \omega_2) = \Phi(\omega_1)\Phi(\omega_2)$$

$$\Psi_{1,rec}(\omega_1, \omega_2) = \Phi(\omega_1)\Psi(\omega_2)$$

$$\Psi_{2,rec}(\omega_1, \omega_2) = \Psi(\omega_1)\Phi(\omega_2)$$

$$\Psi_{3,rec}(\omega_1, \omega_2) = \Psi(\omega_1)\Psi(\omega_2),$$

three wavelet occur. They are depicted with the scaling function for the raised cosine case in the Figs. (5.9 - 5.12).

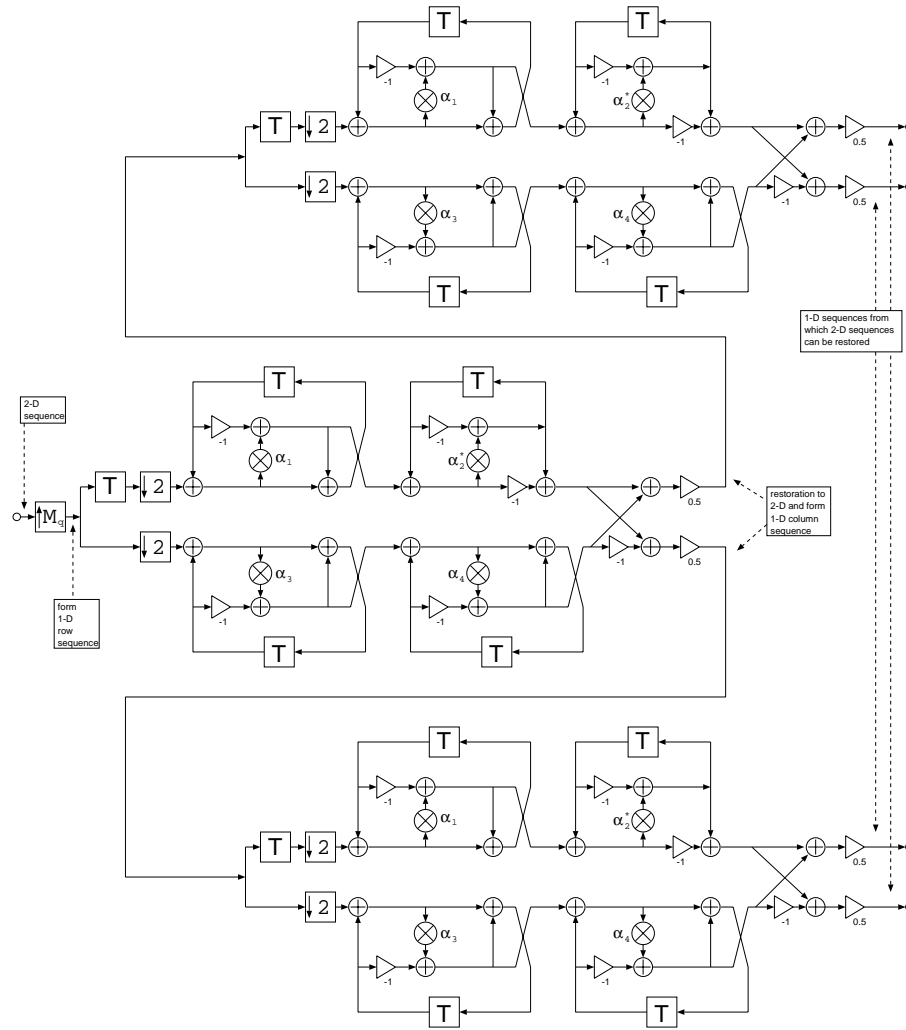


**Figure 5.6:** 2-dimensional, 2-channel nonseparable LWDF bank (analysis part) for quincunx downsampling, expressed in an internal separable way.

## 5.2 Discussions

### 5.2.1 Minimum sampling density for $\mathbf{V}$ related to $\mathbf{M}_q$

Since the shape of  $\varphi(\mathbf{t})$  determines indirectly  $\rho_{min}$ , the (analog/digital) sampling matrix  $\mathbf{V}$  for (5.1) is derived from the (digital/digital) sampling matrix  $\mathbf{M}_q$ . For  $x(\mathbf{n}) = x_a(\mathbf{V}\mathbf{n})$  and with  $\boldsymbol{\Omega} = \mathbf{V}^T \boldsymbol{\omega}$  it follows

$$X(\mathbf{V}^T \boldsymbol{\Omega}) = \frac{1}{|\det(\mathbf{V})|} \sum_{\mathbf{k} \in N} X_a(j(\boldsymbol{\Omega} - \mathbf{U}\mathbf{k})).$$

It is clear from Fig. 5.13, that  $\mathbf{V}$  has for  $\rho_{min}$  (tightest packed  $X(\mathbf{V}^T \boldsymbol{\Omega})$ ) the form

$$\mathbf{V} = \begin{bmatrix} v_0 & 0 \\ 0 & v_1 \end{bmatrix}$$

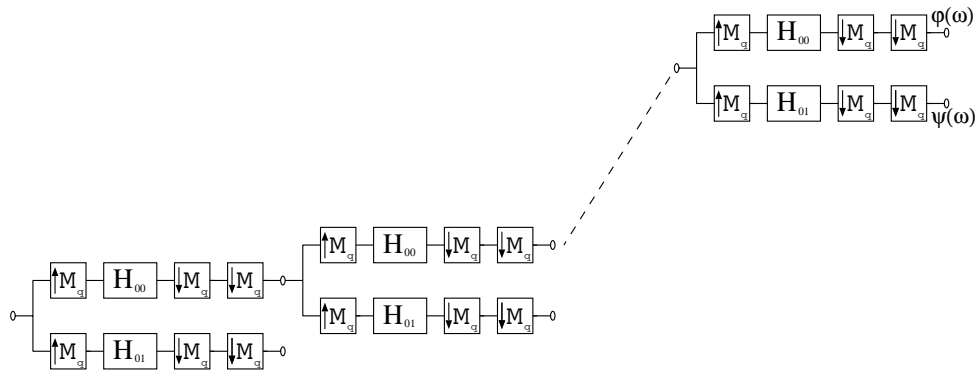


**Figure 5.7:** Computation of the 2-dimensional discrete wavelet transform using a filter bank with quincunx sampling.

or in frequency domain

$$\mathbf{U} = 2\pi \mathbf{V}^{-T} = 2\pi \begin{bmatrix} v_0^{-1} & 0 \\ 0 & v_1^{-1} \end{bmatrix}$$

And aliasing can be avoided for the values

$$v_0 = 1$$

$$v_1 = 1.$$

Thus  $\rho_{min} = 1$ . It can be easily shown that the arrangement in Fig. 5.13 c) yields also  $\rho_{min} = 1$ .

## 5.3 Conclusion

Quincunx sampling is used for two-channel two-dimensional nonseparable sampling. Novel IIR filters for the well-behaved quincunx sampling matrix  $M_q = \begin{pmatrix} 1 & 1 \\ 1 & -1 \end{pmatrix}$ , that leads, when iterated, to orthonormal two-dimensional nonseparable wavelets, are presented. The novel two-dimensional filters are composed of one-dimensional filters and their complexity is surprisingly small. The known Haar filter (FIR) turns out to be the smallest size filter of this design method.

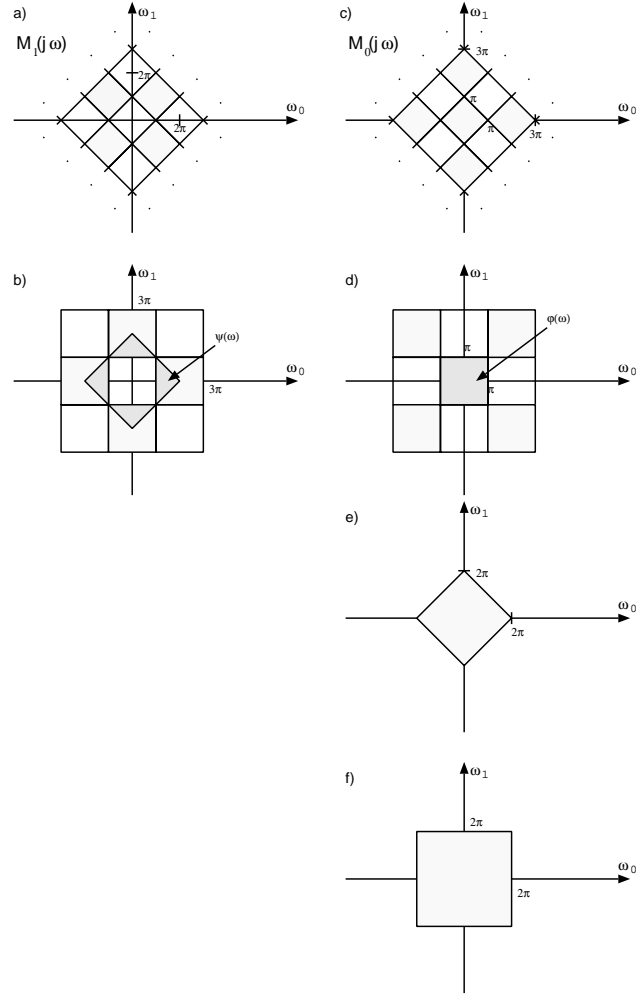


**Figure 5.8:** Various dilated versions of the ideal basic filters shown in a) and c) which take part in the infinite product b), d), e) and f). In b) and d), the wavelet and scaling function are indicated, respectively.

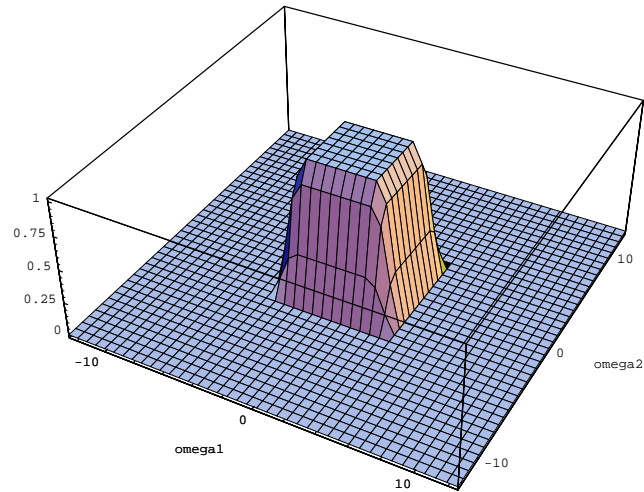


**Figure 5.9:** Two-dimensional Raised-cosine scaling function for digital/digital rectangular sampling for  $\alpha = 0.25$

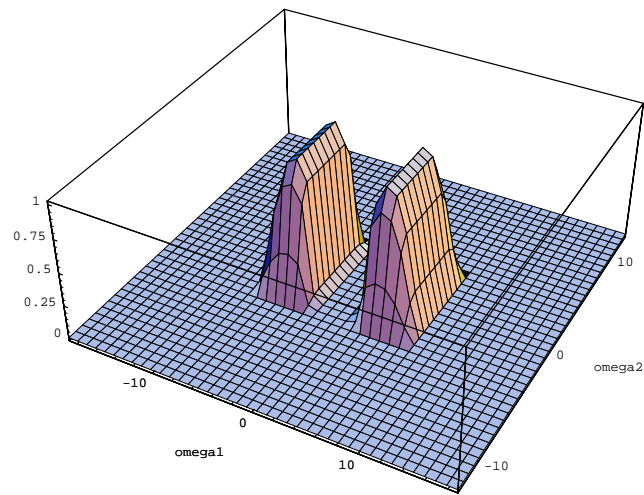


**Figure 5.10:** Two-dimensional Raised-cosine wavelet for digital/digital rectangular sampling,  $|\Psi_{1,rec}(\omega_1, \omega_2)|$ , for  $\alpha = 0.25$ .

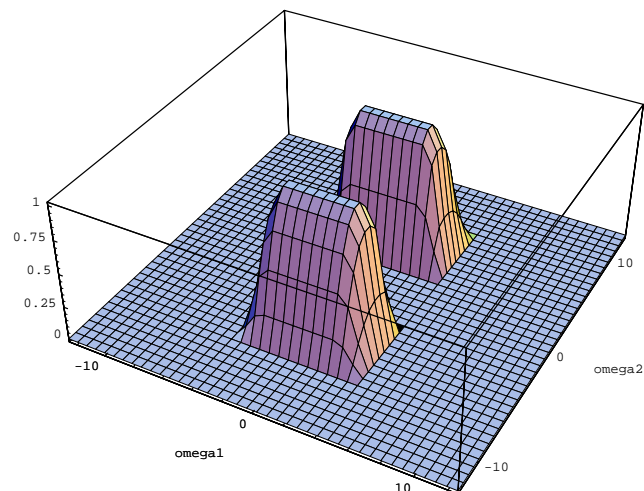


**Figure 5.11:** Two-dimensional Raised-cosine wavelet for digital/digital rectangular sampling,  $|\Psi_{2,rec}(\omega_1, \omega_2)|$ , for  $\alpha = 0.25$ .

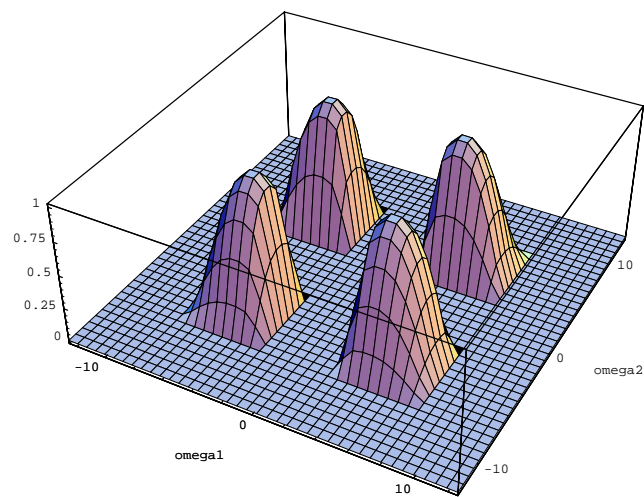


**Figure 5.12:** Two-dimensional Raised-cosine wavelet for digital/digital rectangular sampling,  $|\Psi_{3,rec}(\omega_1, \omega_2)|$ , for  $\alpha = 0.25$ .

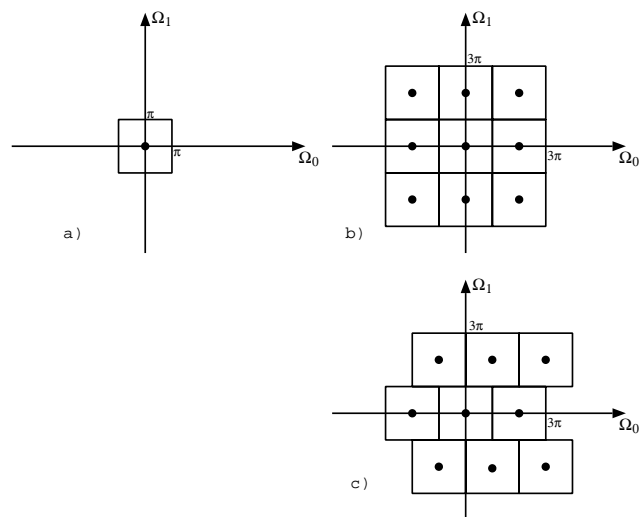


**Figure 5.13:** Ideal (analog/digital) sampling with  $\mathbf{V}$  for (digital/digital) quincunx sampling with  $\mathbf{M}_q$ . a) Support of  $X_a(\boldsymbol{\Omega})$ , b) support of  $X_a(\mathbf{V}^T \boldsymbol{\Omega})$ , rectangular sampling, c) alternative choice for  $\mathbf{V}$ .



# Chapter 6

## Four-Channel Multidimensional Systems

This chapter presents a novel filter design method that can be used for four-channel two- and three-dimensional perfect reconstructing filter banks that, when iterated, generate orthonormal wavelets for nonseparable sampling. A new three-dimensional well-behaved sampling matrix is also presented.

### 6.1 Preliminaries

In the one dimensional case, type 1 (analysis filters) and type 2 (synthesis filters) polyphase decomposition of a WDF (two-channel, bireciprocal case) may be expressed as shown in (3.3-3.6). And the filter coefficients of the PR FB (dependent on the application) can be obtained with the method shown in [Gas85]. A stable implementation of  $G_0(z)$  and  $G_1(z)$  is shown for infinite length signals in chapter 3. In the bireciprocal case, real coefficient WDFs fulfill on the unit circle

$$|H_i(e^{j\omega})|^2 + |H_i(e^{j(\omega+\pi)})|^2 = 1 \quad i = 0, 1$$

[Nos83] and cascading them in a PR WDF system preserves PR and losslessness [Vai93]. In particular, this is shown in [Som93] for M-band tree structures. See also Fig. 2.8 in chapter 2.

In one dimension, for a maximally decimated two-channel (four-channel) perfect reconstruction filter bank, downsampling by 2 (4) is used. In two dimensions, for a maximally decimated two-channel (four-channel) PR FB, a quincunx sampling matrix (hexagonal sampling matrix) having  $|\det(\mathbf{M}_q)| = 2$  ( $|\det(\mathbf{M}_{hex})| = 4$ ) is used. And in three dimensions, for a maximally decimated two-channel (four-channel) PR FB, a face centered cubic sampling matrix (body centered cubic sampling matrix) having  $|\det(\mathbf{M}_{FCCS})| = 2$  ( $|\det(\mathbf{M}_{BCCS})| = 4$ ) is used, see Table 6.1. A decimation ratio,  $r$ , of  $r = 2$  results in a dyadic sampling grid where as  $r = 4$  results in a quartic sampling grid.

	2-channel		4-channel	
	Matrix	Eigenvalues	Matrix	Eigenvalues
2-D	$\mathbf{M}_q = \begin{bmatrix} 1 & 1 \\ 1 & -1 \end{bmatrix}$	$-\sqrt{2}$ $\sqrt{2}$	$\mathbf{M}_{hex} = \begin{bmatrix} 2 & 1 \\ 0 & -2 \end{bmatrix}$	$-2$ $2$
3-D	$\mathbf{M}_{FCCS} = \begin{bmatrix} 1 & 0 & 1 \\ -1 & -1 & 1 \\ 0 & -1 & 0 \end{bmatrix}$	$2^{\frac{1}{3}}$ $-((-1)^{\frac{1}{3}}2^{\frac{1}{3}})$ $(-1)^{\frac{2}{3}}2^{\frac{1}{3}}$	$\mathbf{M}_{BCCS} = \begin{bmatrix} 1 & 0 & 1 \\ -1 & 0 & 1 \\ 1 & -2 & -1 \end{bmatrix}$	$2^{\frac{2}{3}}$ $-((-1)^{\frac{1}{3}}2^{\frac{2}{3}})$ $(-1)^{\frac{2}{3}}2^{\frac{2}{3}}$
2-D	$\mathbf{M}_q^2 = \begin{bmatrix} 2 & 0 \\ 0 & 2 \end{bmatrix}$		$\mathbf{M}_{hex}^2 = \begin{bmatrix} 4 & 0 \\ 0 & 4 \end{bmatrix}$	
3-D	$\mathbf{M}_{FCCS}^3 = \begin{bmatrix} 2 & 0 & 0 \\ 0 & 2 & 0 \\ 0 & 0 & 2 \end{bmatrix}$		$\mathbf{M}_{BCCS}^3 = \begin{bmatrix} 4 & 0 & 0 \\ 0 & 4 & 0 \\ 0 & 0 & 4 \end{bmatrix}$	

**Table 6.1** Well behaved two- and three-dimensional sampling matrices used in a PR FB. Compare [Pet62] for four-dimensional, ..., eight-dimensional sampling matrices (not well-behaved).

## 6.2 Three-Dimensional Nonseparable Orthogonal Perfect Reconstruction Filter Bank using Wave Digital Filters

The aim of this section is the design and implementation of an orthonormal 4-channel PR FB that processes three-dimensional infinite length signals with WDFs. The procedure is similar to the two-channel case presented in the previous chapter.

The block diagram representation of a 4-channel analysis FB can be defined as shown in Fig. 6.1 and will be explained next for PR. (Note that this structure can be used for the FIR and IIR filter design. However, in what follows bireciprocal WDFs will be used since they yield a computationally efficient implementation [Fet86].)

Considering one possible shape of the first Brillouin zone in frequency domain for the BCCS scheme, that is related to the lowpass filter and depicted in Fig. 6.2. One can also illustrate it with three two-dimensional graphs, shown in Fig. 6.3, that, when multiplied with each other, result in the same shape. Since the first Brillouin zone equals to the pass-band of the associated periodic low-pass filter in the Nyquist region, the design of the necessary three-dimensional filter may be carried out by cascading three two-dimensional filters. When properly designed, these filters yield an orthonormal PR FB. The associated blockdiagram, realizing a three-dimensional low-pass filter for an orthonormal 4-channel PR FB, is shown in Fig.6.4, and the associated sampling matrices are

$$\mathbf{M}_1 = \begin{bmatrix} 1 & 1 & 0 \\ 1 & -1 & 0 \\ 0 & 0 & 1 \end{bmatrix}$$

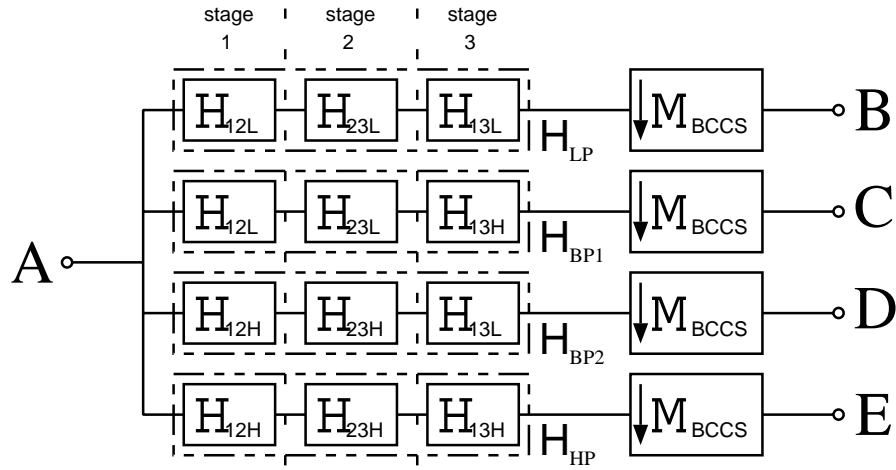


**Figure 6.1:** 4-channel analysis FB that can process three-dimensional infinite length signals. The lowpass-, bandpass- and highpass-filters as well as the nonseparable BCCS down-sampling matrices are shown. Each 3-D filter is split up in three stages. The filters of each stage are 2-D filters. Each 2-D filter can be realized with four 1-D filters and appropriate sampling matrices.

$$\mathbf{M}_2 = \begin{bmatrix} 1 & 0 & 0 \\ 0 & 1 & 1 \\ 0 & 1 & -1 \end{bmatrix}$$

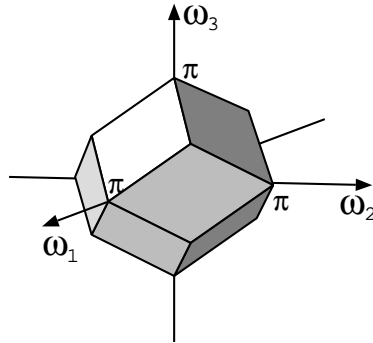


**Figure 6.2:** First Brillouin zone for the BCCS scheme.

$$\mathbf{M}_3 = \begin{bmatrix} 1 & 0 & 1 \\ 0 & 1 & 0 \\ 1 & 0 & -1 \end{bmatrix}.$$

Table 6.2 shows the aliasing frequencies [Coo95], where the frequency response of the

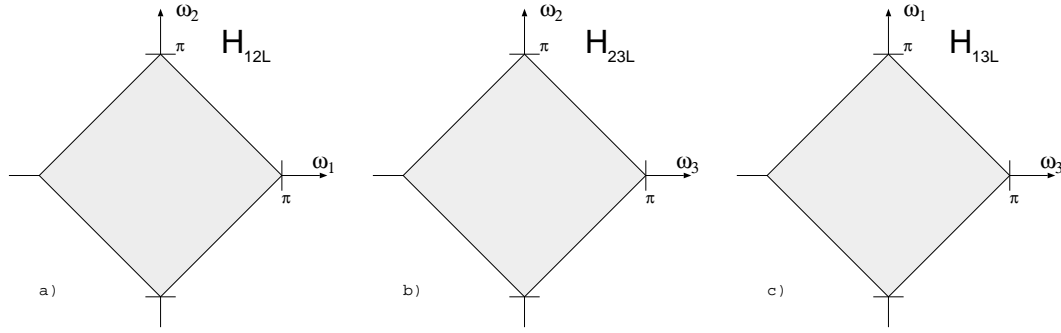


**Figure 6.3:** Nyquist region of the three filters a)  $H_{12L}$ , b)  $H_{23L}$ , c)  $H_{13L}$ , which, when cascaded, result in a three-dimensional low-pass filter (dotted areas show the passband of the filters).

	Aliasing frequencies of the low-pass filter	
	2-channel	4-channel
1-D	$\pi$	$\frac{\pi}{2}, \pi, \frac{3\pi}{2}$
2-D	quincunx sampling $\begin{bmatrix} \pi \\ \pi \end{bmatrix}$	hexagonal sampling $\begin{bmatrix} \pi \\ \frac{\pi}{2} \end{bmatrix}, \begin{bmatrix} 0 \\ \pi \end{bmatrix}, \begin{bmatrix} \pi \\ \frac{3\pi}{2} \end{bmatrix}$
3-D	FCCS $\begin{bmatrix} \pi \\ \pi \\ \pi \end{bmatrix}$	BCCS $\begin{bmatrix} \pi \\ \pi \\ 0 \end{bmatrix}, \begin{bmatrix} \pi \\ 0 \\ \pi \end{bmatrix}, \begin{bmatrix} 0 \\ \pi \\ \pi \end{bmatrix}$

**Table 6.2** Aliasing frequencies of the low-pass filter of a 2-channel and 4-channel filter bank.

lowpass filter has to be zero. The BCCS matrix can be factored as

$$\mathbf{M}_{BCCS} = \mathbf{M}_3 \mathbf{M}_{rest} = \begin{bmatrix} 1 & 0 & 1 \\ 0 & 1 & 0 \\ 1 & 0 & -1 \end{bmatrix} \begin{bmatrix} 1 & -1 & 0 \\ -1 & 0 & 1 \\ 0 & 1 & 1 \end{bmatrix}.$$

Since

$$\mathbf{M}_3^2 = \begin{bmatrix} 2 & 0 & 0 \\ 0 & 1 & 0 \\ 0 & 0 & 2 \end{bmatrix},$$

$H_{13L}$  and  $H_{13H}$  can be operated at lower sampling rate. The filters  $H_{00,1}, H_{00,2}, H_{00,3}$ , are obtained from one-dimensional filters [Got97, Fet90], e.g.

$$H_{00,1}(e^{j(\omega_1, \omega_2)}) = H_L(e^{j\omega_1})H_L(e^{j\omega_2}) + H_H(e^{j\omega_1})H_H(e^{j\omega_2}).$$

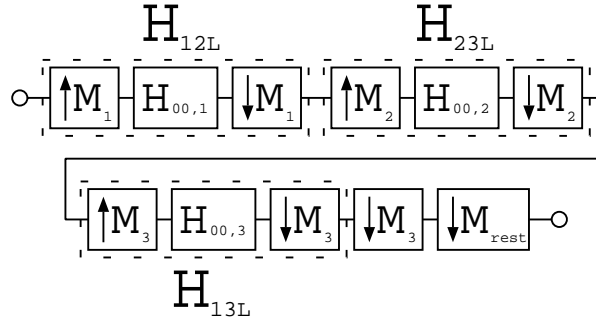


**Figure 6.4:** Realization of a three-dimensional lowpass filter used in a PR FB for BCCS.

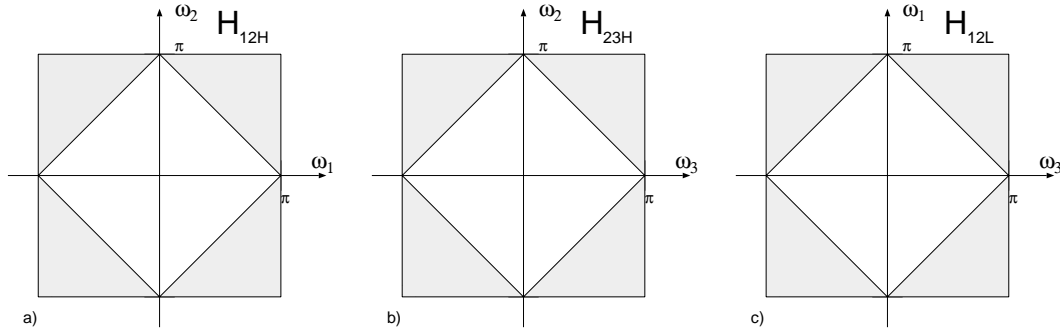


**Figure 6.5:** Nyquist region of the three filters a)  $H_{12H}$ , b)  $H_{23H}$ , c)  $H_{13H}$ , which, when cascaded, result in a three-dimensional high-pass filter (dotted areas show the passband of the filters).

The highpass filters  $H_{12H}$ ,  $H_{23H}$  and  $H_{13H}$  in Fig. 6.5 can be derived in a similar way from the filters  $H_{01,1}$ ,  $H_{01,2}$  and  $H_{01,3}$ . They are also obtained from one-dimensional filters [Got97, Fet90], e.g.

$$H_{01,1}(e^{j(\omega_1, \omega_2)}) = H_L(e^{j\omega_1})H_H(e^{j\omega_2}) + H_H(e^{j\omega_1})H_L(e^{j\omega_2}).$$

As an example, aiming towards the goal to generate Butterworth wavelets, a low-pass/highpass Butterworth realization, having a maximal number of zeros at  $\omega = \pi/\omega = 0$ , is depicted in Fig. 6.6, see [Gas85]. And using this building block in connection with the blockdiagram of Fig. 6.1, the final blockdiagram of a 4-channel PR FB, using a nonseparable BCCS scheme (analysis part), is illustrated in Fig. 6.7, where it is clear that one needs to form one sequence from the two input sequences of the downsampler by adding them together. Additional computational time is not required for the modification of the 3-D sequence into 1-D sequences of the appropriate frequency variables, shown in Fig. 6.7, since one can assign the pointers that take the samples to the appropriate registers, see also [Vet95] and references therein.

As an example, the transfer function of the bireciprocal highpass filter in Fig. 6.6 is

given, by using  $\alpha_2 = -(1 - \alpha_2^*)$ , as

$$H_H(e^{j\omega}) = 0.5(e^{j\omega} \frac{e^{j2\omega} - \alpha_1}{1 - \alpha_1 e^{j2\omega}} \frac{e^{j2\omega} - \alpha_2}{1 - \alpha_2 e^{j2\omega}} - \frac{e^{j2\omega} - \alpha_3}{1 - \alpha_3 e^{j2\omega}} \frac{e^{j2\omega} - \alpha_4}{1 - \alpha_4 e^{j2\omega}})$$

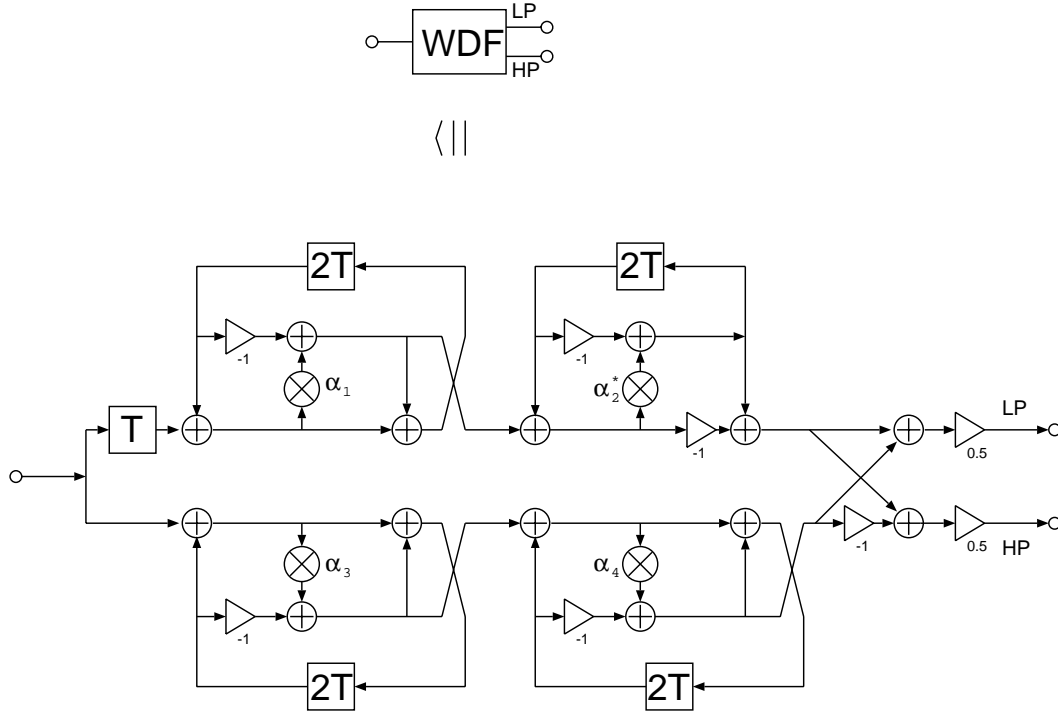


**Figure 6.6:** Butterworth type WDF using four multipliers.  $1/T =$  sampling rate.

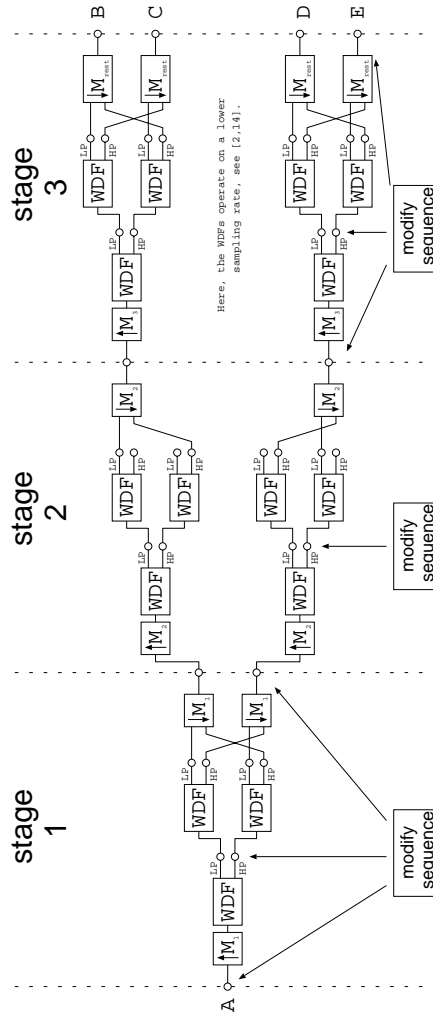


**Figure 6.7:** Analysis FB of a 4-channel PR system using a nonseparable BCCS scheme. The WDFs of stage 3 operate on a lower sampling rate due to the factorization of  $M_{BCCS} = M_3 M_{rest}$ , that allows, because of  $M_3^2$ , to implement this stage similar to a separable system, see also Ref. [Vet95, p.178] or [Got97].

and the filter coefficients are [Gas85] as in chapter 5 for (5.5).

To conclude this section, all the filters to be designed in Fig. 6.1 can be represented with cascades of 1-D filters and sampling matrices. 1-D bi reciprocal Butterworth filters were used. Since cascades of those filters preserves PR and losslessness [Vai93, Fet90], the signal A of Fig. 6.1 can be perfectly reconstructed if the associated analysis filters are designed in the required way shown e.g in [Fet85, Lei94, Mit92]. In other words, the task of reconstructing the signal as well as the design of the filters of the 3-D system is brought back to the 1-D case. And since 1-D bi reciprocal filters in a FB yield a PR system, the above method yield a 3-D PR FB.

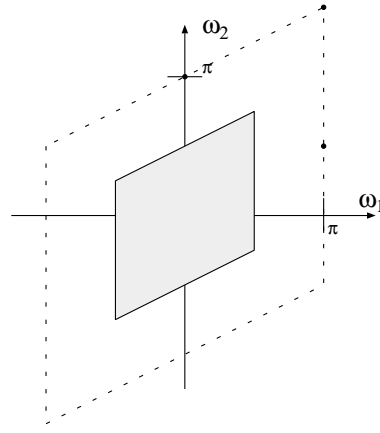


**Figure 6.8:** Frequency response of a digital lowpass filter which is used in a 4-channel multirate system using hexagonal digital/digital sampling.

### 6.3 Four-channel two-dimensional nonseparable orthogonal perfect reconstruction filter bank

The aim of this section is the design of an orthonormal four-channel PR FB that can process two-dimensional infinite length signals with WDF. The procedure is similar to the one in chapter 5 and section 6.2. However, in the previous cases halfband filters were needed exclusively, whereas in this section quarterband filters need to be designed. Two-dimensional hexagonal up/downsampling requires a periodic digital lowpass filter whose frequency response (Nyquist region) is depicted in Fig. 6.8.

The design of the necessary four filters for hexagonally sampled systems is depicted in Fig. 6.9. And the 2-D filters  $H_{00}$ ,  $H_{01}$ ,  $H_{10}$ ,  $H_{11}$  are composed of 1-D quarter band filters, which can be implemented in an internal separable way. The Figs. 6.10-6.13 show the frequency response of the four filters  $H_{LP}$ ,  $H_{BP1}$ ,  $H_{BP2}$ ,  $H_{HP}$  in the region  $-3\pi < \omega_1 < 3\pi$ ,  $-3\pi < \omega_2 < 3\pi$ , respectively. As an example, the filter degree of the quarter band filters in the Figs. 6.10-6.13 were chosen such, that each associated 1-D filter has a filter degree of 9, and the arrangement in Fig. 6.14 helps to determine the quarter band filters

$$\begin{aligned} H_{00}(e^{j(\omega_1, \omega_2)}) &= H_L(e^{j\omega_1})H_L(e^{j\omega_2}) + H_L(e^{j\omega_1})H_H(e^{j\omega_2}) \\ &\quad + H_H(e^{j\omega_1})H_H(e^{j\omega_2}) + H_H(e^{j\omega_1})H_L(e^{j\omega_2}), \end{aligned} \quad (6.1)$$

$$\begin{aligned} H_{01}(e^{j(\omega_1, \omega_2)}) &= H_{BP1}(e^{j\omega_1})H_L(e^{j\omega_2}) + H_{BP1}(e^{j\omega_1})H_H(e^{j\omega_2}) \\ &\quad + H_{BP2}(e^{j\omega_1})H_H(e^{j\omega_2}) + H_{BP2}(e^{j\omega_1})H_L(e^{j\omega_2}), \end{aligned} \quad (6.2)$$



$$H_{10}(e^{j(\omega_1, \omega_2)}) = H_L(e^{j\omega_1})H_{BP1}(e^{j\omega_2}) + H_L(e^{j\omega_1})H_{BP1}(e^{j\omega_2}) + H_H(e^{j\omega_1})H_{BP2}(e^{j\omega_2}) + H_H(e^{j\omega_1})H_{BP2}(e^{j\omega_2}), \quad (6.3)$$

$$H_{11}(e^{j(\omega_1, \omega_2)}) = H_{BP1}(e^{j\omega_1})H_{BP1}(e^{j\omega_2}) + H_{BP1}(e^{j\omega_1})H_{BP2}(e^{j\omega_2}) + H_{BP2}(e^{j\omega_1})H_{BP1}(e^{j\omega_2}) + H_{BP2}(e^{j\omega_1})H_{BP2}(e^{j\omega_2}). \quad (6.4)$$

Note, a cascade of the two half-band (bireciprocal) filters  $H_0(e^{j\omega_1})H_0(e^{j2\omega_1})$  realizes a quarter band filter  $H_L(e^{j\omega_1})$ . Alternatively one can directly design a quarter band filter, e.g. see chapter 7. All the filters in (6.1-6.4) are quarter band filters.

## 6.4 Infinite recursive tree structure (4-channel)

In general, M-band wavelets can be obtained by using an M-channel PR FB system [Som93, Ste93] that fulfills the regularity [Fli94, Str96] criterion. This is indicated in Fig. 6.15 for the N-dimensional 4-channel nonseparable case. The associated formulas, using the normalizations

$M_i(\boldsymbol{\omega}) = H_i(e^{j\boldsymbol{\omega}})/H_i(\mathbf{0})$ ,  $i = LP, BP1, BP2, HP$ , are

$$\Phi(\boldsymbol{\omega}) = \prod_{k=1}^{\infty} M_{LP}(j\mathbf{M}^{-k}\boldsymbol{\omega}) \quad (6.5)$$

$$\Psi_{BP1}(\boldsymbol{\omega}) = M_{BP1}(j\mathbf{M}^{-1}\boldsymbol{\omega})\prod_{k=2}^{\infty} M_{LP}(j\mathbf{M}^{-k}\boldsymbol{\omega}) \quad (6.6)$$

$$\Psi_{BP2}(\boldsymbol{\omega}) = M_{BP2}(j\mathbf{M}^{-1}\boldsymbol{\omega})\prod_{k=2}^{\infty} M_{LP}(j\mathbf{M}^{-k}\boldsymbol{\omega}) \quad (6.7)$$

$$\Psi_{HP}(\boldsymbol{\omega}) = M_{HP}(j\mathbf{M}^{-1}\boldsymbol{\omega})\prod_{k=2}^{\infty} M_{LP}(j\mathbf{M}^{-k}\boldsymbol{\omega}). \quad (6.8)$$

In the two-dimensional case, for hexagonal up/downsampling, (6.5) and (6.7) are separable for the ideal filters in the sense that they can be expressed directly in terms of one dimensional functions, i.e.

$$\Phi_{hex}(\boldsymbol{\omega}) = \Phi(\omega_1)\Phi(\omega_2)$$

$$\Psi_{hex, BP2}(\boldsymbol{\omega}) = \Psi(\omega_1)\Phi(\omega_2)$$

or in time domain as

$$\varphi_{hex}(\mathbf{t}) = \varphi(t_1)\varphi(t_2)$$

$$\psi_{hex, BP2}(\mathbf{t}) = \psi(t_1)\varphi(t_2),$$

compare the Figs. 6.16-6.19.

Note that a tensor product-realization for the four-channel case would result in a system with 15 wavelets and one scaling function.

## 6.5 Conclusion

Novel four-channel two- and three-dimensional filters are presented. They are very much suitable in filter bank applications that use a multidimensional, nonseparable,

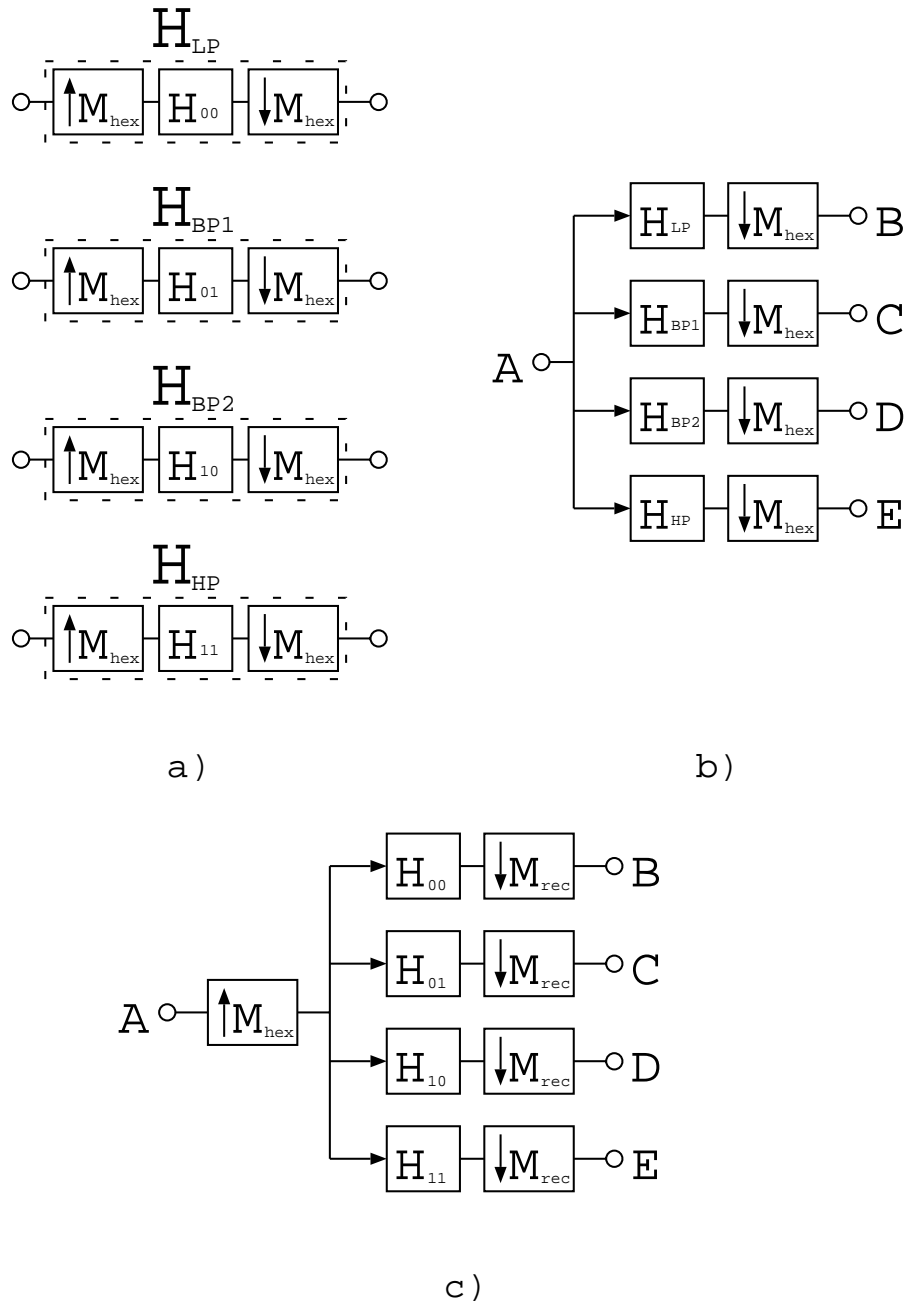


**Figure 6.9:** a) Design of the four two-dimensional filters used in a PR FB for hexagonal digital/digital sampling shown in b). After upsampling with  $M_{hex}$  in c), the right part constitutes a separable filter bank, see [Vet95].

orthonormal wavelet transform. In the three-dimensional case, halfband filters need to be designed, whereas in the two-dimensional case quarterband filters are used. Both four-channel filter designs (two- and three-dimensional) can be treated with one-dimensional filter design techniques.

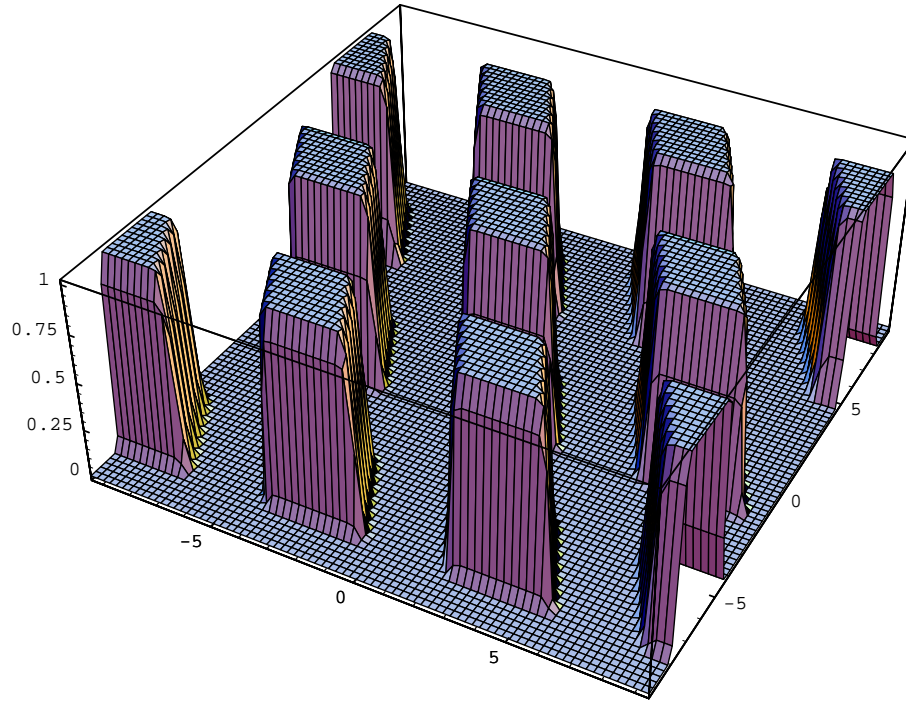


**Figure 6.10:** Frequency response of  $H_{LP}(e^{j\omega})$  in the region  $-3\pi < \omega_1 < 3\pi$ ,  $-3\pi < \omega_2 < 3\pi$ .

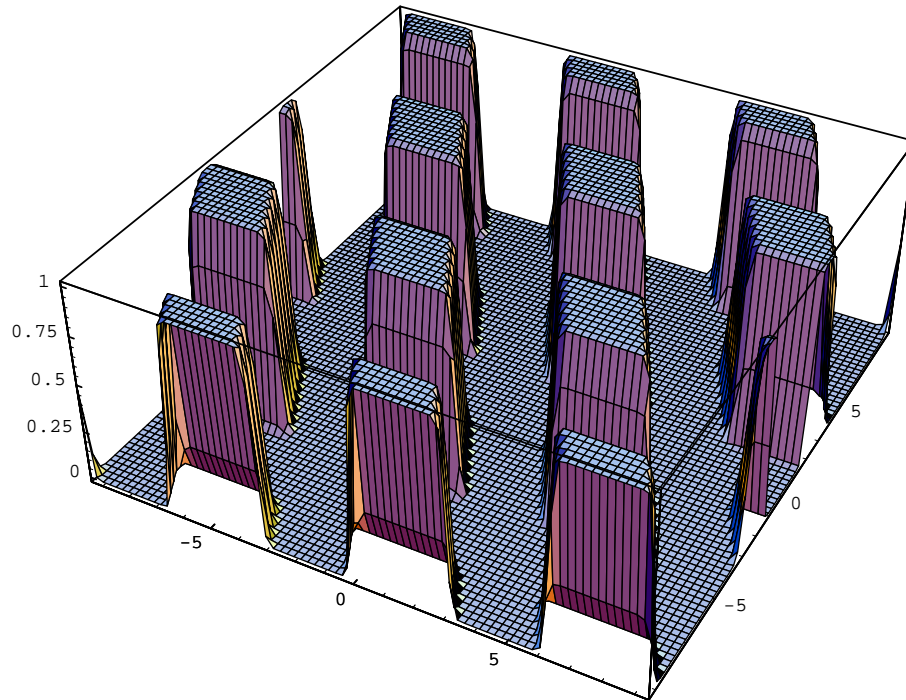


**Figure 6.11:** Frequency response of  $H_{BP1}(e^{j\omega})$  in the region  $-3\pi < \omega_1 < 3\pi$ ,  $-3\pi < \omega_2 < 3\pi$ .

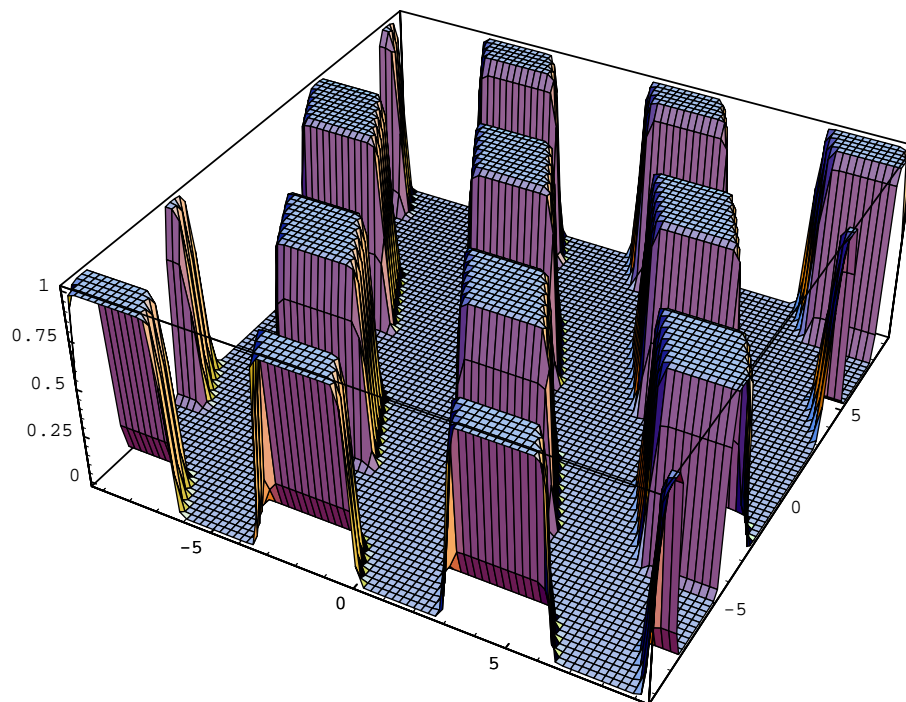


**Figure 6.12:** Frequency response of  $H_{BP2}(e^{j\omega})$  in the region  $-3\pi < \omega_1 < 3\pi$ ,  $-3\pi < \omega_2 < 3\pi$ .

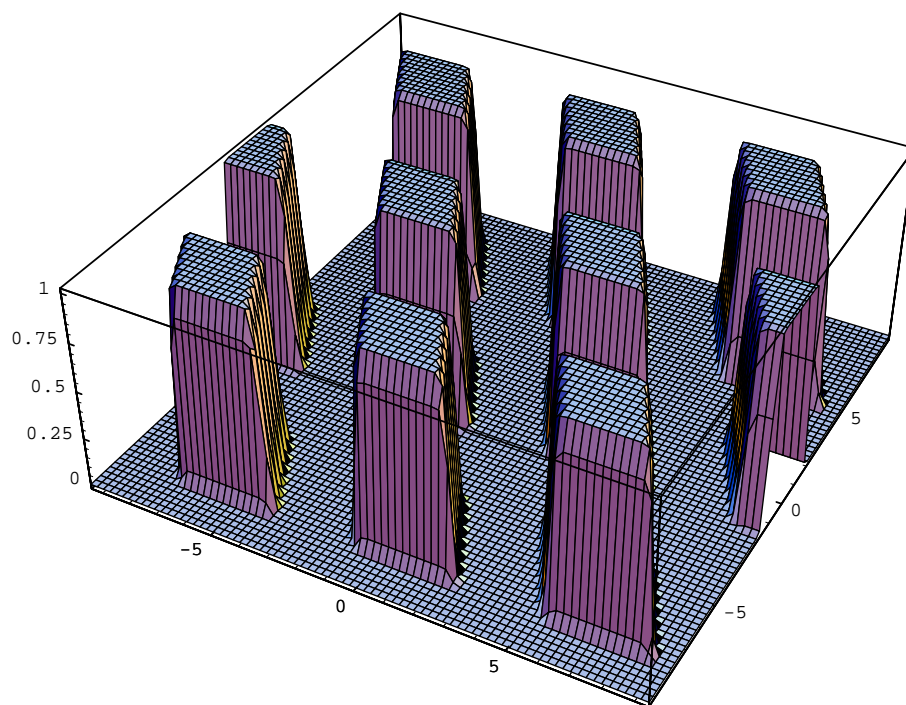


**Figure 6.13:** Frequency response of  $H_{HP}(e^{j\omega})$  in the region  $-3\pi < \omega_1 < 3\pi$ ,  $-3\pi < \omega_2 < 3\pi$ .

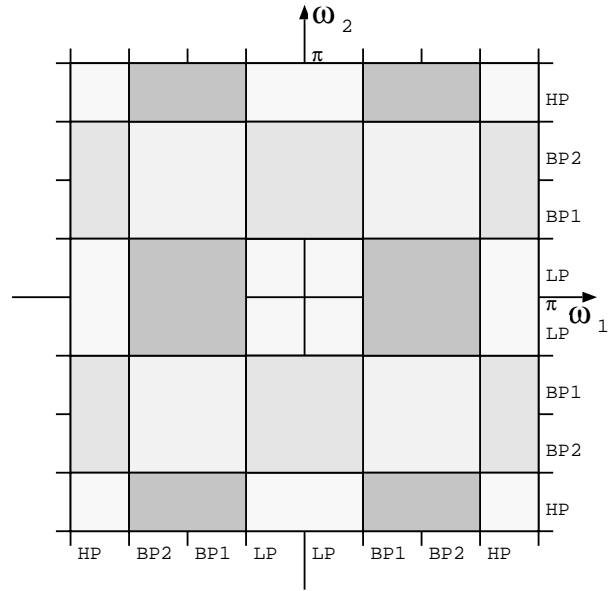


**Figure 6.14:** Arrangement that helps to determine the four quarter band filters.

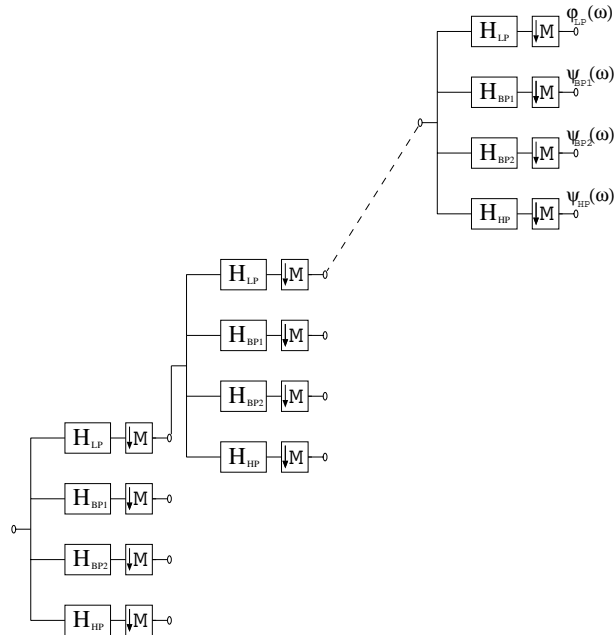


**Figure 6.15:** a) Computation of a 4-channel N-dimensional discrete wavelet transform using a filter bank.

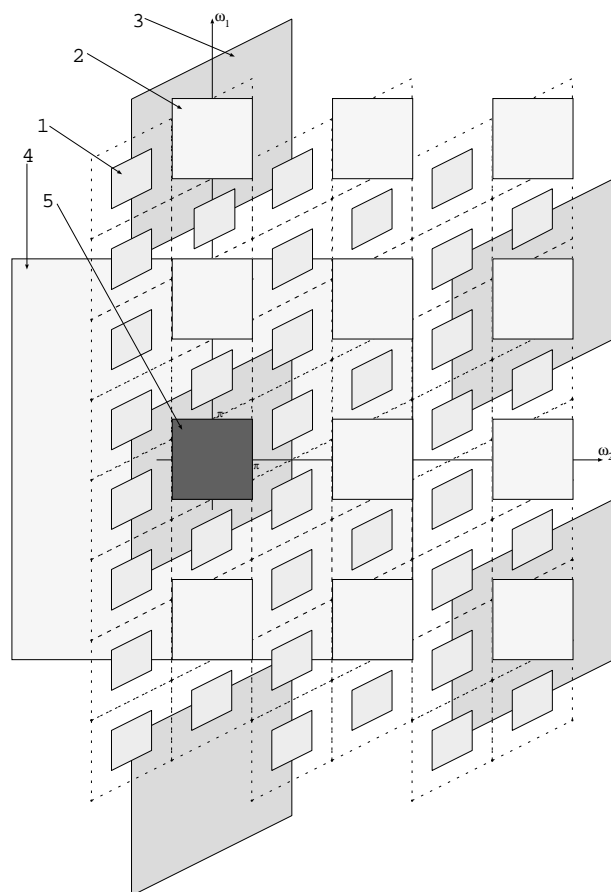


**Figure 6.16:** Various dilated versions of the ideal basic lowpass filter, indicated with 1, 2, 3, and 4, which take part in the infinite product. The separable scaling function,  $\Phi_{hex}(\omega)$ , for hexagonal digital/digital sampling is indicated with number 5.

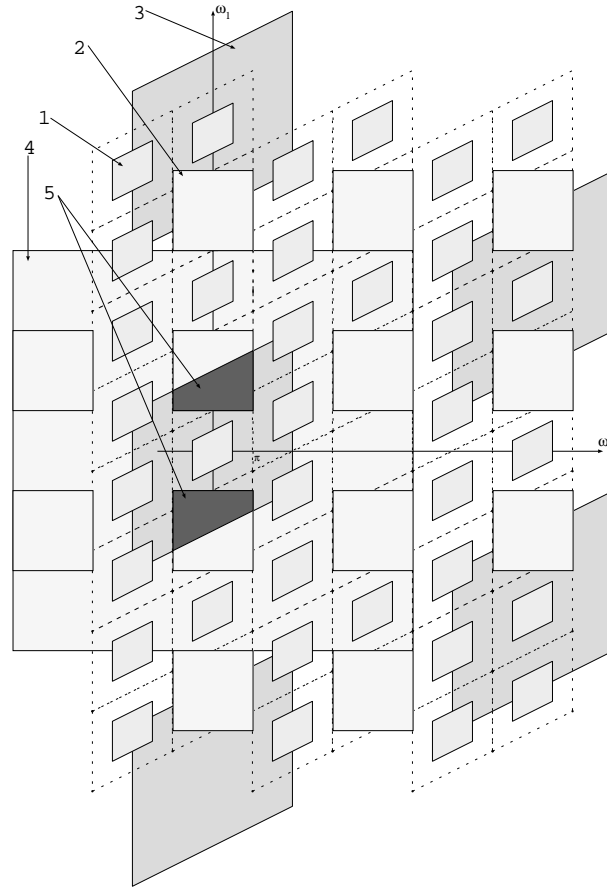


**Figure 6.17:** Various dilated versions of the ideal basic lowpass filter, indicated with 1, 2, 3, and 4, which take part in the infinite product. 2 represents a dilated version of the bandpass filter. The wavelet,  $\Psi_{hex,BP1}(\omega)$ , for hexagonal digital/digital sampling is indicated with number 5.

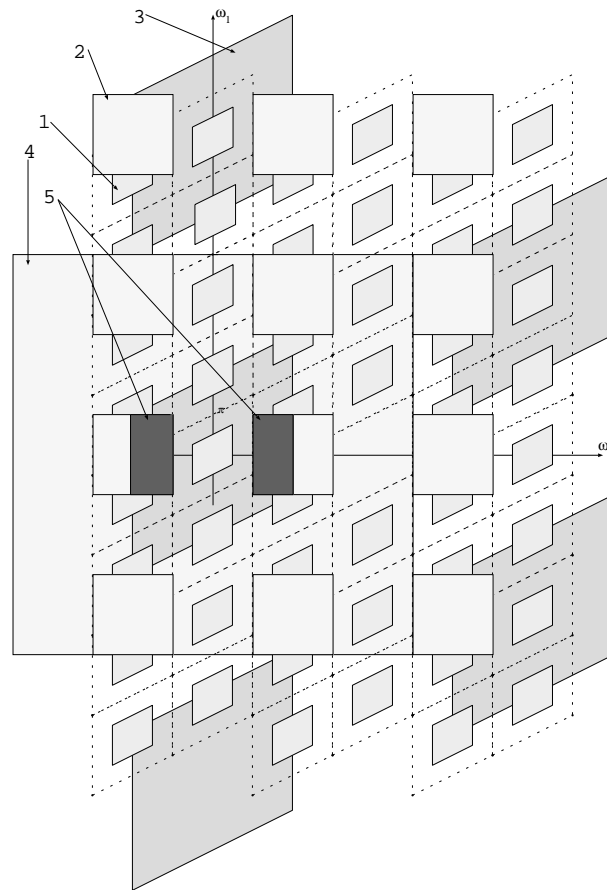


**Figure 6.18:** Various dilated versions of the ideal basic lowpass filter, indicated with 1, 3, and 4, which take part in the infinite product. 2 represents a dilated version of the highpass filter. The separable wavelet,  $\Psi_{hex,BP2}(\omega)$ , for hexagonal up/downsampling is indicated with number 5.



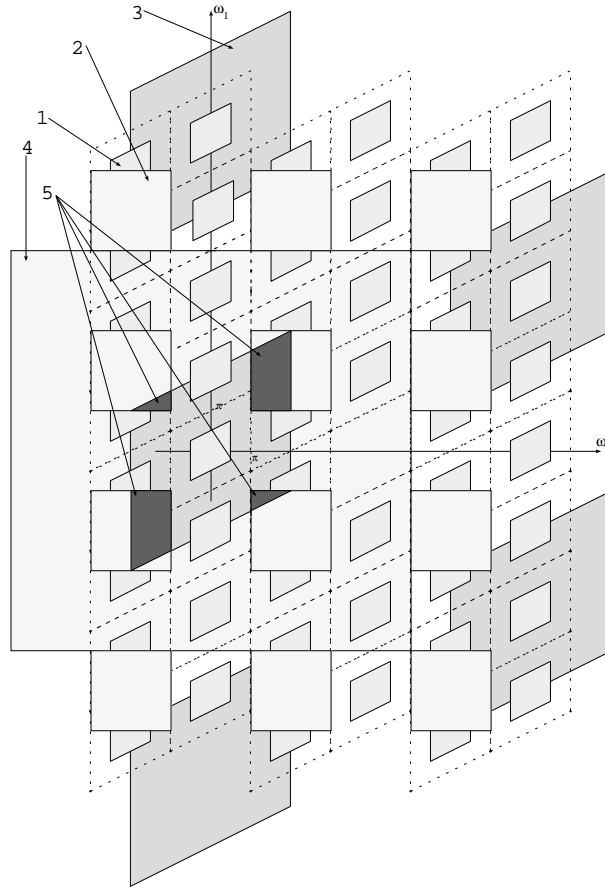


**Figure 6.19:** Various dilated versions of the ideal basic lowpass filter, indicated with 1, 3, and 4, which take part in the infinite product. 2 represents a dilated version of the bandpass filter. The wavelet,  $\Psi_{hex,HP}(\omega)$ , for hexagonal digital/digital sampling is indicated with number 5.

# Chapter 7

## Ladder Wave Digital Filter

In this chapter a novel design method for ladder wave digital filters for four-channel two-dimensional perfect reconstruction filter banks is presented. The presented design method, compared to bireciprocal lattice wave digital filter realizations, gives a better performance, e.g. for a Butterworth filter realization about half filter coefficients are necessary. The filters can readily be used in a hexagonally sampled filter bank, discussed in the previous chapter.

### 7.1 Explicit formulas for IIR filters

Provided that the number of channels is equal to the up/downsampling factor  $M$ , a filter bank has the PR property if and only if the corresponding transmultiplexer has the PR property [Ste93]. For real filter coefficients, this means that the four filters in an analysis 4-channel PR FB have to satisfy

$$|H_{LP}(e^{j\omega})|^2 + |H_{BP1}(e^{j\omega})|^2 + |H_{BP2}(e^{j\omega})|^2 + |H_{HP}(e^{j\omega})|^2 = 1,$$

and if the iterated FB is required to generate wavelet bases, then  $H_{LP}(e^{j\omega})$  has to

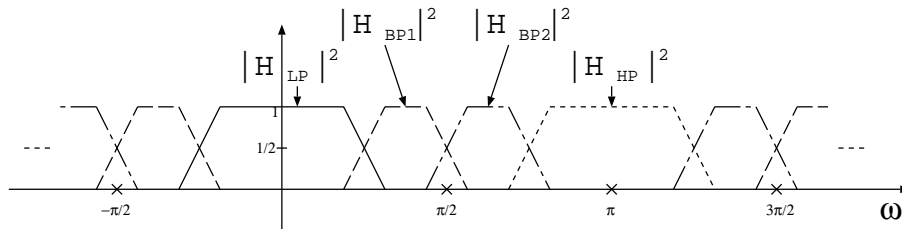


**Figure 7.1:** Magnitude of the filters of a 4-channel PR FB. Aliasing frequency locations of  $H_{LP}$  are indicated with a cross.

have zeros at the aliasing frequencies. They are depicted in Table 7.1. If the associated wavelets are required to have equal differentiability, then the zeros have to be equally distributed. Hence, only odd-order filters having  $3(2i - 1)$  zeros,  $i \in \mathbf{N}/0$ , are of

interest. Figure 7.1 illustrates the filtering scheme.

The aim in this chapter is to design a 2-D quarter band filter for a PR system. In

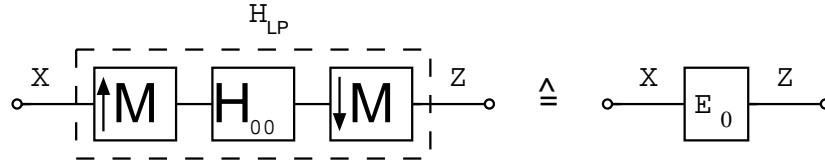


**Figure 7.2:**  $0^{th}$  Type 1 polyphase component of  $H_{00}(e^{j\omega_0, \omega_1})$ .  $E_0(\omega_0, \omega_1 = H_{LP}(\omega_0, \omega_1)$  is used as the proper filter for hexagonal downsampling, see [Got97].

general these filters are nonseparable for hexagonal sampling (4-channel case). However, the proposed method starts with separable filters, see also [Got97]. The  $0^{th}$  type 1 polyphase component of the separable two-dimensional low pass filter  $H_{00}$  is used as the proper low pass filter  $H_{LP}$  for hexagonal sampling, see Fig. 7.2. The necessary other three filters,  $H_{BP1}$ ,  $H_{BP2}$  and  $H_{HP}$  for the filter bank, can be realized similarly. Since the obtained filters are also separable, one can use 1-D tools to show the PR property, namely, cascading of 1-D PR FB preserves the PR property [Vai93, Got97].

Bireciprocal (half band) WDF are very efficient because they can be realized as lattice WDF. Quarter band WDF in a PR system can be efficiently realized with ladder WDF. Such an arrangement is illustrated in Fig. 7.3.

In the 1-D case, cascades of lattice bireciprocal WDF require less filter coefficients compared to quarter band ladder WDF, since the number of multipliers is canonic to the filter degree for a ladder realization and the number of multipliers for the same filter in lattice realization is half! However, this is not true in the considered 2-D case. As will be shown below, a ladder realization results in a structure using less multipliers compared to a lattice realization. This is due to a possible polyphase realization. The  $0^{th}$  polyphase component of  $H_{00}(e^{j(\omega_0, \omega_1)})$  is realized in a polyphase structure.

One advantage of the WDF method over other digital filter design methods is that one has explicit formulas. In what follows, we use Butterworth polynomials. (Rational Chebyshev polynomials could also be used instead.)

The frequency response of a 1-D reference filter of an associated bireciprocal WDF is defined as (low pass):

$$|H_{ref}(s)|^2 = H_{ref}(s)H_{ref}(-s) = \frac{1}{1 - s^{2N}}$$

where  $N$  is the filter degree; e.g. for  $N = 9$

$$H_0(s) = \frac{1}{(1+s)(1+s+s^2)(1+s^3+s^6)}$$

$$H_0(z) = \frac{(1+z^9)}{2z(1+3z^2)(1+33z^2+27z^4+3z^6)}$$

Aliasing frequencies of the lowpass filter		
analog reference filter (T=1)	WDF	
$\Omega_1 = 1$	$\omega_1 = \frac{\pi}{2}$	$z_1 = j$
$\Omega_2 \rightarrow \infty$	$\omega_2 = \pi$	$z_2 = -1$
$\Omega_3 = -1$	$\omega_3 = \frac{3\pi}{2}$	$z_3 = -j$

**Table 7.1** Aliasing frequencies of the lowpass filter.

The frequency response of a 1-D reference filter of an associated quarter band WDF is defined as (using a Butterworth polynomial  $K(s) = (-1)^N s^{2N}$ , for real filter coefficients is N odd):

$$|H_{ref,LP}(s)|^2 = \frac{1}{1 + K(s)} \frac{1}{1 + K(\frac{2s}{1+s^2})} \quad (7.1)$$

$$|H_{ref,HP}(s)|^2 = \frac{1}{1 + K(1/s)} \frac{1}{1 + K(\frac{2s}{1+s^2})}$$

$$|H_{ref,BP1}(s)|^2 = \frac{1}{1 + K(s)} \frac{1}{1 + K(\frac{s^2+1}{2s})}$$

$$|H_{ref,BP2}(s)|^2 = \frac{1}{1 + K(1/s)} \frac{1}{1 + K(\frac{s^2+1}{2s})} \quad (7.2)$$

e.g. for  $N = 9$

$$\begin{aligned} H_{LP}(s) &= (1 + s^2)^9 / ((1 + s)^3 (1 + s + s^2) (1 + 2s + 6s^2 \\ &\quad + 2s^3 + s^4) (1 + s^3 + s^6) (1 + 6s^2 + 8s^3 + 15s^4 + 24s^5 \\ &\quad + 84s^6 + 24s^7 + 15s^8 + 8s^9 + 6s^{10} + s^{12})) \\ H_{LP}(z) &= ((1 + z)^9 (1 + z^2)^9) / (4z^3 (1 + 3z^2) (1 + 3z^4) \\ &\quad (1 + 33z^2 + 27z^4 + 3z^6) (1 + 33z^4 + 27z^8 + 3z^{12})) \end{aligned} \quad (7.3)$$

Note, that the low-pass quarter band filter  $H_{LP}(z)$  is a digital filter, but not a WDF!

## 7.2 Four channel polyphase arrangements

Fig. 7.4 illustrates the deriviation of the four polyphase components generated by

$$\mathbf{M} = \begin{bmatrix} 2 & 1 \\ 0 & -2 \end{bmatrix},$$

$\mathbf{k}_0 = [0 \ 0]^T$ ,  $\mathbf{k}_1 = [1 \ 0]^T$ ,  $\mathbf{k}_2 = [1 \ -1]^T$ ,  $\mathbf{k}_3 = [2 \ -1]^T$  and hence we can draw the type 1 polyphase implementation of a filter with  $M$  as in Fig. 7.5.

To show the effectiveness of this design method, an FIR and IIR example will be presented. As an FIR example we consider a filter with  $N=5$ . In 1-D we can decompose

$$H_{LP}(z) = A + Bz^{-1} + Cz^{-2} + Dz^{-3} + Ez^{-4} + Fz^{-5} \quad (7.4)$$

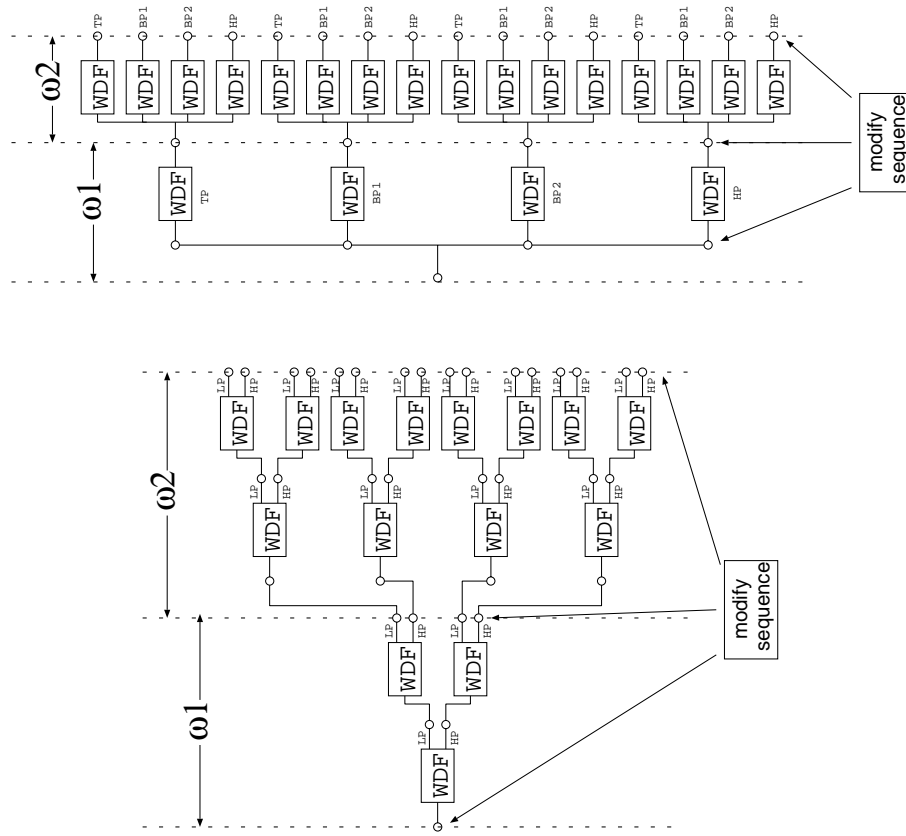


**Figure 7.3:** Possible filter arrangements to realize the 2-D quarter band filters. a) Bireciprocal (half band) WDF arrangement, b) quarter band WDF arrangement. Note, the filters in a) are directly implemented where as the filters in b) are the starting point of the three step design of the polyphase filters in Fig. 7.5.

( $M=4$ ) as shown in Fig. 7.6. And the high pass filter follows as

$$H_{HP}(z) = F - Ez^{-1} + Dz^{-2} - Cz^{-3} + Bz^{-4} - Az^{-5}. \quad (7.5)$$

In 2-D we can decompose (valid for FIR and IIR filters), see also (6.10),

$$\begin{aligned} H_{00}(z_0, z_1) = & H_{LP}(z_0)H_{LP}(z_1) + H_{HP}(z_0)H_{HP}(z_1) + \\ & H_{HP}(z_0)H_{LP}(z_1) + H_{LP}(z_0)H_{HP}(z_1) \end{aligned}$$

as indicated in Fig. 7.7. It is now obvious from Fig. 7.7 that the coefficients surrounded by a circle represent the  $0^{th}$  type 1 polyphase component of  $H_{00}$  from Fig. 7.2. Hence we can write

$$\begin{aligned} H_{LP}(z_0, z_1) = & (A + Cz_0^{-1} + Ez_0^{-2})(A + Cz_1^{-1} + Ez_1^{-2}) \\ & + (A + Cz_0^{-1} + Ez_0^{-2})(F + Dz_1^{-1} + Bz_1^{-2}) \\ & + (F + Dz_0^{-1} + Bz_0^{-2})(F + Dz_1^{-1} + Bz_1^{-2}) \\ & + (F + Dz_0^{-1} + Bz_0^{-2})(A + Cz_1^{-1} + Ez_1^{-2}) \end{aligned} \quad (7.6)$$

It clearly shows, that we can implement  $H_{LP}$  with 1-D filters. And they have only half the coefficients than the ones we started off with. The same can be done with IIR

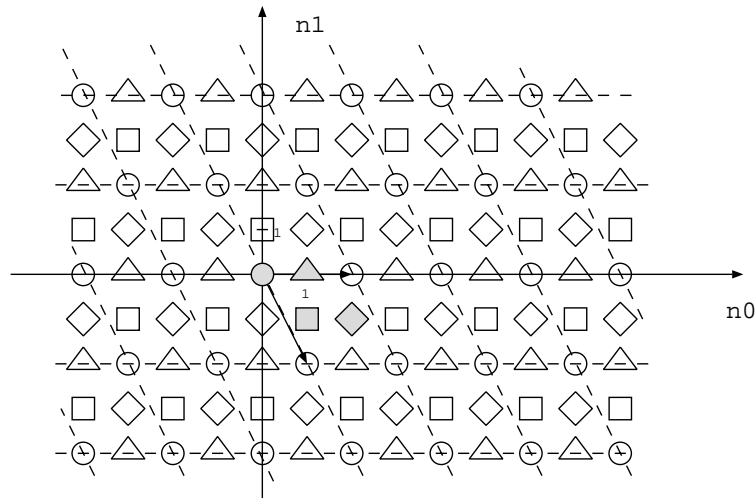


**Figure 7.4:** Demonstrating the four polyphase components generated by  $M$ .

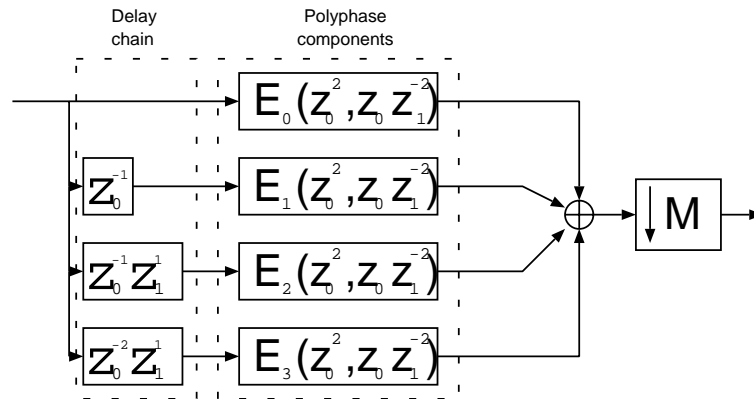


**Figure 7.5:** Type 1 polyphase implementation of a filter with  $M$ .

$$\begin{aligned}
 H_{LP}(z) &= \sum_n h(nM) z^{-nM} \\
 &+ z^{-1} \sum_n h(nM+1) z^{-nM} \\
 &+ z^{-2} \sum_n h(nM+2) z^{-nM} \\
 &+ z^{-3} \sum_n h(nM+3) z^{-nM} \\
 H_{LP}(z) &= \text{A} + \text{B}z^{-1} + \text{C}z^{-2} + \text{D}z^{-3} + \text{E}z^{-4} + \text{F}z^{-5}
 \end{aligned}$$

**Figure 7.6:** Four polyphase components of the 1-D low pass filter.

filters. As we have experienced with our previous FIR example, the coefficients of the odd powers of  $z_i$ ,  $i=0,1$ , are set to zero and the even powers of  $z_i$  are renumbered. In the IIR case this is done in the numerator as well as in the denominator, e.g. (using (7.3),

$$H_{LP}(z_0, z_1) = \frac{(1+z_0)^9(3+z_0)(3+27z_0+33z_0^2+z_0^3)}{z_0(1+3z_0)(1+3z_0^2)(1+33z_0+27z_0^2+3z_0^3)(1+33z_0^2+27z_0^4+3z_0^6)} \cdot \frac{(1+z_1)^9(3+z_1)(3+27z_1+33z_1^2+z_1^3)}{z_1(1+3z_1)(1+3z_1^2)(1+33z_1+27z_1^2+3z_1^3)(1+33z_1^2+27z_1^4+3z_1^6)} \quad (7.7)$$

The other three filters follow as

$$H_{HP}(z_0, z_1) = \frac{(-1+z_0)^9(3+z_0)(3+27z_0+33z_0^2+z_0^3)}{z_0(1+3z_0)(1+3z_0^2)(1+33z_0+27z_0^2+3z_0^3)(1+33z_0^2+27z_0^4+3z_0^6)} \cdot \frac{(1+z_1)^9(3+z_1)(3+27z_1+33z_1^2+z_1^3)}{z_1(1+3z_1)(1+3z_1^2)(1+33z_1+27z_1^2+3z_1^3)(1+33z_1^2+27z_1^4+3z_1^6)}$$

$$H_{BP1}(z_0, z_1) = \frac{(-1+z_0)^9(3+z_0)(3+27z_0+33z_0^2+z_0^3)}{z_0(1+3z_0)(1+3z_0^2)(1+33z_0+27z_0^2+3z_0^3)(1+33z_0^2+27z_0^4+3z_0^6)} \cdot \frac{(-1+z_1)^9(3+z_1)(3+27z_1+33z_1^2+z_1^3)}{z_1(1+3z_1)(1+3z_1^2)(1+33z_1+27z_1^2+3z_1^3)(1+33z_1^2+27z_1^4+3z_1^6)}$$

$$H_{BP2}(z_0, z_1) = \frac{(1+z_0)^9(3+z_0)(3+27z_0+33z_0^2+z_0^3)}{z_0(1+3z_0)(1+3z_0^2)(1+33z_0+27z_0^2+3z_0^3)(1+33z_0^2+27z_0^4+3z_0^6)} \cdot \frac{(-1+z_1)^9(3+z_1)(3+27z_1+33z_1^2+z_1^3)}{z_1(1+3z_1)(1+3z_1^2)(1+33z_1+27z_1^2+3z_1^3)(1+33z_1^2+27z_1^4+3z_1^6)}$$

Having obtained the two 1-D filters from the  $\mathbf{0}^{th}$  type 1 polyphase component of  $Q_0$  from Fig. 7.2, one simply goes back to the s-domain by using (3.2) and applies the standard method to design a WDF, see also (2.25) and Fig. 2.4. Note, the four 2-D filters can be realized with three 1-D WDF.

Fig. 7.3a) needs 80 and, again assuming a canonical ladder realization with respect to multipliers. The proposed design method requires 39 operations per output sample.

So far we have realized the  $\mathbf{0}^{th}$  type 1 polyphase component from Fig. 7.2. However, we can still improve the filter bank. For the quarter band case this is due to the fact that one can apply again a polyphase decomposition. Both realizations reduce the number of required operations again.

The four polyphase components of the ladder WDF realization are again composed of separable 1-D filters.  $E'_0(z_0, z_1)$  (starting from  $H_{LP}(z_0, z_1)$ ) is composed of the even

coefficients of the 1-D filter in  $z_0$  and of the even coefficients of the 1-D filter in  $z_1$ . Continuing the previous FIR example

$$\begin{aligned} E'_0(z_0, z_1) &= (A + Ez_0^{-1})(A + Ez_1^{-1}) + (A + Ez_0^{-1})(F + Bz_1^{-1}) \\ &+ (F + Bz_0^{-1})(F + Bz_1^{-1}) + (F + Bz_0^{-1})(A + Ez_1^{-1}). \end{aligned} \quad (7.8)$$

$E'_1(z_0, z_1)$ ,  $E'_2(z_0, z_1)$  and  $E'_3(z_0, z_1)$  are also separable 2-D filters and it is now straight forward to derive them with the help of Fig. 7.7.

$$\begin{aligned} E'_1(z_0, z_1) &= (\text{odd of } z_0)(\text{even of } z_1) \\ E'_2(z_0, z_1) &= (\text{odd of } z_0)(\text{odd of } z_1) \end{aligned} \quad (7.9)$$

$$E'_3(z_0, z_1) = (\text{even of } z_0)(\text{odd of } z_1) \quad (7.10)$$

Note, if one combines analog reference filters in (7.1-7.2), e.g. elliptic filters and Butterworth filters, then one can reduce the regularity and increase the frequency selectivity of the wavelet.

## 7.3 Conclusion

This chapter presents a new filter design method to design FIR and IIR filters for hexagonally sampled signals. The resulting filters in ladder structure have much less complexity compared to filters in lattice structure. A similar statement is true for FIR filters.



**Figure 7.7:** Four polyphase components of the 2-D low pass filter. The circles mark the filter coefficients that belong to  $E_0(z_0^2, z_0 z_1^{-2})$ . The triangles mark the filter coefficients that belong to  $E_1(z_0^2, z_0 z_1^{-2})$ . The squares mark the filter coefficients that belong to  $E_2(z_0^2, z_0 z_1^{-2})$ . The diamonds mark the filter coefficients that belong to  $E_3(z_0^2, z_0 z_1^{-2})$ . The periodicity of the filter is indicated in one direction. The shifted delay chain is also indicated (shaded elements).

# Chapter 8

## Conclusion

This thesis shows new filters of analog as well as of digital type. Their design purpose lies in the wavelet transform for one-, two- and three-dimensions. Application examples of the wavelet transform were not discussed. However they can be found e.g. in [Fli94, Vet95, Ans96, Rao96]. Especially wave digital filters (WDF) were used. They turn out to be best suited filters for the wavelet transform. This is due to their low-sensitivity property as well as due to the efficiency with which they can be implemented (big hardware savings compared to other existing structures, e.g. direct structure, are possible). The novel multidimensional wave digital filters are used in an orthonormal filter bank for nonseparable sampling. Furthermore, new wavelets, such as the raised cosine wavelet and the Chebyshev wavelet, are presented. In addition a filter of very low complexity that performs a shift  $\tau \in \mathbf{R}$  on the expansion coefficients (wavelet coefficients) is given. Scaling functions are classified into "valid" and "approximating" scaling functions in respect to Shannon sampling, since Shannon sampling offers a lower minimum sampling rate than wavelet sampling.

# Appendix A

## Sampling lattice

First, 2-D sampling lattices will be briefly shown in this section. For more details it is referred to, e.g., [Pet62, Vai93, Vet95]. Finally a proof for the design of the two dimensional, orthonormal, nonseparable filters in chapter 5 is presented.

### Sampling lattices

Let sampling of an analog 2-D signal  $x(t_0, t_1)$  result in  $x(n_0, n_1)$ , where the set of all sample points is the set

$$\mathbf{t} = \begin{bmatrix} t_0 \\ t_1 \end{bmatrix} = V \begin{bmatrix} n_0 \\ n_1 \end{bmatrix}.$$

$V$  is called sampling matrix and is a real, nonsingular matrix. The lattice (marked with cross points) generated by  $V$  (using  $U = 2\pi V^{-T}$ ,  $T_0 = T_1 = \pi/\sigma$ ,  $\Omega_0 = \omega_0/T_0$ ,  $\Omega_1 = \omega_1/T_1$ ) for

$$V = \begin{bmatrix} T_0 & 0 \\ 0 & T_1 \end{bmatrix} \quad (\text{A.1})$$

is depicted in figure A.1 b), the lattice generated by (using  $T_0 = \sqrt{3}T_1 = \pi/\sigma$ )

$$V = \begin{bmatrix} T_0 & -T_0 \\ T_1 & T_1 \end{bmatrix} \quad (\text{A.2})$$

is depicted in figure A.1 c). The sampling density, (see (5.1)), for (A.1) is  $\frac{\sigma^2}{\pi^2}$ , for (A.2) is  $\frac{\sqrt{3}\sigma^2}{\pi^2}$ . For the above, rectangular sampling under circular support and hexagonal sampling under circular support was assumed, respectively. It is shown in [Pet62] that for 2-D systems there is no more efficient sampling scheme for circularly bandlimited signals than hexagonal sampling. The sampling efficiency under circular support for rectangular sampling is 78.5%; for hexagonal sampling 90.8%. Intermediate solutions exist. Figure A.1 depicts the effect of rectangular and hexagonal sampling under circular support. It can be seen that the circles are more tightly packed for hexagonal sampling.

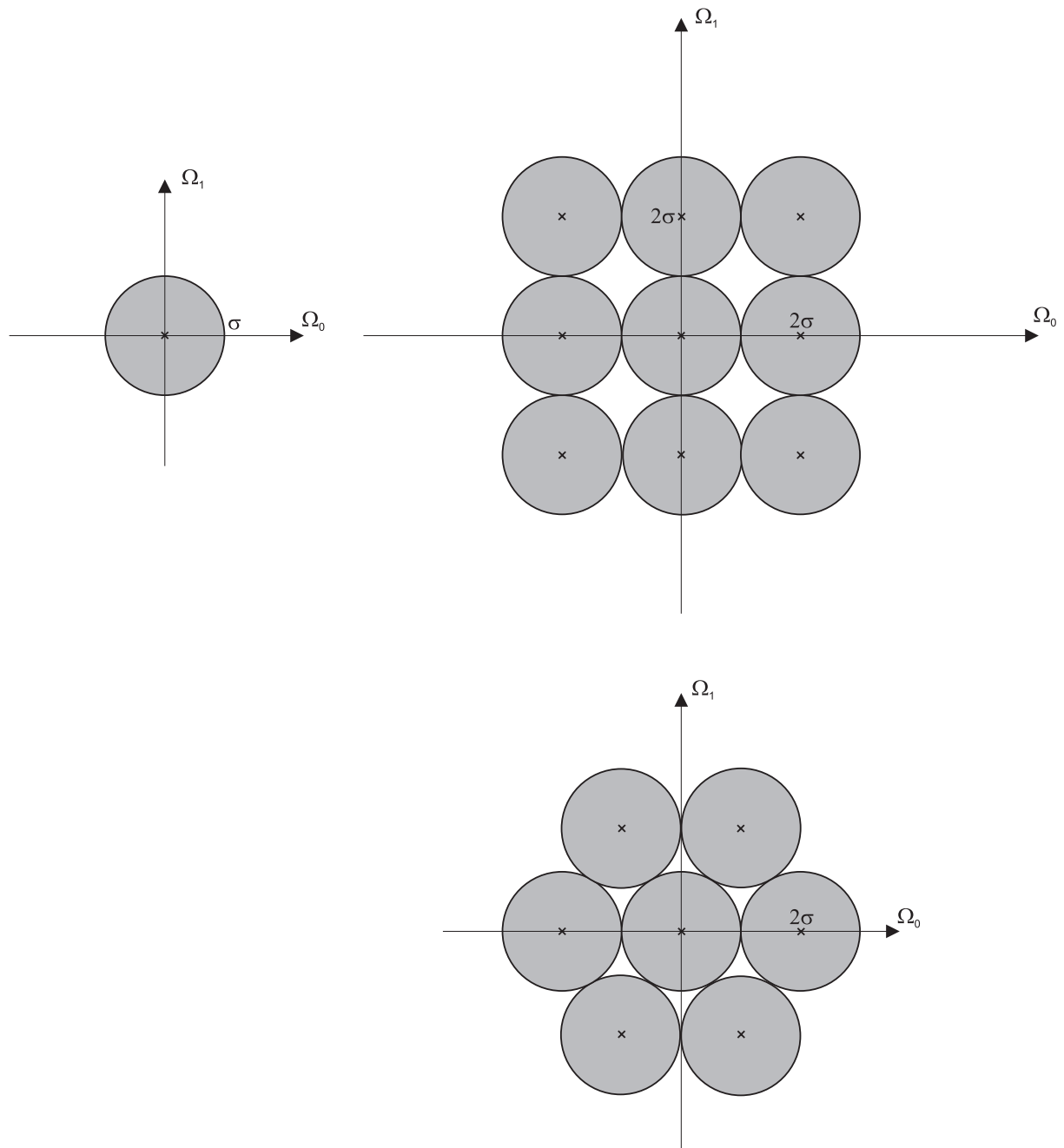


**Figure A.1:** Effect of sampling under circular support: a) support of a 2-D lowpass signal, b) effect of rectangular sampling and c) effect of hexagonal sampling.

One can show that there exist infinite number of sampling matrices resulting in the same lattice, see [Vai93]. The same is true for (digital/digital) downsampling matrices. However, whereas sampling matrices can have real valued entries, downsampling matrices can only have integer entries.

Coding gain in subband coding is maximized by opting nonseparable systems [Vet95].

Thus, in a two dimensional system, quincunx downsampling is often used for a two channel subband coding system, and hexagonal downsampling is often used for a four channel subband coding system.

One can fit hexagonal patterns into lattices generated by rectangular, hexagonal or quincunx matrices, see figure A.2. Hence, one needs to be careful with the term hexagonal [Vai93].

In figure A.2, sampling density is reduced by a factor of four for the separable downsampling, four for the hexagonal downsampling and by a factor of two for quincunx downsampling, see also chapter 5 and 6. If images have circularly symmetric power spectrums that decrease with higher frequencies, then the quincunx lowpass filter will retain more of the original signal's energy than a separable lowpass filter [Vet95]. Using the same argument, the hexagonal lowpass filter is then better than the corresponding lowpass filter in a separable system with downsampling by two in each dimension [Vet95]. Such preprocessing (using nonseparable downsampling) has been used in socalled intraframe coding of high definiton television (HDTV) [Rao96].

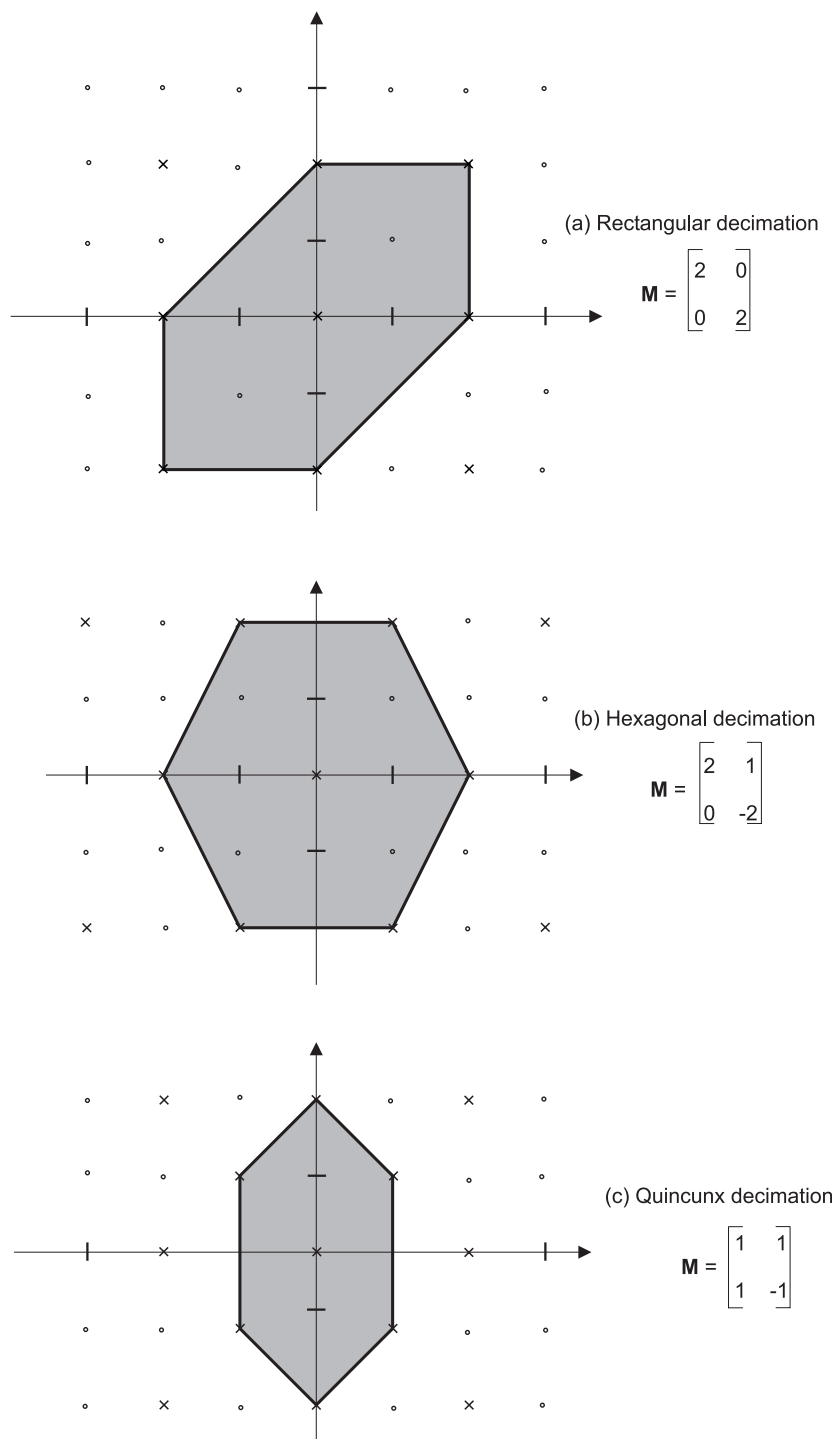


**Figure A.2:** Decimation matrices: a) for (digital/digital) rectangular downsampling, b) for (digital/digital) hexagonal downsampling, c) for (digital/digital) quincunx downsampling. The circles mark the sample values that are discarded after downsampling took place, the cross mark the ones that are still preserved.

## Proof for quincunx grid

Proof for the design of the two-dimensional, orthonormal, nonseparable filters in chapter 5.

**Proof :**

Let  $H_0(e^{j\omega})$  be a one-dimensional low-pass filter satisfying (3.3 - 3.6), hence

$$|H_0(e^{j\omega})|^2 + |H_0(-e^{j\omega})|^2 = 1,$$

$$|H_0(e^{j\omega}) \pm H_0(-e^{j\omega})| = 1$$

and

$$M_q = \begin{pmatrix} 1 & 1 \\ 1 & -1 \end{pmatrix}.$$

Define

$$Q_0(e^{j\boldsymbol{\omega}}) = H_0(e^{j\omega_0})H_0(e^{j\omega_1}) + H_1(e^{j\omega_0})H_1(e^{j\omega_1})$$

and

$$Q_1(e^{j\boldsymbol{\omega}}) = H_0(e^{j\omega_0})H_1(e^{j\omega_1}) + H_1(e^{j\omega_0})H_0(e^{j\omega_1}).$$

Then, using upsampling

$$Y_1(\boldsymbol{\omega}) = X(M_q^T \boldsymbol{\omega})$$

and downsampling

$$Z(\boldsymbol{\omega}) = \frac{1}{|\det M_q|} \sum_{k \in \mathbf{N}(M^T)} Y_2(M^{-T}(\boldsymbol{\omega} - 2\pi k))$$

one can write

$$Y_2 = Q_0(e^{j\boldsymbol{\omega}})Y_1(\boldsymbol{\omega}).$$

With

$$2\pi M_q^{-T} \begin{pmatrix} 1 \\ 0 \end{pmatrix} = \begin{pmatrix} \pi \\ \pi \end{pmatrix}$$

follows

$$Z(\boldsymbol{\omega}) = \frac{1}{2} [Y_2(M_q^{-T} \boldsymbol{\omega}) + Y_2(M_q^{-T}(\boldsymbol{\omega} + \begin{pmatrix} \pi \\ \pi \end{pmatrix}))] X(\boldsymbol{\omega} + 2\pi \begin{pmatrix} 1 \\ 0 \end{pmatrix}).$$

Since periodicity implies

$$\boldsymbol{\omega} + 2\pi \begin{pmatrix} 1 \\ 0 \end{pmatrix} = \boldsymbol{\omega}$$

it follows that

$$Z(\boldsymbol{\omega}) = \frac{1}{2} [Q_0(e^{jM_q^{-T} \boldsymbol{\omega}}) + Q_0(e^{j(M_q^{-T} \boldsymbol{\omega} + (\pi, \pi))})] X(\boldsymbol{\omega})$$

$$Z(\boldsymbol{\omega}) = Q_0(e^{jM_q^{-T} \boldsymbol{\omega}}) X(\boldsymbol{\omega}).$$

Next, it will be shown that

$$|H_0(e^{j(\omega_0, \omega_1)})|^2 + |H_0(e^{j[(\omega_0, \omega_1) + (\pi, \pi)]})|^2 = 1$$

is satisfied. For convenience, let

$$\frac{\omega_0 + \omega_1}{2} = v_0$$

and

$$\frac{\omega_0 - \omega_1}{2} = v_1.$$

Then, with

$$(\omega_0, \omega_1) = M_q \begin{pmatrix} v_0 \\ v_1 \end{pmatrix}$$

follows

$$|Q_0(e^{j(v_0, v_1)})|^2 + |Q_0(e^{j[(v_0, v_1) + (\pi, \pi)]})|^2 = 1.$$

The latter equation can be written as

$$\begin{aligned} & [H_0(e^{jv_0})H_0(e^{jv_1}) + H_0(-e^{jv_0})H_0(-e^{jv_1})] \cdot \\ & [H_0(e^{-jv_0})H_0(e^{-jv_1}) + H_0(-e^{-jv_0})H_0(-e^{-jv_1})] + \\ & [H_0(-e^{jv_0})H_0(e^{jv_1}) + H_0(e^{jv_0})H_0(-e^{jv_1})] \cdot \\ & [H_0(-e^{-jv_0})H_0(e^{-jv_1}) + H_0(e^{-jv_0})H_0(-e^{-jv_1})] = \\ & |H_0(e^{jv_0})H_0(e^{jv_1})|^2 + |H_0(-e^{jv_0})H_0(-e^{jv_1})|^2 + \\ & |H_0(-e^{jv_0})H_0(e^{jv_1})|^2 + |H_0(e^{jv_0})H_0(-e^{jv_1})|^2 + \\ & H_0(e^{jv_0})H_0(e^{jv_1})H_0(-e^{-jv_0})H_0(-e^{-jv_1}) + \\ & H_0(-e^{jv_0})H_0(-e^{jv_1})H_0(e^{-jv_0})H_0(e^{-jv_1}) + \\ & H_0(-e^{jv_0})H_0(e^{jv_1})H_0(e^{-jv_0})H_0(-e^{-jv_1}) + \\ & H_0(e^{jv_0})H_0(-e^{jv_1})H_0(-e^{-jv_0})H_0(e^{-jv_1}) = \\ & 1 + H_0(e^{jv_0})H_0(e^{jv_1})H_0(-e^{-jv_0})H_0(-e^{-jv_1}) + \\ & H_0(-e^{jv_0})H_0(-e^{jv_1})H_0(e^{-jv_0})H_0(e^{-jv_1}) + \\ & H_0(-e^{jv_0})H_0(e^{jv_1})H_0(e^{-jv_0})H_0(-e^{-jv_1}) + \\ & H_0(e^{jv_0})H_0(-e^{jv_1})H_0(-e^{-jv_0})H_0(e^{-jv_1}) = 1 \diamond \end{aligned}$$

Note that

$$\begin{aligned} & |H_0(e^{jv_0})H_0(e^{jv_1})|^2 + |H_0(-e^{jv_0})H_0(-e^{jv_1})|^2 + \\ & |H_0(-e^{jv_0})H_0(e^{jv_1})|^2 + |H_0(e^{jv_0})H_0(-e^{jv_1})|^2 = \\ & (|H_0(e^{jv_0})|^2 + |H_0(-e^{jv_0})|^2)(|H_0(e^{jv_1})|^2 + |H_0(-e^{jv_1})|^2) = 1 \end{aligned}$$

and

$$|H_0(e^{jv_0})| = |H_0(e^{-jv_0})|$$

for symmetric filters.



# Appendix B

## Zusammenfassung

Obwohl diese Dissertation sich überwiegend mit digitaler (diskreter) Signalverarbeitung befaßt, ist es das Ziel, analoge (zeitkontinuierliche) Signalverarbeitung durchzuführen. Die Verbindung zwischen beiden ist ein Abtastatz. Der Sinn eines Abtastatzes liegt darin, eine Vorschrift anzugeben, welche eine Repräsentation eines analogen Signals durch ein diskretes Signal erlaubt; in einer Weise, daß keine Information verloren geht. Weiterhin gibt er an, welche Mindestabstände zwischen zwei Abtastwerten notwendig sind, um eine fehlerfreie Rückgewinnung des ursprünglichen kontinuierlichen Signals aus dessen diskreter Version zu erreichen. Der Hauptgrund, warum man einen digitalen Schaltkreis anstelle eines analogen Schaltkreises verwendet ist der, daß für bestimmte Frequenzbereiche digitale Schaltkreise weniger störanfällig sind als analoge Schaltkreise.

Wenn eine diskrete Folge mit einem digitalen Filter gefaltet wird, dann wurde schon zuvor die gewünschte Filterstruktur (Mögliche Strukturen sind z.B. Direkt-, Parallel-, Kaskaden-, Abzweig- und Kreuzgliedstruktur) ausgewählt. Eine sehr gute Wahl der Filterstruktur für eine Anwendung, welche gute Koeffizientengenauigkeit, guten dynamischen Bereich und Stabilität unter der Bedingung endlicher Arithmetik erfordert, sind Abzweig- und Kreuzglied-Wellendigitalfilter-Strukturen (WDF). Rekursive WDF, z.B. Butterworth- und Cauer-Filter, können unter Zuhilfenahme von expliziten Formeln entworfen werden. Nichtrekursive WDF werden durch Optimierungsmethoden entworfen. Für sie können, bei einem hohen Filtergrad, numerische Probleme auftreten. Um die gleichen Filterspezifikationen zu erreichen, braucht man für nichtrekursive digitale Filter einen höheren Filtergrad als bei rekursiven digitalen Filtern. Linearphasige Filter und multipliziererfreie Strukturen können für beide Filtertypen angegeben werden.

Digitale Filter, welche in einer Filterbank angeordnet sind und zusätzlichen Bedingungen genügen, können benutzt werden, um Wavelets zu generieren. Biorthogonale Filter sind solche Filter. Orthogonale Filter sind eine Untermenge von biorthogonalen Filtern, welche die geringste Komplexität aufweisen. Entwurfsverfahren für orthogonale Filter sind für den eindimensionalen Fall bekannt [Gas85, Flie94, Vai93, Vet95]. Eine Entwurfsmethode der orthogonalen Filter für die mehrdimensionale, nichtseparierbare Abtastung, außer für ein triviales Filter (Haar Filter), wurde noch nicht gefunden. Im Gegensatz zur separablen Abtastung (Diagonal-Matrix), welche aus einem Skalarprodukt des eindimensionalen Falls hervorgeht und in einer Skalierungsfunktion und drei verschiedenen Wavelets resultiert, existiert für nichtseparierbare Abtastung eine

Skalierungsfunktion und nur ein Wavelet für den zweidimensionalen Fall mit zwei Kanälen. Eine ähnliche Aussage über die Anzahl der Wavelets gilt für mehr als zwei Kanäle und für mehr als zwei Dimensionen.

Mögliche Kandidaten für einen Abtastsatz sind der Nyquist-Abtastsatz oder der Wavelet-Abtastsatz. Das Filter mit welchem ein analoges Signal vor der Abtastung gefaltet wird ist die Skalierungsfunktion. Ein möglicher Kandidat für eine nichtseparierbare Abtastmatrix in zwei Dimensionen ist eine Quincunx-Matrix für die Zweikanal-Filterbank und eine Hexagonal-Matrix für die Vierkanal-Filterbank. In drei Dimensionen ist das eine FCCS-Matrix für die Zweikanal-Filterbank und eine BCCS-Matrix für die Vierkanal-Filterbank.

Die Stärke der Wavelet-Methoden liegt in der Fähigkeit, lokale Ereignisse genauer beschreiben zu können, als es mit der traditionellen Fourieranalyse der Fall ist. Deshalb sind Wavelets ideal für Anwendungen, in welchen ein Ansatz für das Beschreiben von Übergangsverhalten benötigt wird, wie z.B. bei seismologischen Signalen oder bei der Bildverarbeitung. Operatoren, die mit Wavelets assoziiert sind, wie z.B. die Calderon-Zygmund-Operatoren, scheinen dafür prädestiniert zu sein, noch nicht gelöste Probleme in der komplexen Analyse und bei partiellen Differentialgleichungen zu lösen. Deshalb sind Wavelets und der Entwurf orthogonaler Filter, realisiert als Wellendigitalfilter, für die nichtseparierbare Abtastung bei mehrdimensionalen Problemen sehr gefragt. Sie werden von Ingenieuren, die sich mit Teilbandkodierung befassen, Physikern, die sich mit den sogenannten "coherent states" in der Quantenphysik befassen, und Mathematikern, die sich mit den Calderon-Zygmund-Operatoren befassen, hauptsächlich benötigt. Verschiedene Industrienormen haben inzwischen die Wavelet-Transformation mit einbezogen, siehe z.B. [Rao96].

Das Kernziel dieser Dissertation ist der Entwurf von orthogonalen, mehrdimensionalen Wellendigitalfiltern für nichtseparierbare Abtastmatritzen. Damit der Leser einen einfacheren Einstieg in den Filterentwurf hat, sind einige Grundlagen elektrischer Netzwerke und Filter vom analogen als auch vom digitalen Typ in Kapitel 2 angegeben. Als motivierendes Beispiel einer Anwendung ist ein elektrisches Netzwerk angegeben, welches eine dreidimensionale Navier-Stokes-Gleichung repräsentiert. Dieses Netzwerk kann herangezogen werden, wenn numerische Lösungswerte der Gleichung berechnet werden sollen. Wichtiges Beiwerk, welches digitale Filter mit der Wavelet-Transformation verknüpfen, ist zusammengefaßt, und es wird weiterführende Literatur angegeben, die diesen Stoff ausführlicher behandelt. Weiterhin werden wichtige Abtastsätze präsentiert. Ein angegebener Vergleich über die minimale Abtastrate zeigt einen interessanten Aspekt bezüglich der Mindestabstände zwischen zwei Abtastwerten.

Kapitel 3 zeigt Verbindungen von Wellendigitalfiltern zu ihren analogen Referenzfiltern auf. Weiterhin wird gezeigt wie man eine perfekte Rekonstruktion mit Filterbänken erreicht ohne eine spektrale Faktorisierung durchführen zu müssen. Diesbezüglich ist Feldkellers Gleichung während des Entwurfs von Abzweig- und Kreuzglied-Wellendigitalfiltern wichtig. Es ist exemplarisch gezeigt, wie man ein perfektes Rekonstruktionssystem mit rekursiven, orthogonalen Kreuzglied-Wellendigitalfiltern entwerfen kann. Es ist auch gezeigt, wie man nichtkausale Filter implementieren und wie man Signale unendlicher Länge verarbeiten kann.

Bekannte Wavelets, wie z.B. Meyer Wavelets, Sinc Wavelet (Littlewood-Paley Wavelet), Haar Wavelet, Daubechies Wavelet und Butterworth Wavelet, sind in Kapitel 4 präsentiert. Ebenfalls sind bekannte Filter präsentiert, die (sofern einige Einschränkungen eingehalten werden) benutzt werden können, um neue orthonormale Wavelets, nämlich Cosinus-Rolloff-Wavelet und Chebyshev-Wavelet, zu generieren. Ferner sind in Kapitel 4 zwei Eigenschaften der Wavelet-Transformation, die Verschiebung und die Faltung aufgeführt. Unter Zuhilfenahme bekannter Filterentwurfsverfahren ist die Verschiebeoperation für Verschiebungen um  $\tau \in \mathbf{R}$  erweitert.

Die Neuheiten der Kapitel 5, 6, und 7 sind:

- Eine Entwurfsmethode für quincunx-abgetastete, nichtseparierbare, orthogonale Wellendigitalfilter (zweikanalig) ist in Kapitel 5 angegeben. Die Entwurfsmethode basiert auf eindimensionalen Filtern sowie aus sogenannten gutartigen Abtastmatritzen. Eine Polyphasenzerlegung ist angewendet und resultiert in einer sehr effizienten Filterstruktur.
- Eine zweite Entwurfsmethode für hexagonal-abgetastete sowie BCCS-abgetastete, nichtseparierbare, orthogonale Wellendigitalfilter (vierkanalig) ist in Kapitel 6 angegeben. Es wurden, wie in Kapitel 5, gutartige Abtastmatritzen gefunden, die während des Filterentwurfs, der ebenfalls mit eindimensionalen Filtern durchgeführt wird, verwendet werden. Ein Beispiel (Butterworth-Filter) ist aufgeführt. Jedoch ist die Methode nicht nur auf Butterworth-Filter beschränkt.
- In den Kapiteln 5 und 6 werden Kreuzglied-Wellendigitalfilter bevorzugt, da sie sehr effizient realisiert werden können. Jedoch, wie im Kapitel 7 gezeigt wird, führt eine Abzweigstruktur der Wellendigitalfilter für hexagonal abgetastete Signale auf effizientere Implementierungen. Eine neue Filterentwurfsmethode ist für diesen Fall aufgezeigt, und baut auf expliziten Formeln auf.

Die Dissertation ist im Kapitel 8 zusammengefaßt.

# Bibliography

- [Ans96] R. Ansari, "IIR filter banks and wavelets," in A. N. Akansu, M. J. T. Smith, "Subband and wavelet transforms, Design and applications," Kluwer Academic Publishers, 1996.
- [Bel68] V. Bellevitch, "Classical Network Synthesis," Holden Day, San Francisco, CA, 1968.
- [Bey92] G. Beylkin, "On the representation of operators in bases of compactly supported wavelets," *SIAM J. Numer. Anal.*, **6**, (6), pp.1716-1740, December 1992.
- [Can94] V. F. Candela, "Computation of shift operators in orthonormal compactly supported wavelet bases," *SIAM J. Numer. Anal.*, **31**, (3), pp.768-787, June 1994.
- [Che91] T. Chen, P. P. Vaidyanathan, "Multidimensional Multirate Filters derived from one Dimensional Filters," *Electronics Letters*, vol.27, pp.225-228, Jan. 1991.
- [Coo95] T. Cooklev, "Regular Perfect-Reconstruction Filter Banks and Wavelet Bases," Doctoral dissertation, Tokyo Institute of Technology, 1995.
- [Cro83] R. E. Crochiere, L. R. Rabiner, "Multirate digital signal processing," Englewood Cliffs, Prentice Hall, 1983.
- [Che95] G. Chen, "Representation, Approximation and Identification," in W. K. Chen "The Circuits and Filters Handbook," CRC Press, Inc. 1995.
- [Cle79] J. H. Mc Clellan, T. W. Parks, L.R. Rabiner, "FIR linear phase filter design program," in programs for digital signal processing, New York: IEEE, pp. 5.1-1-5.1-13, 1979.
- [Coh90] A. Cohen, "Ondelettes, Analyses Multiresolutions et Traitement Numerique du Signal," PhD Thesis, Universite Paris IX Dauphine, Paris, France, 1990.
- [Coh93] A. Cohen, I. Daubechies, "Nonseparable bidimensional wavelet bases," *Rev. Mat. Iberoamericana*, vol.9, no.1, pp.51-137, 1993.
- [Dav95] A. M. Davis, "Approximation," in W. K. Chen, "The Circuits and Filters Handbook," CRC Press, Inc. 1995.

- [Dau92] I. Daubechies, "Ten lectures on wavelets," SIAM Philadelphia, PA, 1992
- [Djo94] I. Djokovic, P.P. Vaidyanathan, "Generalized Sampling Theorems in Multiresolution Subspaces," Technical Report, California Institute of Technology, Aug. 1994
- [Eur93] L. Eurp, M. Gardener, R. A. Harris, "Interpolation in Digital Modems-Part II: Implementation and Performance," *IEEE Trans. on Commun.*, **41**, (6),pp. 998-1008, December 1993.
- [Far92] M. Farge, E. Goirand, Y. Meyer, F. Pascal, M. V. Wickerhauser, "Improved predictability of two-dimensional turbulent flows using wavelet packet compression," *Fluid Dynamics Research*, vol. 10, pp.229-250, 1992.
- [Far88] C. W. Farrow, "A continuously variable digital delay element," *IEEE Proc. Int. Symp. Circuits & Syst.*, Espoo, Finnland, pp.2641-2645, June 1988.
- [Fet92] A. Fettweis, "Discrete Modeling of Lossless Fluid Dynamic Systems," *Archiv fuer el. Uebertr.*, vol. 46, no. 4, pp. 209-218, Apr. 1992.
- [Fet70] A. Fettweis, "Entwurf von Digitalfiltern in Anlehnung an Verfahren der klassischen Netzwerktheorie," in *Proc. NTG-Fachtagung, "Analyse und Synthese von Netzwerken,"* pp.17-20, 1970
- [Fet86] A. Fettweis, "Wave digital filters:Theory and Practice," *Proc.IEEE*, vol.74,no.2, pp.270-327, Feb.1986.
- [Fet85] A. Fettweis, J. A. Nossek, K. Meerkoetter, "Reconstruction of Signals after Filtering and Sampling Rate Reduction," *IEEE Trans. on Acoustic and Signal Processing*, vol. ASSP-33, no.4, Aug. 1985.
- [Fet90] A. Fettweis, T. Leickel, M. Bolle, U. Sauvagerd, "Realization of Filter banks by means of wave digital filters," *IEEE Int. Symp. on Circuits and Systems*, 1990.
- [Fli91] N. J. Fliege, "Systemtheorie," B.G. Teubner, 1991
- [Fli94] N. Fliege, "Multirate Digital Signal Processing," John Wiley & Sons Ltd, 1994.
- [Fri96] M. Fries, "Numerical integration of Euler flow by means of multidimensional wave digital principals," Shaker, 1996
- [Gas85] L. Gaszi, "Explicit formulae for lattice wave digital filters," *IEEE Trans.*, vol.CAS-32, pp.68-88, Jan. 1985.
- [Got98a] A. Gottscheber, "Passive Two- and Three-dimensional Wave Digital Filters used in a Multirate System having Perfect Reconstruction," To be published in *Signal Processing* 1997.

- [Got97a] A. Gottscheber, A. Nishihara, "Passive Two-dimensional Wave Digital Filters used in a Multirate System having Perfect Reconstruction," IEICE Trans. on Fundamentals, vol. E80-A, no.1, pp.133-139, Jan. 1997.
- [Got98] A. Gottscheber, A. Nishihara, "Chebyshev wavelets, Butterworth wavelets and Wave Digital Filter," To be published in IMR 1998.
- [Got96] A. Gottscheber, A. Nishihara, "Filter bank implementation of the shift operation in orthonormal wavelet bases," Trans. IEICE, vol. E79-A, no.3, pp.291-296, Mar. 1996.
- [Got97] A. Gottscheber, A. Nishihara, "Wavelet bases derived from the raised-cosine filter," IEICE Trans. on Fundamentals, vol. E80-A, no.1, pp.126-132, Jan. 1997.
- [Hay95] S. Haykin, "Adaptive filter theory," Prentice Hall, 1995
- [Hem95] G. Hemetsberger, "Numerische Integration hyperbolischer partieller Differentialgleichungen unter Verwendung mehrdimensionaler Wellendigitalfilter," Doctoral dissertation, Ruhr-Univ. Bochum, 1995.
- [Her93] C. Herley, M. Vetterli, "Wavelets and Recursive Filter Banks," IEEE Trans. on Signal Proc., vol.41, no.8, pp.2536-2556, Aug. 1993.
- [Iee79] IEEE DSP Comm., IEEE New York: Programs for digital signal processing, 1979.
- [Jaw94] B. Jawerth, W. Sweldens, "An overview of wavelet based multiresolution analysis," SIAM Review, Vol.36, No. 3, pp.377-412, September 1994
- [Jer77] A. J. Jerri, "The Shannon sampling theorem-Its various extensions and applications: A tutorial review," Proc. IEEE, vol. 65, pp. 1565-1596, 1977.
- [Kar97] T. Karp, "Modifizierte DFT-Filterbnke," doctoral dissertation, VDI Verlag, 1997.
- [Kim92] C. W. Kim, R. Ansari, A. E. Cetin, "A class of linear phase biorthogonal wavelets," Proc. Int. Conf. on Acoustics, Speech and Signal Processing, pp.673-676, March 1992.
- [Kov92] J. Kovacevic, M. Vetterli, "Nonseparable Multidimensional Perfect Reconstruction Filter Banks and Wavelet Bases for  $R^n$ ," IEEE Trans. on Inform. Theory, vol.38, no.2, Mar. 1992.
- [Kov95] J. Kovacevic, "z-Transform," in W. K. Chen, "The Circuits and Filters Handbook," CRC Press, Inc. 1995.
- [Law90] S. Lawson, A. Mirzai, "Wave Digital Filters," Ellis Horwood Ltd., 1990.
- [Law93] W. Lawton, "Applications of complex valued wavelet transforms to subband decomposition", *IEEE Trans. on Signal Proc.*, **41**, (12), pp.3566-3568, Dec. 1993.

- [Lei94] T. Leickel, "Entwurf und Realisierung diskreter Filterbaenke," Doctoral dissertation, Ruhr-Univ. Bochum, 1994.
- [Lim95] Y. C. Lim, "Lattice Filters," in W. K. Chen, "The Circuits and Filters Handbook," CRC Press, Inc. 1995.
- [Lin84] G. Linnenberg, "Ueber die discrete Verarbeitung mehrdimensionaler Signale unter Verwendung von Wellendigitalfiltern," Doctoral dissertation, Ruhr-Univ. Bochum, 1984.
- [Lor83] G. G. Lorentz, K. Jetter, S. D. Riemenschneider, "Birkhoff Interpolation," Reading, MA: Addison-Wesley, 1983.
- [Lou94] A. K. Louis, P. Maass, A. Rieder, "Wavelets," B.G. Teubner, 1994.
- [Mal89] S. Mallat, "A theory for multiresolution signal decomposition: The wavelet representation," IEEE Trans. Patt. Recog. and Mach. Intell., vol. 11, no. 7, pp. 674-693, Jul. 1989.
- [Mer83] R. M. Merserau, T. C. Speake, "The Processing of periodically Sampled Multidimensional Signals," IEEE Trans. Acoust., Speech, Signal Proc., vol. ASSP-31, pp.188-194, Feb. 1983.
- [Mey92] Y. Meyer, "Wavelets and operators," Cambridge Uni. Press, 1992
- [Mit92] S. K. Mitra, C. Creusere, H. Babic, "A novel implementation of perfect reconstruction QMF banks using IIR filters for infinite length signals," IEEE Int. Symp. on Circuits and Systems, pp.2312-2315, 1992.
- [Nar94] R. Naresh, K. Keshab, "Pipelined adaptive digital filters," Kluwer, 1994.
- [Nit93] G. Nitsche, "Numerische Lsung partieller Differentialgleichungen mit Hilfe von Wellendigitalfiltern," VDI Verlag, 1993
- [Nos83] A. Nossek, H. D. Schwarz, "Wave digital lattice filters with applications in communication systems," Proc. IEEE Int. Symp. Circuits and Systems, pp.845-848, May 1983.
- [Oko71] H. P. Okolowitz, "Zur Synthese verlustfreier Zweitore durch Faktorzerlegung der Betriebsparametermatrizen," Doctoral dissertation, Ruhr-Univ. Bochum, 1971.
- [Owe92] K. A. Owenier, "Uniform recurrence formulae for the characteristic function of classical LC-filters, wave digital filters, and VIS-SC-filters, with Tchebycheff pass-band," Proc. IEEE ISCAS, vol. 2, pp.337-340, 1992.
- [Pet62] D. P. Peterson, D. Middleton, "Sampling and reconstruction of wave-number-limited functions in N-dimensional Euclidean spaces," Information and Control, vol. 5, pp. 279-323, 1962.

- [Ram84] T. A. Ramstad, "Digital methods for conversion between arbitrary sampling frequencies", *IEEE Trans. Acoustic, Speech, SignalProcessing*, **ASSP-32**, pp. 577-591, June 1984.
- [Rao96] K. R. Rao, J. J. Hwang, "Techniques and Standards for Image and Audio Coding," Engelwood Cliffs, Prentice Hall, 1996.
- [Sch73] R. W. Schafer, L. R. Rabiner, "A digital signal processing approach to interpolation," *Proc. IEEE*, **61**, pp. 692-702, June 1973.
- [Sch90] R. Schaumann, M. S. Ghausi, K. R. Laker, "Design of analog filters," Prentice hall, 1990.
- [Sel97] I. W. Selesnick, "Explicit formulas for orthogonal IIR wavelets," preprint, 1997.
- [Skl88] B. Sklar, "Digital Communications," Prentice Hall, 1988.
- [Smi91] M. J. T. Smith, "IIR Analysis/Synthesis Systems," in J. W. Woods, "Subband Image Coding," Kluwer Academic Publishers, 1991.
- [Som93a] A. K. Soman, P. P. Vaidyanthan, T. Q. Nguyen, "Linear Phase Paraunitary Filter Banks: Theory, Factorizations and Designs," *IEEE Trans. on Signal Processing*, vol. 41, no.12, pp. 3480-3496, Dec. 1993.
- [Som93] A. K. Soman, P. P. Vaidyanthan, "On Orthonormal Wavelets and Paraunitary Filter Banks," *IEEE Trans. on Signal Processing*, vol. 41, no.3, pp. 1170-1183, March 1993.
- [Ste93] P. Steffen, P. N. Heller, A. Gopinath, C. S. Burrus, "Theory of Regular M-Band Wavelet Bases," *IEEE Trans. on Signal Processing*, vol. 41, no.12, pp. 3497-3511, Dec. 1993.
- [Str96] G. Strang, T. Q. Nguyen, "Filter banks and wavelets," Wellesley-Cambridge Press, 1996.
- [Tan95] S. Tantaratana, "Design of IIR Filters," in W. K. Chen, "The Circuits and Filters Handbook," CRC Press, Inc. 1995.
- [Tch96] P. Tchamitchian, "Wavelets, Functions, and Operators," in G. Erlenbacher, M. Y. Hussanini, L. M. Jameson, "Wavelets, Theory and Applications," Oxford Univ. Press, Inc. 1996.
- [The73] G. C. Themes, S. K. Mitra, "Modern Filter Theory and Design," John Wiley & Sons, inc. 1973.
- [Thi77] J. P. Thiran, "On unit element structures for wave digital filters," *IEEE Trans. on Circuits and Systems*, vol. CAS-24, no. 1, pp.20-28, Jan. 1977.
- [Unb93] R. Unbehauen, "Netzwerk und Filtersynthese," Oldenbourg, 1993



- [Vai93] P. P. Vaidyanathan, "Multirate Systems and Filter Banks," Engelwood Cliffs, Prentice Hall, 1993.
- [Vai93a] P.P. Vaidyanathan, "Orthonormal and Biorthonormal Filter Banks as Convolvers, and Convolutional Coding Gain," IEEE Trans. Signal Proc., vol. 41, pp.2110-2130, June 1993.
- [Vet95] M. Vetterli, J. Kovacevic, "Wavelets and subband coding," Engelwood Cliffs, Prentice Hall, 1995.
- [Wal92] G.G. Walter, "A sampling theorem for wavelet subspaces," IEEE Trans. Information Theory, vol. 38, pp. 881-884, 1992
- [Wic92] M. V. Wickerhauser, "Acoustic signal compression with wavelet packets," in C. K. Chui, "Wavelets: A tutorial in theory and application," pp.679-700, Academic Press, N. Y. 1992.
- [Xia93] X.G. Xia, Z. Zhang, "On Sampling Theorem, Wavelets, and Wavelet transforms," IEEE Trans. on Signal Processing, vol. 41, no. 12, pp. 3524-3535, Dec. 1993

# LEBENS LAUF

## Achim GOTTSCHER

Geburtstag / Geburtsort	01.01.1965 / Bad Wimpfen
Schulbesuch	1971-74 Grundschule in Grombach bis 1980 Hauptschule in Kirchardt
Berufsausbildung	1980-83 Lehre als Energieanlagenelektroniker (Badenwerk AG, Sinsheim)
Praktische Tätigkeit	1983-86 als Elektromonteur (Badenwerk AG, Sinsheim)
Schulbesuch	1984-86 Abendrealschule der Volkshochschule Sinsheim e.V.
Grundwehrdienst	01.07.1986-30.09.1987
Schulbesuch	Einjähriges Berufskolleg zum Erwerb der Fachhochschulreife Schuljahr 1987-88
Praktische Tätigkeit	01.07.1988-30.09.1988 als Monteur (Vollert AG, Weinsberg)
Studium	WS 88/89-SS 92 FH Aalen, Fachbereich Elektronik, Diplom-Ingenieur (FH)
Studium	WS 90/91 Teesside University in Middlesbrough (UK), Department of Instrumentation and Control Engineering (ERASMUS-Austauschprogramm)
Praktische Tätigkeit	01.03.1991-31.08.1991 2. Praxissemester (SEW Eurodrive, Bruchsal)
Studium	1992-93 University of London, King`s College, Department of Electronic and Electrical Engineering, Master of Science
Praktische Tätigkeit	28.06.1993-31.08.1993 Praktikum (Britisch Telecom, Ipswich, UK)
Sprachstudium	01.09.1993-31.03.1994 Japanisch, Universität Heidelberg
Studium	01.04.1994-30.09.1994 Tokyo Institute of Technology, Department of Physical Electronics, Research Student
Sprachstudium	01.10.1994-31.03.1995 Fachbuchübersetzung Englisch→Japanisch, Titel: "Multirate Digital Signal Processing", von N. J. Fliege, 1994
Studium	01.04.1995-31.03.1997 Tokyo Institute of Technology, Department of Physical Electronics, Studium zum Erlangen des Grades eines Doktor-Ingenieurs (DAAD/Monbusho-Stipendium)
Gastwissenschaftler	01.06.1995-31.08.1995 Ruhr-Universität Bochum, bei A. Fettweis im Lehrstuhl für Nachrichtentechnik 01.06.1996-31.08.1996 Ecole Polytechnique Federale de Lausanne (S), bei M. Vetterli im Dept. d` Electricite 20.06.1996-07.07.1996 Jerome University Aix (F), bei P. Tchamitchian im Laboratoire de Mathematiques
Studium	01.04.1997-31.01.1998 Universität Mannheim, Lehrstuhl für Elektrotechnik, bei N. J. Fliege, Dissertation
Praktische Tätigkeit	01.02.1998-... Forschungszentrum Karlsruhe, Nachwuchswissenschaftler in der Hauptabteilung Prozeßdatenverarbeitung und Elektronik